High-Performance Robot Motion Control Based on Wideband and Friction-Free Force Sensation

広帯域と摩擦フリー力覚情報に基づく高性能ロボットモーションコントロール

TRAN PHUONG THAO

Supervisor: Prof. Kiyoshi OHISHI

Energy and Environment Sciences

Nagaoka University of Technology

Table of Contents

List of Figures

List of Tables

Acknowledgements

This PhD thesis is the summary of research activities in Doctoral course at Professor Ohishi's laboratory, Department of Electrical Engineering, Nagaoka University of Technology, Japan.

I would never have been able to finish my dissertation without the guidance of my Professors, help from friends, and support from my family.

First and foremost, I would like to express my deepest gratitude to my supervisor, Professor Kiyoshi Ohishi, for the insightful guidance and tremendous support of my study and research, for his patience, encouragement, enthusiasm, and immense knowledge. It is my honor to be a student under his supervision.

I would like to thank Professor Toshimasa Miyazaki for his helpful advice and comments during my research work. I also wish to thank Professor Shiro Urushihara, who is with Takamatsu National College of Technology, for his great support and help when I first started my life in Japan.

I would like to sincerely thank Professor Seiji Kondo, Professor Yuji Hirao, Professor Yasuhiro Wada, Professor Takabumi Fukuda, Professor Jun-ichi Itoh and Assistant Professor Yuki Yokokura for their invaluable comments and discussions to improve my research and modify this thesis.

I would like to thank all members in Ohishi laboratory for their kind help and support, for creating good research environment and friendships. Special thanks to Dr. Chowarit Mitsantisuk, Dr. Manuel Nandayapa, Dr. Kenji Takahashi and Dr. Naoki Shimada, who are always willing to help and give their best suggestions. Many thanks to our secretary, Ms. Akiko Nagumo, for her friendliness and helpfulness in many cases.

The financial support from the Ministry of Education, Culture, Sport, Science, and Technology, Japan (MEXT), including the scholarship and the research fund during my five years of study and research is acknowledged. I also thank Nagaoka University of Technology because of the good support for all international students at GIDAI.

I would like to give many thanks to my parents, Tran Minh Chanh and Lai Thi Bach Cuc, and all other family members. There is no word to acknowledge the encouragement and love of my parents. I could not have finished the long journey of my study without their love and encouragement.

Finally, I would like to thank my beloved husband, Banh Quoc Tuan. He was always there cheering me up and stood by me through the good times and bad.

Sincerely,

TRAN Phuong Thao

July, 2013

Chapter 1

Introduction

In this chapter, the research background on force sensing technology in motion control and sensorless force estimation method, which induce the motivation of my research, are presented. The objectives of this research are clearly described and the outline of the thesis is briefly introduced.

1.1 Research Background

1.1.1 Overview of Force Sensing Technology in Robot Motion Control

In developed countries, the evolvement of technology is much more concentrating on improving the standard of human living. Robots and mechatronic systems are expected to support human activities in daily life, industry, entertainment, service, outer space and medicine. In order to competently support human activities, the robots should have the ability to recognize the real world based on human actions. Haptic technology which refers to sensing and manipulation through touch is concerned with acquisition and transmission of haptic or tactile information in order to enable human to perceive the real environment through devices.

Force sensing method plays a very vital role in haptics applications of human-robot interaction manipulators, machine tools, railway systems, and robotic surgery [1-10]. The measurement of force in a force control system is of greatest importance since the accuracy of the force measurement affects the performance of the system directly. Wideband force sensing is necessary to achieve a high-performance force control system [11]. To increase patient safety in a tele-robotic surgery system, it is essential to obtain the precise force feedback information to give the surgeon the vivid feeling that he is directly operating with his own hands on the patient body [12]. An industrial robot arm requires knowledge of the contact force while performing specific tasks to guarantee that the contact force is regulated

within a safe level so that the environment and human operator are not in danger when in contact with the robot [13].

The bandwidth of force sensing is inversely proportional to a sampling period of the control system. In order to increase the bandwidth of force sensation, a shortened sampling period is necessary. However, conventionally, a motion controller is executed by CPU or DSP, and the sampling period is not fast enough to estimate the frequency range of forces that human can feel. Together with the rapid development of very large scale integration (VLSI) technology and the demand on a suitable device for high speed motion controllers, a field programmable gate array (FPGA) has become a good candidate for implementing the motion controller. FPGA has brought their advantages of hard-wired programmability, fast time-to-market, shorter design cycle, embedded systems, low of power consumption and higher density for digital implementation. There is much research focusing on applying the controller in FPGA [14-23]. The feature of parallel processing enables FPGA to significantly shorten the sampling time of the control algorithm.

Generally, force measurement is realized using force sensors. Although commercial force sensors benefit from their accuracy, flexibility, and reliability, the use of force sensors in a force control system has its own noteworthy downsides. Most force sensors are not very durable and are vulnerable to impact. Besides, high-precision force sensors are not economical for limited budget projects. Moreover, force sensors are susceptible to the noise effect that results in a narrow force-sensing bandwidth and are not usually suitable for all environments or applications. These drawbacks to some extent limit the use of force sensors.

Therefore, many approaches have been proposed to develop alternative force observers. One popular force-sensor-less observer method is the disturbance observer [24-26]. Essentially, the disturbance observer is used instead of a force sensor to estimate and compensate the disturbance force. Since being invented, it has become one of the most preferred solutions in motion control [27-40]. The disturbance observer is designed for making estimates by taking parameter variation, nonlinear friction, and other disturbances into consideration as a single state variable. By using the disturbance observer, the disturbance force is rejected, and robust motion control is attained. Moreover, a large number of elegant approaches to develop the disturbance observer as well as improve its performance

have been proposed. Xiong and Saif have proposed a state functional disturbance observer to estimate disturbances with a bounded error [41]. In this method, the disturbance observer state does not precisely track the system states, which is an advantage that simplifies the estimation error dynamics. To provide satisfactory control performance, Chen et al. have proposed a new nonlinear disturbance observer scheme and applied it to a robotic system [42]. Kato et al. have introduced a modified disturbance observer with a Smith predictor for time-delay compensation [43]. This method achieved robust stability in a control system in which time-delay transmission occurred.

With the position-sensor-based disturbance observer, the bandwidth of force sensing is limited by the position sensor and the derivative noise because the disturbance observer obtains the force information by the second-order derivative of a position response. In order to solve this problem, Katsura et al. have proposed a combination of position and acceleration signals to construct a position-acceleration integrated disturbance observer [27]. This technique combines the position signal and acceleration signal to construct the high frequency bandwidth force sensing. Nevertheless, in industrial applications, the performance of the disturbance observer is deteriorated by noise problems. Consequently, the inaccuracy of the force sensation and the instability of the force control system sometimes happen. Another approach has introduced a Kalman-filter-based disturbance observer (KFDOB) to enhance the performance of force estimation by improving the bandwidth of force sensing without noise [44]. However, the possibility of widening the bandwidth of the disturbance observer is also restricted by the sampling period of $100\,\mu s$ of CPU based on the RT-Linux operating system.

In fact, the performance of a force control system is determined by how the force is properly detected. In many control systems, the drive motor is connected to the load through a ball screw or gear mechanism. Due to mechanical imperfections in these connections, there always exists some friction. Friction is usually described as the resistance to motion of two surfaces in contact. Friction is one of the greatest obstacles in high-precision control systems. In a force control system, friction can deteriorate the force-sensing performance as well as the control performance. In motion control, a possible way to minimize the influence of friction is to compensate for it. Many model-based friction estimation and compensation

methods have been proposed [45-50]. Friedland et al. have proposed a reduced-order nonlinear observer to estimate the velocity-dependent coefficient of the classical nonlinear friction model with velocity measurements [51]. Canudas et al. have proposed a new dynamic model for friction including the Stribeck effect, hysteresis, spring-like characteristics for stiction, and a varying break-away force [52]. Nicholas et al. have presented a hybrid compensation method that is applied to compensate friction in a haptic display [53]. The hybrid compensator combined a model-based feed-forward compensator and force feedback to cancel friction. Xia et al. have employed a velocity observer based on a state-space nonlinear friction model and designed an adaptive controller that achieved a semi-global asymptotic stability [54]. The velocity observer is a model-based estimator that requires plant parameters to estimate the velocity.

The inherent disadvantage of the model-based technique lies in the model complexity and accuracy. A very simple way to eliminate the effect of friction is to use a non-model-based friction compensation method known as "dithering." Dithering is a technique characterized by the addition of a high-frequency, low-amplitude signal to the desired reference signal. The effect of the dither signal is the ability to smooth the discontinuity of friction. Another version of the dithering method is the Knocker, for use in industrial valves [55]. In [56], the effect of the dither signal in a system with dynamic friction has also been presented. However, the use of a dither signal has the disadvantage of introducing more disturbances into the control process. The oscillatory disturbance caused by dither signal can affect the performance of the force sensing as well as the control system.

Therefore, to achieve the high performance force control system, it is vital to develop a wideband force sensing method with effective friction reduction and noise suppression in force estimation.

1.1.2 Robustness in Motion Control Systems

A motion control system in an open environment requires various stiffnesses corresponding to each task. Control stiffness is defined in the following equation:

$$k = \frac{\partial f}{\partial x} \tag{1.1}$$

where k denotes control stiffness, f denotes generated force, and x denotes position. The ideal position control should have infinite stiffness; however, the ideal force control should have zero stiffness. A modern motion system requires the ability to be compliant with a contact environment. Motion control should take plural modes of environment into account. The environmental information is a key to be compliant to an unknown environment. Motion control taking environmental information into account makes various machines including robots more adaptive and versatile.

The high performance motion control system capable of performing skillful motions should be robust against the load change and parameter variation. To satisfy these requirements, the controller should have a wide range of control stiffness, keeping the system highly robust.

Acceleration control can set the control stiffness independent of the robustness. A disturbance observer is a well-known method for attaining robust acceleration control. A disturbance observer identifies the total mechanical load force and parameter change. In other words, the identification of disturbance torque is essential for motion control robustness to realize various applications.

1.1.3 Sensorless Force Estimation Method

Motion control systems are concerned with the actuation of all devices in a manufacturing process to satisfy specific motion requirements. In a force control system, the control requirement is to dictate the desired force on the environment. Traditionally, this motion requirement can be achieved with the utilization of force sensors. However, it is well known that force sensors have many drawbacks such as sensor noise, narrow bandwidth, instability due to the soft structure of force sensors, complex electronic setups and wirings. These drawbacks limit the use of force sensors and motivate the development of force observers to provide alternative methods for force sensing process.

A disturbance observer [24-26], which is proposed to replace the use of a force sensor, is an effective method to achieve robustness against disturbances and model uncertainties. The disturbance observer is a technique to estimate and compensate the disturbance forces by identifying the total load force and the parameters of the motor inertia and force coefficient.

Using the disturbance observer, the robust acceleration control is achieved. In comparison with force sensors, the disturbance observer offers the advantages of faster response, wider bandwidth, free from sensor noise and increasing of system stability. The sensorless force control based on disturbance observer has arisen in literature and reality with a variety of applications. In addition, the disturbance observer is an efficient tool in most of industrial force control applications because it can be combined with most of the relevant existing force control techniques such as hybrid position/force control, stiffness control, acceleration based force control, and impedance control.

1.2 Objectives of Research

Based on the reasoning in the previous section, my research proposes a methodology to achieve the high-performance robot motion control based on the wideband, friction-free and noise-free force sensing to be applied in human-robot interaction systems, machine tools, power assisted devices, surgery, education and training systems.

The objectives of this research are clearly described as follows.

a. High performance force control system with wideband force sensing based on Multi-sensor integration in Kalman-filter-based disturbance observer (DOB)

Linear shaft motor is used to construct the haptic device: In haptics applications, a proper mechanism is required to allow human to easily maneuver an object. A linear shaft motor has a simple construction that features its outstanding characteristics of precision positioning, compact and lightweight, operation under adverse environmental conditions, and especially frictionless mechanism. Therefore, the linear shaft motor is well suited for haptic device configuration, notably in medical applications of tele-surgery robots.

Multi-sensor integration in Kalman-filter-based disturbance observer: The Kalman-filter with multi-sensor is used in combination with the disturbance observer for force sensing operation. The Kalman-filter uses position signals and acceleration signals as its inputs to estimate the velocity. By using Kalman-filter with multi-sensor integration, the noise in velocity estimation is suppressed effectively and the improved velocity information is obtained, especially during the impact motions with high acceleration. As the result, the force estimated by disturbance observer is markedly enhanced and the superior wideband force sensing of 10 kHz is achieved.

b. Enhanced force sensing performance based on wideband, friction-free and noise-free force estimation

Force control system constructed by a ball-screw mechanism: Ball screws are widely used in various applications such as machine tools, robots, automobile industry, aircraft industry, military equipment, medical equipment or precision assembly equipment owing to their characteristics of high loading ability, long life, high stiffness, easy travel and high

speed reliability. Therefore, my research develops a high performance and wideband, friction-free and noise-free force control system based on the ball-screw mechanism.

Friction compensation using dithering method: Force control systems in which a ball screw is employed to connect the drive motor to the load are generally affected by friction due to mechanical imperfections in the connections. In my research, the friction compensation method is inspired by the dithering method's simplicity of implementation. Thus, a periodic signal is inserted into the control signal to reduce the effect of friction on force estimation. The effect of the dither signal is the ability to smooth the discontinuity of friction.

Wideband, friction-free and noise-free force observation: The dither signal also generates oscillatory disturbances affecting the performance of control system and force estimation by conventional DOB. Therefore, my research proposes a friction-free DOB for force sensing operation and elimination of periodic disturbances in force estimation. To make the force observation design practical, the problem of noise in the measurement is taken into account. A Kalman filter is used for velocity estimation to reduce effects of noise on force estimation. The force-sensing bandwidth is significantly improved owing to the effective noise reduction by Kalman filter. Hence, using a friction-free DOB and a Kalman filter provides high performance force control system with friction-free and wideband force sensing.

c. High performance power assisted bilateral control system of different configurations based on friction-free force observer

The increasing of aging population in the world has led to an enormous demand for power assist devices that can enhance human ability to manipulate. Therefore, the proposed research constructs a bilateral control system with different mechanisms of the master and slave sides operating as a power assisted control system. The master device is a friction-less linear shaft motor while the slave device is a ball-screw system with high friction.

The proposed bilateral control is based on acceleration control and consists of a conventional disturbance observer and a friction-free disturbance observer for the master and slave, respectively. Although bilateral control of different mechanism is well research in literatures, there is no consideration for improving force sensation using dither technique and

friction-free DOB. The proposed bilateral control system offers the advantages of friction-free force observation, high transparency, ability to do tasks with heavy load on the slave side, and enhancement of the manual capability of the human operator as a power assisted device. Additionally, the friction-free DOB effectively suppresses the harmonic disturbances in the force estimation in both the master and slave.

d. FPGA-based controller

Since the force sensing bandwidth is inversely proportional to the sampling period of the control system. In order to increase the bandwidth of force sensation, a shortened sampling period is necessary. The feature of parallel processing enables FPGA to significantly shorten the sampling time of control algorithms. Therefore, in my research, all control algorithms are implemented in FPGA to improve the control performance. The shortened sampling time of control system is $5\,\mu s$.

1.3 Outline of the Thesis

The Thesis is organized in 6 chapters as follows:

Chapter 1 – Introduction. This chapter introduces the background and the objectives of the research. The outline of the Thesis is also briefly described in this chapter.

Chapter 2 – High performance force control based on FPGA. This chapter initially introduces the force sensing by conventional disturbance observer methods and the motion control system based on FPGA. After that, the research strategy as well as the breakthroughs that are developed and achieved during this research work are presented.

Chapter 3 – Wideband force sensing based on multi-sensor integration in Kalman-filter-based disturbance observer utilizing FPGA. This chapter describes the principles of the Kalman-filter-based disturbance observer using multi-sensor and clarifies the effectiveness of the proposed method through experimental results.

Chapter 4 – FPGA-based wideband force control system with friction-free and noise-free force observation. This chapter describes the principles and design method of the friction-free disturbance observer. The effectiveness of the friction-free DOB is verified by experimental results.

Chapter 5 – High performance power assisted bilateral control system of different configurations based on friction-free force observer. This chapter describes the principles of the proposed bilateral control system with different master and slave mechanism using the friction-free disturbance observer. The effectiveness of the proposed method is verified by experimental results.

Chapter 6 – Summary of the dissertation. This chapter presents the overall conclusions of this research work and describes the future developments of the research in motion copying system and system safety technology.

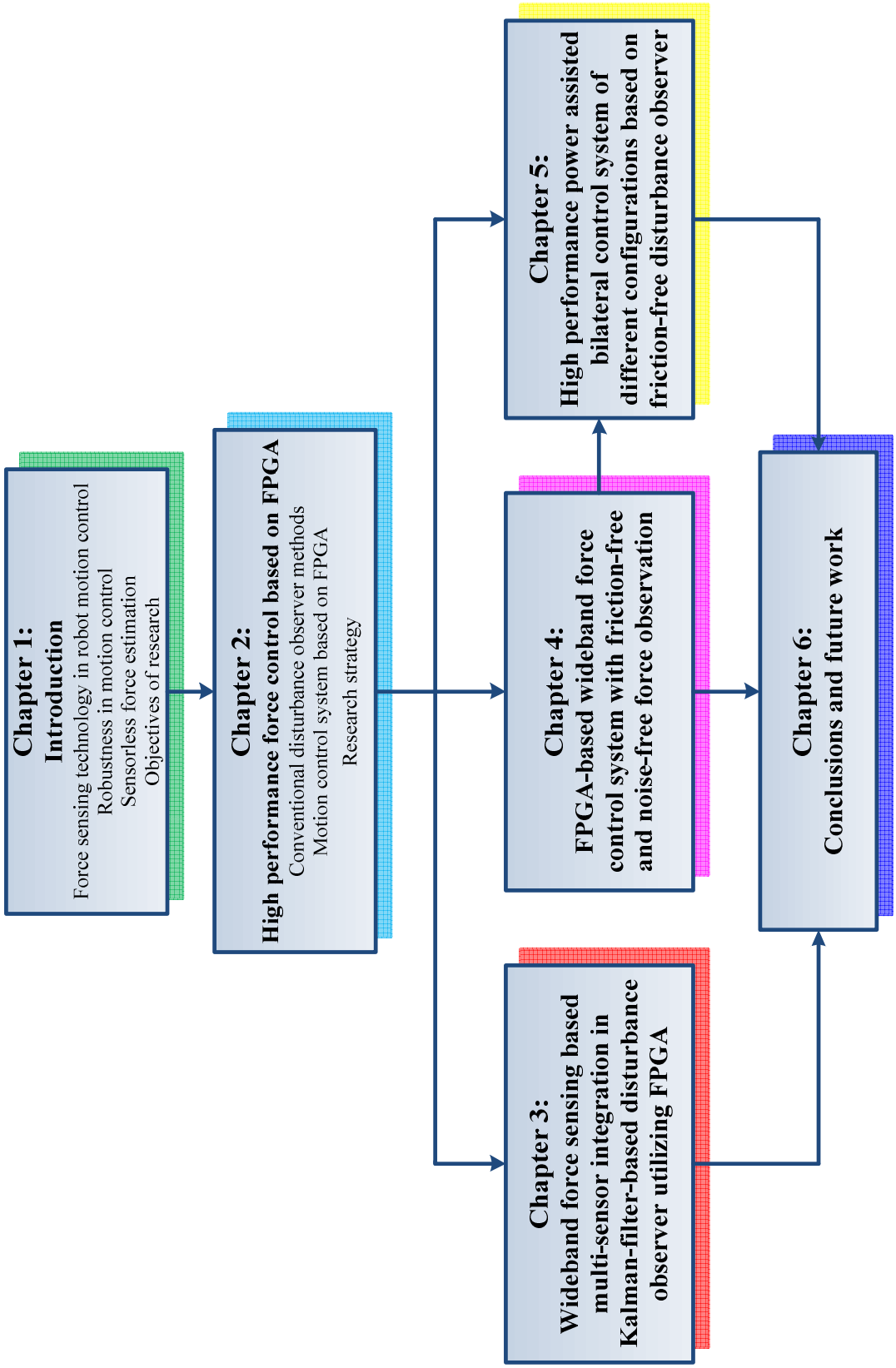

Fig. 1.1. Overview of the outline of the thesis

Chapter 2

High Performance Force Control Based on FPGA

This chapter initially introduces the force sensing by conventional disturbance observer methods and the motion control system based on FPGA. After that, the research strategy as well as the breakthroughs that are developed and achieved during this research work are presented.

2.1 Force Estimation by Conventional Disturbance Observer Methods

2.1.1 Position-sensor-based Disturbance Observer (PDOB)

In motion control system, servomechanism needs self-tuning to adjust dynamics and kinematics of the system. This self-tuning has to compensate effects of internal and external disturbances: model uncertainty, load, and friction for instances. Normally, the controlled system consists of a plant and a controller which is used to shape both transient and steady state responses of the controlled plant to the desired characteristics.

Recent force feedback control systems require the robustness to adapt to the variable stiffness of the environments. A disturbance observer is a solution to attain the robust acceleration control. The disturbance observer is a technique to estimate and compensate the disturbance force by identifying the total load force and the parameters of the motor inertia and force coefficient. Fig. 2.1 shows the block diagram of the position-sensor-based disturbance observer with a model of the linear motor. In Fig. 2.1, M denotes the mass of the motor, K_t denotes the force coefficient, I_m is the motor current, $x_m, \dot{x}_m$ and $\ddot{x}_m$ are the motor position, velocity and acceleration, respectively. F_g denotes the generated force and F_{dis} is the disturbance force.

The dynamic equation of the motor is expressed by (2.1).

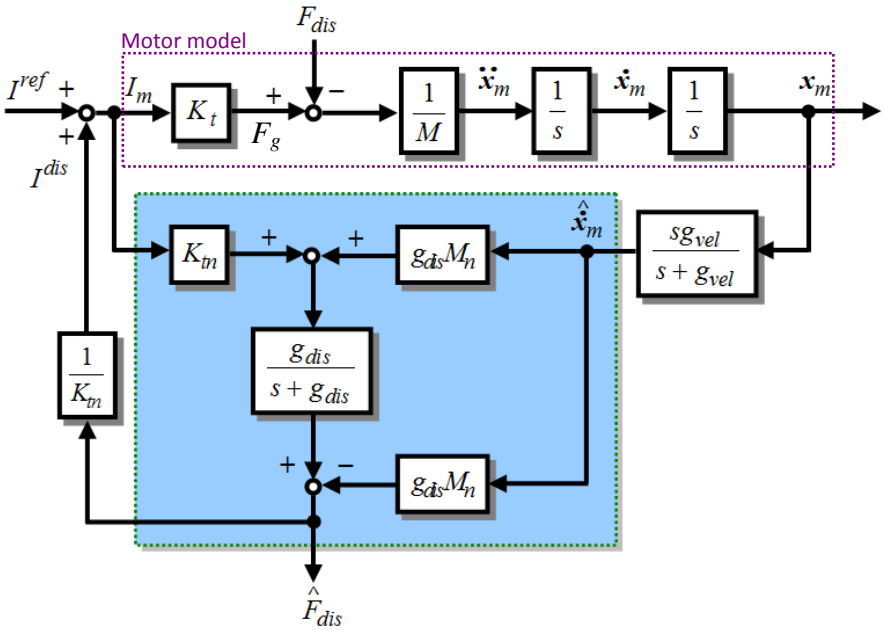

Fig. 2.1. Block diagram of the position-sensor-based disturbance observer

$$M\ddot{x} = F_g - F_{dis} \tag{2.1}$$

The total generated force is given simply as shown in (2.2).

$$F_g = K_t I_m \tag{2.2}$$

The disturbance force F_{dis} is defined as a summation of the external force, the friction force and the force caused by parameter variations, and is represented as shown in (2.3).

$$F_{dis} = F_{ext} + F_c + D\dot{x}_m + \Delta M\ddot{x}_m + \Delta K_t I_m \tag{2.3}$$

where F_{ext} denotes the external force, F_c denotes the Coulomb friction and $D\dot{x}_m$ denotes the viscous friction. $\Delta M\ddot{x}_m$ is the force caused by the self-mass variation. $\Delta K_t I_m$ is the force ripple due to the variation of the force coefficient. The disturbance observer obtains the disturbance force from the motor current and the second derivative of position signal, as expressed in (2.4).

$$F_{dis} = K_{tn} I_m - M_n \ddot{x}_m \tag{2.4}$$

where K_{tn} denotes the nominal force coefficient and M_n denotes the nominal mass. To suppress the high-frequency noise, the disturbance force is estimated through a first-order low-pass filter, and (2.4) is transformed into (2.5) as follows.

$$\hat{F}_{dis} = \frac{g_{dis}}{s + g_{dis}}(K_{tn} I_m + g_{dis} M_n \hat{\dot{x}}_m) - g_{dis} M_n \hat{\dot{x}}_m \tag{2.5}$$

$$= \frac{g_{dis}}{s + g_{dis}} F_{dis}$$

where g_{dis} is the cut-off frequency of the low-pass filter. It determines the bandwidth of the force sensing by disturbance observer. The compensation current for the disturbance force I^{dis} is calculated as follows.

$$I^{dis} = \frac{1}{K_{tn}} \hat{F}_{dis} \tag{2.6}$$

The robust acceleration control is achieved by feeding back the compensation current.

The disturbance torque estimated by (2.5) is used for a realization of robust motion control. The robust motion controller makes a motion system an acceleration control system, as shown in Fig. 2.2.

As shown in Fig. 2.2, the effect of the disturbance torque is represented as a transfer function $S_{(s)}$, which is defined as

$$S_{(s)} = \frac{s}{s + g_{dis}^{\#}} F_{dis} \tag{2.7}$$

$$g_{dis}^{\#} = \frac{K_t}{K_{tn}} \frac{M_n}{M} g_{dis} \tag{2.8}$$

$S_{(s)}$ represents a sensitivity showing how the disturbance force influences the motion system and is called a sensitivity function. As a result, the acceleration reference $\ddot{x}_m^{ref}$ is attainable within the bandwidth of the disturbance observer.

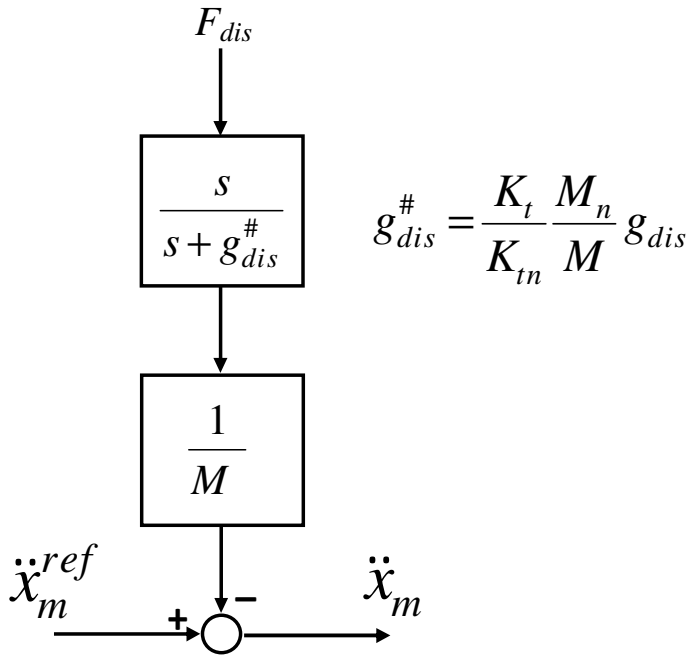

Fig. 2.2. Robust acceleration control system by the disturbance observer

In (2.5), the estimated disturbance force is dependent on the accuracy of velocity estimation. Commonly, the estimated velocity is obtained from the derivative of position signal with respect to time and high frequency noise is filtered out by a low-pass filter as shown in (2.9).

$$\hat{\dot{x}}_m = \frac{s g_{vel}}{s + g_{vel}} x_m \tag{2.9}$$

where g_{vel} denotes the cut-off frequency of the low-pass filter. The position information x_m is measured by a position sensor. However, with this method of velocity calculation, the accuracy of force estimation as well as the bandwidth of the position-sensor-based disturbance observer is limited by both the noise problem and the performance of measurement devices.

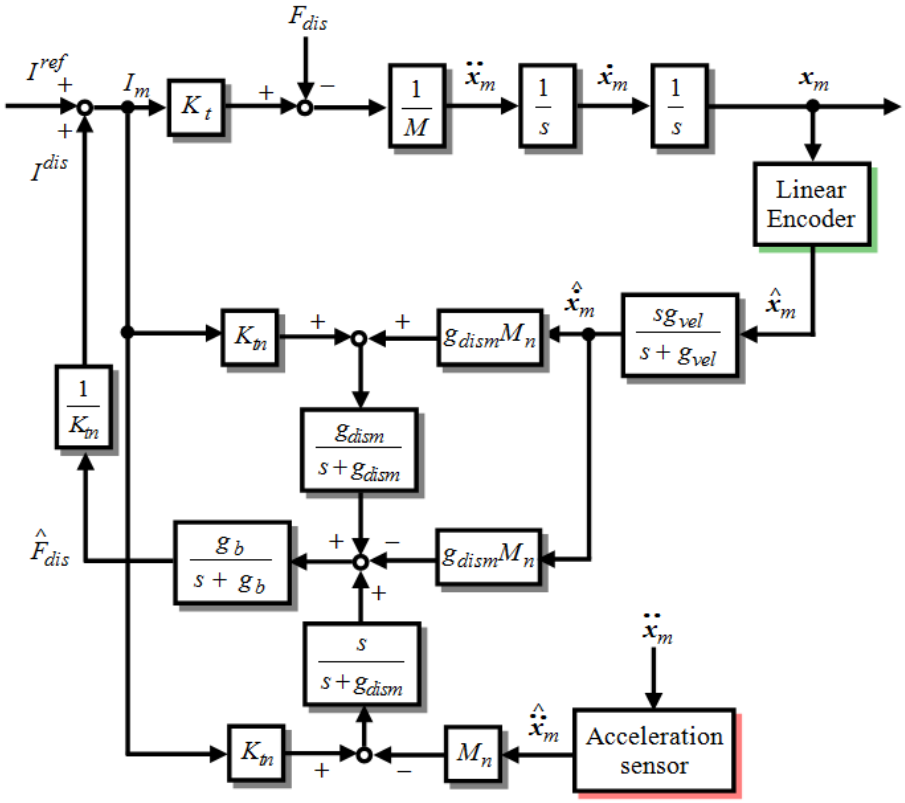

Fig. 2.3. Block diagram of PAIDO

2.1.2 Position-Acceleration Integrated Disturbance Observer (PAIDO)

In the position-sensor-based disturbance observer (PDOB) discussed in section 2.2.1, the bandwidth of force sensing is limited by both the derivative noise and the performance of measurement device. Another method named as position-acceleration integrated disturbance observer (PAIDO) was introduced to enhance the force estimation. The block diagram of PAIDO is shown in Fig. 2.3.

The PAIDO uses both the position sensor for the force estimation in the low frequency range determined by a low-pass filter and the acceleration sensor to obtain the force information in the high frequency range decided by a high-pass filter. The cut-off frequencies of the low-pass filter and the high-pass filter are set to the same value g_{dism} for enlargement

of the bandwidth. The bandwidth of the PAIDO is determined by the cut-off frequency g_b. The disturbance force is computed by using the following equation

$$\hat{F}_{dis} = \frac{g_b}{s+g_b}\left[\frac{g_{dism}}{s+g_{dism}}\left(K_{tn}I_m + g_{dism}M_n\hat{\dot{x}}_m\right) - g_{dism}M_n\hat{\dot{x}}_m + \frac{s}{s+g_{dism}}\left(K_{tn}I_m - M_n\hat{\ddot{x}}_m\right)\right] \quad (2.10)$$

In actual applications, this method has the drawback caused by the noise effect of the acceleration sensor. Therefore, the ability to widen the force sensing bandwidth of the PAIDO is also limited.

The next section shows the demonstrations of the force sensing performance of the two disturbance observers discussed above.

2.1.3 Demonstrations of Force Sensing Performance of PDOB and PAIDO

For evaluations of the two methods discussed above, Fig. 2.4 shows the force responses estimated by the PDOB and the PAIDO at the bandwidth of 6280 rad/s. These results are obtained by implementing both methods whose sampling time is 5 μs in FPGA. FPGA implementation and experimental set up will be discussed in section 3.4. The cut-off frequency of velocity estimation in the PDOB (g_{vel}) is also set to 6280 rad/s. The cut-off frequencies of the low-pass filter, the high-pass filter and the velocity estimation in the PAIDO (g_{dism} and g_{vel}) are set to 1000 rad/s.

Fig. 2.4(a) shows that the force response estimated by the PDOB is totally corrupted by the peak-to-peak noise level of 0.9 N at the bandwidth of 6280 rad/s.

In Fig. 2.4 (b), the force response is improved by the PAIDO with the noise level of 0.25N. However, with the PAIDO, the acceleration signal is directly used for the force sensing algorithm. This is the drawback of the PAIDO since the acceleration sensor has a high sensitivity to noise. Therefore, it is impossible for the PAIDO to further increase the bandwidth of force sensing.

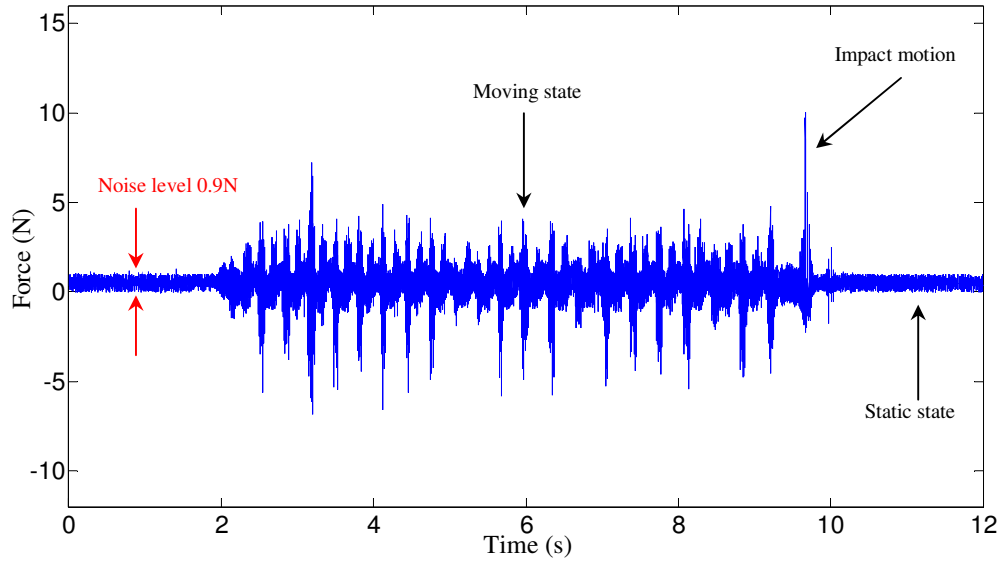

(a) Estimated by PDOB

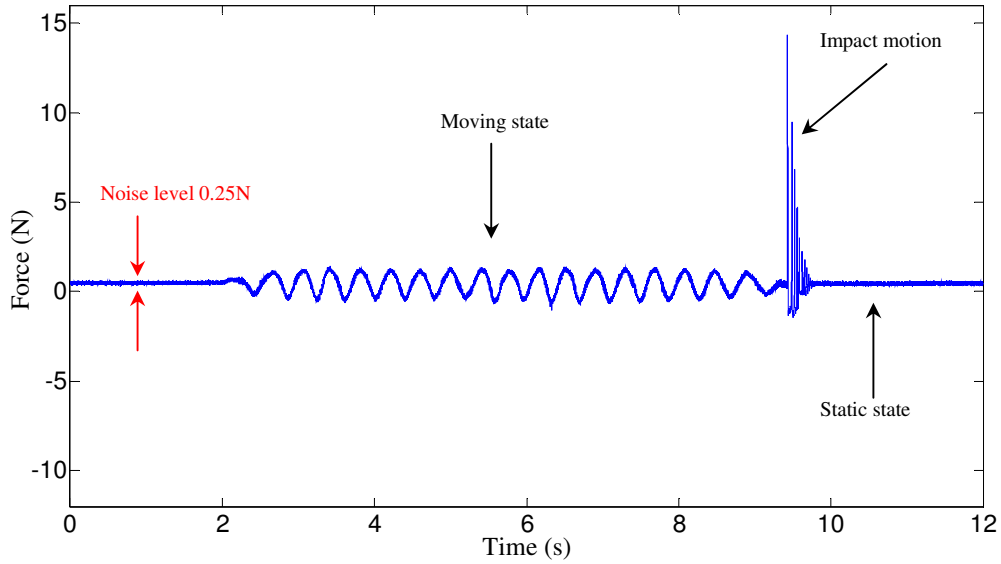

(b) Estimated by PAIDO

Fig. 2.4. Force responses at the force sensing bandwidth of 6280 rad/s

Since the purpose of this research is to further broaden the force sensing bandwidth up to 62800 rad/s (≈10 kHz), the PDOB and the PAIDO cannot satisfy this performance. Therefore, this research proposes a Kalman-filer-based disturbance observer with multi-sensor implemented in FPGA to attain the wideband force sensing as well as the high performance force estimation.

The advantages of FPGA based controller and the strategy of the research to achieve the research objectives are discussed in sections 2.2 and 2.3.

2.2 Motion Control System Based on FPGA

In advanced mechatronics and digital control, FPGA-based systems on a chip (SoCs) promise to succeed older technologies, such as microcontrollers and DSPs. The use of advanced control algorithms depends upon being able to perform complex calculations within demanding timing constraints, where system dynamics can require feedback response in as short as several of microseconds. Developing and implementing such capable feedback controllers is currently a hard goal to achieve for systems based on CPU or DSP, and there is much technological challenge in making it more affordable.

Owing to the major technological breakthroughs in recent years, and the sustained rapid progress in the fields of very large scale integration (VLSI) and electronic design automation, FPGA devices have reached a level of development that puts them on the edge of microelectronics fabrication technology advancements. FPGAs provide many advantages with respect to their non-reconfigurable counterparts such as the general purpose microprocessors and DSP processors. Taking advantage of hardware parallelism, FPGAs exceed the computing power of CPU and DSP by breaking the paradigm of sequential execution and accomplishing more per clock cycle. FPGA technology offers flexibility and rapid prototyping capabilities in the face of increased time-to-market concerns. In fact, FPGA-based systems achieve better performance-cost compromise, and with a moderate design effort they can afford the implementation of a powerful and flexible embedded system.

Exploiting the FPGA technology benefits for industrial control systems has been the source of intensive research during last decade in order to boost their control performances [57-60]. Important and constant improvement in FPGA devices, synthesis, place-and-route tools, and debug capabilities has made FPGA prototyping more available and practical to ASIC/SoC designers than ever before. Consequently, FPGA-based prototypes can be efficiently implemented for motion control applications to achieve improved performance of the advanced control algorithms through high sampling period, short-design cycles, simple simulation, and rapid verification.

2.3 Research Strategy

In order to reach the goal of this research on achieving high-performance robot motion control based on the superior *wideband, friction-free and noise-free* force sensing, the following research strategy as well as the breakthroughs are developed and achieved during this research work.

Wideband force sensing based on Kalman-filter-based disturbance observer with multi sensors:

Because the force sensing bandwidth of the conventional force estimation method by the disturbance observers (DOBs), which are described in section 2.1, is limited by the noise problem, this research proposed the force sensing by the Kalman-filter-based disturbance observer. The Kalman filter brings up the effective noise suppression in force estimation. Therefore, the combination of Kalman filter and disturbance observer provides a wider bandwidth of force sensing.

Besides, the Kalman-filter-based disturbance observer is constructed with multi sensors to improve the force sensing performance. With the single-sensor-based DOB, the force sensing performance and frequency bandwidth of are also limited by the position sensor. Therefore, the proposed method introduces the development of the DOB by combining the multi-sensor fusion in Kalman-filter to obtain the high performance force sensing. The use of multiple types of sensors increases the accuracy with which a quantity can be observed and characterized. Thus, the proposed method employs the Kalman-filter data fusion algorithm for a linear encoder and an acceleration sensor. The Kalman-filter-based DOB with multi-sensor fusion achieves the significant noise reduction, highly accurate force information and wider bandwidth of force sensing.

Furthermore, the possibility of increasing the force sensing bandwidth is also dependent on the sampling period of the control system. In order to increase the bandwidth of force sensation, a shortened sampling period is necessary. Conventionally, motion controllers are implemented in CPU or DSP that cannot achieve the fast sampling period of several micro seconds. On the other hand, the FPGAs have more advantages in performance compared to the conventional CPU and DSP as shown in section 2.2. The feature of parallel processing

enables FPGA to significantly shorten the sampling time of control algorithms. Therefore, in this research, all control algorithms are implemented in FPGA to achieve the shortened sampling time of $5\,\mu s$ that enables widening force sensing bandwidth and ensures the high performance of control system when the control algorithm is highly complex.

Using the proposed method, the force sensing bandwidth is widened to 10 kHz. This bandwidth is superior to human bandwidth of tactile sensation (400 Hz). It is useful for human-robot interaction and haptics applications (such as human interfaces, haptic devices, surgical robots, surgical tele-operation, exercise robots) to achieve the high efficiency in haptic information reproduction and transmission with the attained wideband force sensing.

Wideband, friction-free and noise-free force sensing based on friction-free disturbance observer and Kalman filter:

The development of force sensing method in this research is also focuses on improving the force sensing performance by reducing the effect of friction as well widening the force sensing bandwidth. To deal with the effect of friction, a novel force sensing method named as friction-free disturbance observer is proposed. The friction compensation method is inspired by the dithering method's simplicity of implementation. Thus, a periodic signal is inserted into the control signal to reduce the effect of friction on force estimation. The effect of the dither signal is the ability to smooth the discontinuity of friction. The disadvantage of the dithering method is that it generates an oscillatory disturbance that can affect the performance of the control system. The proposed friction-free disturbance observer is designed for force sensing operation and elimination of periodic disturbance in force estimation.

To increase the force sensing bandwidth, the problem of noise in the measurement is taken into account. A Kalman filter is used in combination with the friction-free disturbance observer to reduce the effect of noise on the force estimation. The force-sensing bandwidth is significantly improved owing to the effective noise reduction by Kalman filter. The influence of the periodic signal on force estimation is effectively rejected by the friction-free disturbance observer. The proposed method attains effective friction reduction in force estimation and a wider force sensing bandwidth of 1000 rad/s. The proposed method is useful

for sensor-less force control applications such as robots, machine tools, power assisted devices and bilateral control systems.

Moreover, all control algorithms are also implemented in FPGA to achieve the shortened sampling time of $5\,\mu s$ that enables widening force sensing bandwidth and ensures the high performance of control system when the control algorithm is highly complex.

Power assisted bilateral control system of different mechanism based on friction-free disturbance observer:

Based on the development of this research on force sensing methodology described in the previous paragraphs, this research also presents a new force sensing approach based on the friction-free disturbance observer to improve the performance of a bilateral control system with different mechanisms of the master and the slave operating as a power assisted control system. The master device is a friction-less linear shaft motor while the slave device is a ball-screw system with high friction.

In a bilateral control system, human operator manipulates the master to assign tasks to the slave. The slave senses the interaction force with the environment and transmits force to the master so that the operator can perceive the task operation as if he directly contacts the remote environment. To achieve high transparency, robustness, and contact stability of control system, the proposed bilateral control is based on acceleration control, consisting of a conventional DOB for force sensation on the master, and a friction-free DOB for force sensation on the slave. Although bilateral control of different mechanism is well research in literatures, there is no consideration for improving force sensation using dither technique and friction-free DOB.

Using the proposed method, the oscillatory disturbance in the force responses is reduced effectively on both master and slave sides; the good tracking in the position and force responses of the master and the slave devices is achieved, even when the mechanisms of the master and the slave are different; the human operator is assisted to manipulate the device with a small operational force, while still perceiving the impedance of the remote environment. Additionally, the friction-free DOB effectively suppresses the harmonic

disturbances in the force estimation in both the master and slave. The proposed method is feasible for application to human assist systems or in industrial applications.

FPGA implementation is always employed for all control algorithms to achieve the very high sampling rate of the control cycle of 5 μs that enables widening force sensing bandwidth and ensures the high performance of control system when the control algorithm is highly complex.

Chapter 3

Wideband Force Sensing Based on Multi-Sensor Integration in Kalman-Filter-Based Disturbance Observer Utilizing FPGA

3.1 Introduction

Force sensation plays an important role in force control systems. The bandwidth of force sensing is vital to reproduce the vivid force information. Generally, sensor-less force control systems use the position-sensor-based disturbance observer for force estimation. The bandwidth of force sensation as well as the control performance, however, is limited by the noise problems. This research proposes a method to achieve the high performance force control based on wideband force sensing. In the research, the force estimation operation is performed by a combination of a Kalman-filter with multi-sensor and a disturbance observer implemented in a field programmable gate array (FPGA). The wide bandwidth force sensing is attained owing to the shortened sampling time by FPGA. Moreover, the noise in the force information is suppressed effectively by the Kalman-filter. The experimental results show the viability of the proposed method.

3.2 The Kalman-filter Theory

3.2.1 The Kalman-filter Concept

The Kalman-filter is named after Rudolph E. Kalman, who in 1960 published his famous paper describing a recursive solution to the discrete-data linear filtering problem [61].

The Kalman-filter is essentially a set of mathematical equations that implement a predictor-corrector type estimator that is optimal in the sense that it minimizes the estimated error covariance. Since being introduced, the Kalman-filter has been the subject of extensive research and application, particularly in the area of autonomous or assisted navigation. The filter is very powerful in several aspects: it supports estimations of past, present, and even future states, and it can do so even when the precise nature of the modeled system is unknown.

Theoretically, a Kalman-filter is an estimator for what is called the linear-quadratic problem, which is the problem of estimating the instantaneous "state" of a linear dynamic system perturbed by white noise, by using measurements linearly related to the state but corrupted by white noise. The resulting estimator is statistically optimal with respect to any quadratic function of estimation error.

Originally, a filter solves the problem of separating unwanted components of mixtures. In other word, the filter preferentially attenuates unwanted frequencies of signals that are mixtures of different frequency components. However, with Kalman filtering the term "filter" assumes a meaning that is well beyond the original idea of separation of the components of a mixture. It has also come to include the solution of an inversion problem, in which one knows how to represent the measurable variables as functions of the variables of principle interest. In essence, it inverts this functional relationship and estimates the independent variables as inverted functions of the dependent (measurable) variables. These variables of interest are also allowed to be dynamic, with dynamics that are only partially predictable.

The mathematical foundations of the Kalman-filter are consisted of Least squares, Probability theory, Dynamic systems, Least mean squares and Stochastic systems. The Kalman filtering is itself a part of the foundations of another discipline, modern control theory, and a proper subset of statistical decision theory.

3.2.2 The Model of The Process to be Estimated by Kalman filter

The Kalman-filter addresses the general problem of trying to estimate the state $x \in \Re^n$ of a discrete-time controlled process that is governed by the following equation

$$x_k = Ax_{k-1} + Bu_{k-1} + w_{k-1} \tag{3.1}$$

with a measurement $z \in \Re^m$

$$z_k = Hx_k + v_k \tag{3.2}$$

The random variables w_k and v_k represent the process noise and measurement noise, respectively. They are assumed to be independent of each other, white, and with normal probability distributions

$$p(w) \sim N(0, Q) \tag{3.3}$$

$$p(v) \sim N(0, R) \tag{3.4}$$

Q is the process noise covariance matrix and R is the measurement noise covariance matrix. In practice, Q and R matrices might change with each time step or measurement, however here they are assumed to be constant.

The $n \times n$ matrix A in the equation (3.1) relates the state at the previous time step *k-1* to the state at the current step *k*, in the absence of either a driving function or process noise. The $n \times l$ matrix B relates the optional control input $u \in \Re^l$ to the state x. The $m \times n$ matrix H in the measurement equation (3.2) relates the state to the measurement z_k. In practice A and H might change with each time step or measurement, but here they are assumed to be constant.

3.2.3 The Derivation of The Kalman-filter Equations

We define $\hat{x}_{k-1} \in \Re^n$ to be a prior state estimate at step k given knowledge of the process prior to step k, and $\hat{x}_k \in \Re^n$ to be a posterior state estimate at step k given measurement z_k. We can then define a prior and a posterior estimate errors as

$$e_{k-1} \equiv x_k - \hat{x}_{k-1} \tag{3.5}$$

and $$e_k \equiv x_k - \hat{x}_k \tag{3.6}$$

Then the prior estimate error covariance is

$$P_{k-1} = E\left[e_{k-1} e_{k-1}^T \right] \tag{3.7}$$

and the posterior estimate error covariance is

$$P_k = E\left[e_k e_k^T \right] \tag{3.8}$$

To derive the equations for the Kalman-filter, we begin with the goal of finding an equation that computes a posterior state estimate $\hat{x}_k$ as a linear combination of a prior estimate $\hat{x}_{k-1}$ and a weighted difference between an actual measurement z_k and a measurement prediction $H\hat{x}_{k-1}$ as shown in equation (3.9).

$$\hat{x}_k = \hat{x}_{k-1} + K(z_k - H\hat{x}_{k-1}) \tag{3.9}$$

The difference $(z_k - H\hat{x}_{k-1})$ in (3.9) is called the measurement innovation, or the residual. The residual reflects the variance between the predicted measurement $H\hat{x}_{k-1}$ and the actual measurement z_k. A residual of zero means that the two are in complete agreement.

The $n \times m$ matrix K in (3.9) is chosen to be the gain or blending factor that minimizes the posterior error covariance in (3.8).

The derivation of the Kalman-filter's mathematical equations can be accomplished by the following steps:

The optimal linear estimate is equivalent to the general (nonlinear) optimal estimator if the variants x and z are jointly Gaussian. Therefore, it suffices to seek an updated estimate $\hat{x}_k$ based on the observation z_k, which is a linear function of the prior estimate and the measurement z:

$$\hat{x}_k = K_k^1 \hat{x}_{k-1} + K_k z_k \tag{3.10}$$

The matrices K_k^1 and K_k are as yet unknown. We seek those values of K_k^1 and K_k such that the new estimate $\hat{x}_k$ will satisfy the orthogonality principle. This orthogonality condition can be written in the form

$$E\left\langle \left[x_k - \hat{x}_k \right] z_i^T \right\rangle = 0, \qquad i = 1, 2, \ldots, k\text{-}1 \tag{3.11}$$

$$E\left\langle \left[x_k - \hat{x}_k \right] z_k^T \right\rangle = 0 \tag{3.12}$$

If we substitute the formula for x_k from (3.1) and for $\hat{x}_k$ from (3.10) into (3.11), then we will observe from (3.1) and (3.2) that the data $z_1, \ldots, z_k$ do not involve the noise term w_k. Therefore, because the random sequences w_k and v_k are uncorrelated, it follows that $E w_k z_i^T = 0$ for $1 \le i \le k$.

Using this result, we can obtain the following relation:

$$E\left[\left\langle A_{k-1} x_{k-1} + w_{k-1} - K_k^1 \hat{x}_{k-1} - K_k z_k \right\rangle z_i^T \right] = 0, \quad i = 1, 2, \ldots, k\text{-}1 \tag{3.13}$$

But because $z_k = H x_k + v_k$, (3.13) can be rewritten as

$$E\left[A_{k-1} x_{k-1} - K_k^1 \hat{x}_{k-1} - K_k H_k x_k - K_k v_k \right] z_i^T = 0, \; i = 1, 2, \ldots, k\text{-}1 \tag{3.14}$$

We also know that (3.11) and (3.12) hold at the previous step, that is,

$$E\left\langle \left[x_{k-1} - \hat{x}_{k-1} \right] z_i^T \right\rangle = 0, \qquad i = 1, 2, \ldots, k\text{-}1 \tag{3.15}$$

and

$$E\left\langle v_k z_i^T \right\rangle = 0, \qquad i = 1, 2, \ldots, k\text{-}1 \tag{3.16}$$

Then (3.14) can be reduced to the form

$$A_{k-1}Ex_{k-1}z_i^T - K_k^1 E\hat{x}_{k-1}z_i^T - K_k H_k A_{k-1}E x_{k-1} z_i^T - K_k E v_k z_i^T = 0$$

$$A_{k-1}Ex_{k-1}z_i^T - K_k^1 E\hat{x}_{k-1}z_i^T - K_k H_k A_{k-1}E x_{k-1} z_i^T = 0$$

$$E\left\langle \left[x_k - K_k H_k x_k - K_k^1 x_k \right] - K_k^1 \left(\hat{x}_{k-1} - x_k \right) \right\rangle z_i^T = 0$$

$$\left[I - K_k^1 - K_k H_k \right] E x_k z_i^T = 0 \tag{3.17}$$

(3.17) can be satisfied for any given x_k if

$$K_k^1 = I - K_k H_k \tag{3.18}$$

Clearly, this choice of K_k^1 causes (3.10) to satisfy a portion of the condition given by (3.11). The choice of K_k is such that (3.12) is satisfied.

Let the errors

$$e_k \triangleq \hat{x}_k - x_k \tag{3.19}$$

$$e_{k-1} \triangleq \hat{x}_{k-1} - x_k \tag{3.20}$$

$$e_{z_k} \triangleq \hat{z}_{k-1} - z_k = H_k \hat{x}_{k-1} - z_k \tag{3.21}$$

The parameter $\hat{x}_k$ depends linearly on x_k, which depends linearly on z_k. Therefore, from (3.12)

$$E\left[x_k - \hat{x}_k \right] z_{k-1}^T = 0 \tag{3.22}$$

and also (by subtracting (3.12) from (3.22)

$$E\left[x_k - \hat{x}_k \right] e_{z_k}^T = 0 \tag{3.23}$$

Substitute for x_k , $\hat{x}_k$ and e_{z_k} from (3.1), (3.10) and (3.21), respectively. Then

$$E\left[A_{k-1}x_{k-1} + w_{k-1} - K_k^1 \hat{x}_{k-1} - K_k z_k \right]\left[H_k \hat{x}_{k-1} - z_k \right]^T = 0 \tag{3.24}$$

However, by the system structure

$$E w_k z_k^T = E w_k \hat{x}_k^T = 0 \tag{3.25}$$

$$E\left[A_{k-1}x_{k-1} - K_k^1 \hat{x}_{k-1} - K_k z_k \right]\left[H_k \hat{x}_{k-1} - z_k \right]^T = 0 \tag{3.26}$$

Substituting for K_k^1 , z_k and e_{k-1} and using the fact that $E e_{k-1} v_k^T = 0$, this last result can be modified as follows:

$$\begin{aligned} 0 &= E\left\langle \left[A_{k-1}x_{k-1} - \hat{x}_{k-1} + K_k H_k \hat{x}_{k-1} - K_k H_k x_k - K_k v_k \right]\left[H_k \hat{x}_{k-1} - H_k x_k - v_k \right]^T \right\rangle \\ &= E\left\langle \left[\left(x_k - \hat{x}_{k-1} \right) - K_k H_k \left(x_k - \hat{x}_{k-1} \right) - K_k v_k \right]\left[H_k e_{k-1} - v_k \right]^T \right\rangle \\ &= E\left\langle \left[-e_{k-1} + K_k H_k e_{k-1} - K_k v_k \right]\left[H_k e_{k-1} - v_k \right]^T \right\rangle \end{aligned} \tag{3.27}$$

By definition, the prior covariance (the error covariance matrix before the update) is

$$P_{k-1} = E\left[e_{k-1} e_{k-1}^T \right]$$

It satisfies the equation

$$\left[I - K_k H_k \right] P_{k-1} H_k^T - K_k R_k = 0$$

and therefore, the gain can be expressed as

$$K_k = P_{k-1} H_k^T \left[H_k P_{k-1} H_k^T + R_k \right]^{-1} \tag{3.28}$$

which is the solution we seek for the gain as a function of the prior covariance.

We can derive a similar formula for the posterior covariance (the error covariance matrix after update), which is defined as

$$P_k = E\left[e_k e_k^T \right] \tag{3.29}$$

By substituting (3.18) into (3.10), we obtain the equations

$$\hat{x}_k = \left(I - K_k H_k \right) \hat{x}_{k-1} + K_k z_k$$

$$\hat{x}_k = \hat{x}_{k-1} + K_k \left(z_k - H_k \hat{x}_{k-1} \right) \tag{3.30}$$

Subtract x_k from both sides of the latter equation to obtain the equations

$$\hat{x}_k - x_k = \hat{x}_{k-1} + K_k H_k x_k + K_k v_k - K_k H_k \hat{x}_{k-1} - x_k$$

$$e_k = e_{k-1} - K_k H_k e_{k-1} + K_k v_k$$

$$e_k = \left(I - K_k H_k \right) e_{k-1} + K_k v_k \tag{3.31}$$

By substituting (3.31) into (3.29) and noting that $E e_{k-1} v_k^T = 0$, we obtain

$$P_k = E\left\{ \left[I - K_k H_k \right] e_{k-1} e_{k-1}^T \left[I - K_k H_k \right]^T + K_k v_k v_k^T K_k^T \right\}$$

$$= \left(I - K_k H_k \right) P_{k-1} \left(I - K_k H_k \right)^T + K_k R_k K_k^T \tag{3.32}$$

This last equation is the so-called "Joseph form" of the covariance update equation. By substituting for K_k from (3.28), it can be put into the following forms:

$$P_k = P_{k-1} - K_k H_k P_{k-1} - P_{k-1} H_k^T K_k^T + K_k H_k P_{k-1} H_k^T K_k^T + K_k R_k K_k^T$$

$$= \left(I - K_k H_k \right) P_{k-1} - P_{k-1} H_k^T \underbrace{K_k^T + K_k \left(H_k P_{k-1} H_k^T + R_k \right)}_{P_{k-1} H_k^T} K_k^T$$

$$= \left(I - K_k H_k \right) P_{k-1} \tag{3.33}$$

The last of which is the one most often used in computation. This implements the effect that conditioning on the measurement has on the covariance matrix of estimation uncertainty.

Error covariance extrapolation models the effects of time on the covariance matrix of estimation uncertainty, which is reflected in the prior values of the covariance and state estimates,

$$P_{k-1} = E\left[e_{k-1} e_{k-1}^T \right]$$

$$\hat{x}_{(k/k-1)} = A_{k-1} \hat{x}_{(k-1/k-1)} \tag{3.34}$$

Subtract x_k from both sides of the last equation to obtain the equations

$$\hat{x}_{(k/k-1)} - x_k = A_{k-1} \hat{x}_{(k-1/k-1)} - x_k$$

$$e_{k-1} = A_{k-1} \left[\hat{x}_{(k-1/k-1)} - x_{(k-1/k-1)} \right] - w_{k-1}$$

$$= A_{k-1} e_{(k-1/k-1)} - w_{k-1}$$

for the propagation of the estimation error. Postmultiply it by e_{k-1}^T (on both sides of the equation) and take the expected values. Use the fact that $E e_{k-1} w_{k-1}^T = 0$ to obtain the results

$$P_{(k/k-1)} = E\left[e_{k-1} e_{k-1}^T \right]$$

$$= A_{k-1} E\left[e_{(k-1/k-1)} e_{(k-1/k-1)}^T \right] A_{k-1}^T + E\left[w_{k-1} w_{k-1}^T \right]$$

$$= A_{k-1} P_{(k-1/k-1)} A_{k-1}^T + Q_{k-1} \tag{3.35}$$

which gives the prior value of the covariance matrix of estimation uncertainty as a function of the previous posterior value.

The equation for computing the Kalman gain (3.28) can be rewritten in the following form:

$$K_k = P_{k-1}H^T(HP_{k-1}H^T + R)^{-1}$$

$$= \frac{P_{k-1}H^T}{HP_{k-1}H^T + R} \tag{3.36}$$

In equation (3.36), when the measurement error covariance R approaches zero, the gain K weights the residual more heavily:

$$\lim_{R_k \to 0} K_k = H^{-1} \tag{3.37}$$

On the other hand, when the prior estimate covariance P_{k-1} approaches zero, the gain K weights the residual less heavily:

$$\lim_{P_{k-1} \to 0} K_k = 0 \tag{3.38}$$

The concept of the weighting by gain K can be rephrased in another way: When the measurement error covariance R approaches zero, the actual measurement z_k is "trusted" more and more, while the predicted measurement $H\hat{x}_{k-1}$ is trusted less and less. In contrast, when the prior estimate error covariance P_{k-1} approaches zero, the actual measurement z_k is trusted less and less, while the predicted measurement $H\hat{x}_{k-1}$ is trusted more and more.

3.3 Force Sensing Using Kalman-Filter-Based Disturbance Observer with Multi Sensors

3.3.1 Kalman-Filter Implementation with Multi Sensors for Velocity Estimation

Since the performance of force sensing by disturbance observer is related to how the velocity is precisely estimated in all speed ranges, in this research, a Kalman-filter using multi-sensor integration is employed to obtain the accurate velocity estimation.

The Kalman-filter estimates the state of the multi-sensor measuring process that is formulated in the following equations

$$\boldsymbol{x}_{(k+1)} = \boldsymbol{A}\boldsymbol{x}_{(k)} + \boldsymbol{B}\boldsymbol{u}_{(k)} + \boldsymbol{w}_{(k)} \tag{3.39}$$

$$\boldsymbol{z}_{(k)} = \boldsymbol{H}\boldsymbol{x}_{(k)} + \boldsymbol{v}_{(k)} \tag{3.40}$$

where k refers to the sampling time index, $\boldsymbol{x}_{(k)}$ is the state vector, $\boldsymbol{z}_{(k)}$ is the measurement vector and $\boldsymbol{u}_{(k)}$ is the control input vector. The random variables $\boldsymbol{w}_{(k)}$ and $\boldsymbol{v}_{(k)}$ represent the process noise and the measurement noise, respectively. The matrix $\boldsymbol{A}$ relates the state at the previous sampling time to the state at the current sampling time, the matrix $\boldsymbol{B}$ relates the optional control input $\boldsymbol{u}$ to the state $\boldsymbol{x}$, and the matrix $\boldsymbol{H}$ relates the state $\boldsymbol{x}$ to the measurement $\boldsymbol{z}$.

Commonly, the Kalman-filter is used to estimate the velocity based on the model shown by (3.39) and (3.40), in which the observed state variable $\boldsymbol{x}_{(k)}$ includes position and velocity while acceleration is used as a known input variable to the system $\boldsymbol{u}_{(k)}$ and can be measured by an acceleration sensor; the system output variable $\boldsymbol{z}_{(k)}$ is only the measured position. According to this common state space representation, the values of position and velocity depend on the accuracy of the measured acceleration. However, as the acceleration sensor has the high sensitivity to noise, the state estimation is also affected by this noise problem.

For the above reason, in the proposed method, acceleration is introduced as an observed state variable (not a system input variable) together with position and velocity. When acceleration is the state variable to be estimated by Kalman-filter, the noise in the

acceleration information is reduced. Therefore, when the estimated acceleration is applied in the state estimation, the estimation accuracy is improved. The discrete state matrices then are given as shown in (3.41).

$$\boldsymbol{A}=\begin{bmatrix}1 & T_s & 0.5T_s^2\\ 0 & 1 & T_s\\ 0 & 0 & 1\end{bmatrix},\ \boldsymbol{B}=\begin{bmatrix}0\\0\\0\end{bmatrix},\ \boldsymbol{H}=\begin{bmatrix}1 & 0 & 0\\ 0 & 0 & 1\end{bmatrix} \tag{3.41}$$

where T_s is the sampling time of the control system.

Additionally, in the proposed method, both acceleration and position are used as the measured state variables for enlarging the bandwidth of the measurement system. The system output $\boldsymbol{z}_{(k)}$ includes position measured by an encoder and acceleration measured by an acceleration sensor. On condition of only position measurement, due to the bandwidth limitation of measurement device, the imprecise velocity estimation often occurs during the impact motions with high accelerations. Generally, the bandwidth of an acceleration sensor covers from 1Hz to more than 10 kHz without DC range. In order to cover the DC range, the measurement information is obtained by a position sensor. Acceleration measurement contributes primarily to the accurate velocity acquisition during the impact motions. Therefore, the Kalman-filter using multi-sensor can provide the accurate velocity estimation and the effective noise suppression. With the improved velocity information, it is possible for the disturbance observer to attain the high performance force sensing. When the sampling rate is sufficiently high, a wide bandwidth force sensing is achieved.

In the state space representation shown in (3.39) and (3.40), both the process noise $\boldsymbol{w}_{(k)}$ and the measurement noise $\boldsymbol{v}_{(k)}$ are assumed to be uncorrelated zero-mean Gaussian white noise with the covariance matrix of process noise $\boldsymbol{Q}$ and the covariance matrix of measurement noise $\boldsymbol{R}$. The covariance matrices $\boldsymbol{Q}$ and $\boldsymbol{R}$ are defined as:

$$\boldsymbol{Q}=E\left[ww^T\right] \tag{3.42}$$

$$\boldsymbol{R}=E\left[vv^T\right] \tag{3.43}$$

in which $\boldsymbol{Q}$ and $\boldsymbol{R}$ are the nonnegative definite matrices, and $E[\ ]$ denotes the expected value.

The values of $\boldsymbol{Q}$ and $\boldsymbol{R}$ are used for tuning the accuracy of the filter and can be determined by using the testing simulations of the measurement sensor signals, which are based on the actual experimental data. The susceptibility of the Kalman-filter to the measurement noise depends on the process noise covariance matrix $\boldsymbol{Q}$ and the measurement noise covariance matrix $\boldsymbol{R}$.

Fig. 3.1 shows the algorithm of the Kalman-filter. The Kalman-filter uses the form of feedback control to estimate the state $\boldsymbol{x}$. The filter estimates the state ahead in time and then obtains the feedback in the form of measurements corrupted by noise. The current state and the estimation error are projected forward in time by the predictor equations as shown in the following equations.

$$\boldsymbol{x}_{(k|k-1)} = \boldsymbol{A}\boldsymbol{x}_{(k-1|k-1)} + \boldsymbol{B}\boldsymbol{u}_{(k-1)} \tag{3.44}$$

$$\boldsymbol{P}_{(k|k-1)} = \boldsymbol{A}\boldsymbol{P}_{(k-1|k-1)}\boldsymbol{A}^{T} + \boldsymbol{Q} \tag{3.45}$$

where $\boldsymbol{P}$ is the estimate error covariance matrix derived from the variance between the predicted state estimation and the improved state estimation. The Kalman-filter gain matrix $\boldsymbol{K}$, which is based on the total uncertainty measurement, is computed to minimize the error covariance using the following equation.

$$\boldsymbol{K}_{(k)} = \boldsymbol{P}_{(k|k-1)}\boldsymbol{H}^{T}(\boldsymbol{H}\boldsymbol{P}_{(k|k-1)}\boldsymbol{H}^{T} + \boldsymbol{R})^{-1} \tag{3.46}$$

The next step is to update the prior state estimation and the prior error covariance. The actual measurement $\boldsymbol{z}_{(k)}$ provided by position sensor and acceleration sensor at every sampling time is incorporated into the previous estimations to obtain the improved estimates using the corrector equations as follows.

$$\boldsymbol{x}_{(k|k)} = \boldsymbol{x}_{(k|k-1)} + \boldsymbol{K}_{(k)}(z_{(k)} - \boldsymbol{H}\boldsymbol{x}_{(k|k-1)}) \tag{3.47}$$

$$\boldsymbol{P}_{(k|k)} = \boldsymbol{P}_{(k|k-1)} - \boldsymbol{K}_{(k)}\boldsymbol{H}\boldsymbol{P}_{(k|k-1)} \tag{3.48}$$

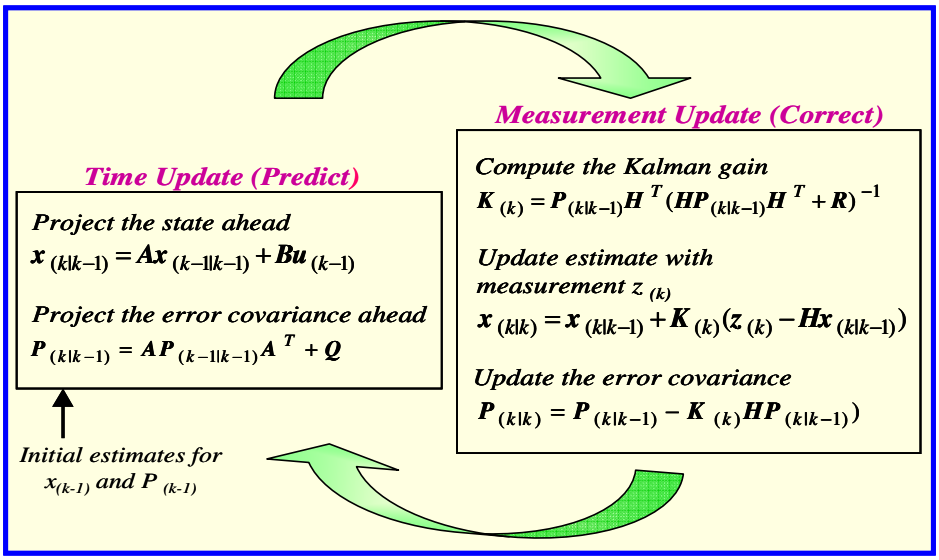

Fig. 3.1. Recursive adaptive Kalman-filter algorithm

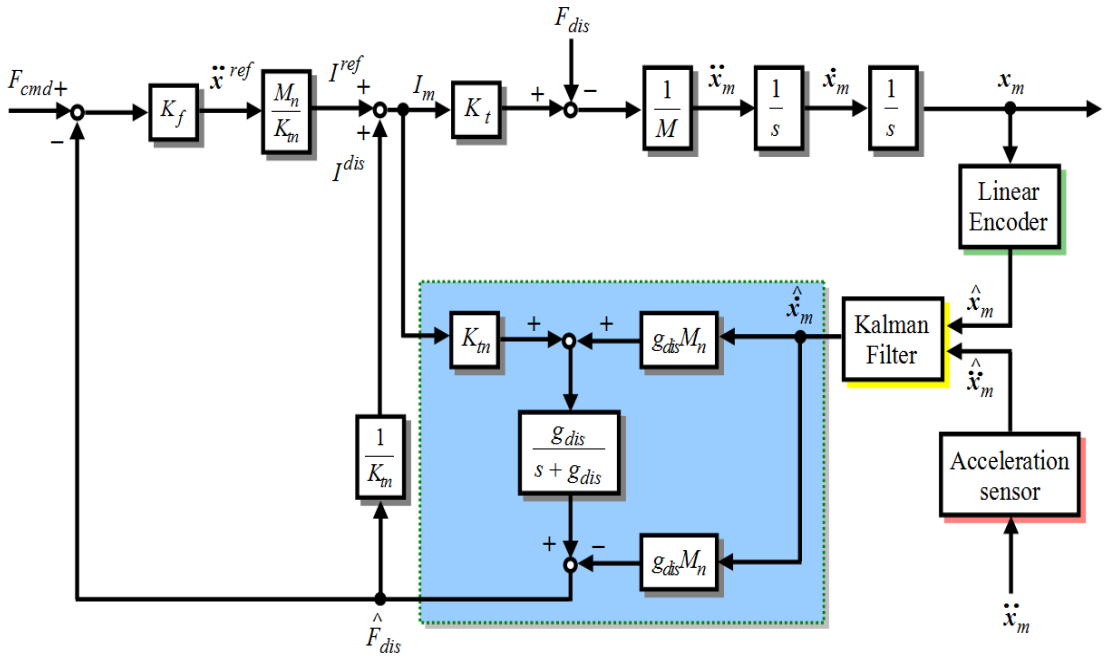

Fig. 3.2. Block diagram of force control using Kalman-filter-based disturbance observer with multi-sensor

The updated velocity estimation by Kalman-filter is applied to the disturbance observer in order to attain the force information as shown in Fig. 3.2.

3.3.2 Force Controller Design

The block diagram of the force control using Kalman-filter-based disturbance observer with multi-sensor is shown in Fig. 3.2. The research considers the relation between the gain of disturbance observer and that of Kalman-filter. At first, the Kalman-filter gain is determined based on the process noise covariance matrix Q and the measurement noise covariance matrix R. After that, the gain of the disturbance observer is decided.

The force control in Fig. 3.2 consists of two control loops. The compensation current computed from the estimated disturbance force is used to cancel the effects of the disturbance force on the motor and the modeling errors. By feeding back the compensation current, the force control system attains the robustness against the unknown environments. In the force feedback loop, the estimated force applying on the motor is compared with the force command to derive the force variation. Based on the force variation between the force command and the estimated force, the linear proportional controller is designed as follow

$$\hat{I}_m = (F_{cmd} - \hat{F}_{dis}) K_f \frac{M_n}{K_{tn}} + \hat{F}_{dis} \frac{1}{K_{tn}} \tag{3.49}$$

where F_{cmd} is the force command and K_f represents the force control gain.

3.3.3 FPGA Implementation of Force Sensing

An FPGA is a type of programmable logic device (PLD). The structure of an FPGA is composed of a matrix of configurable logic blocks, an interconnection programmable network and a ring of configurable input/output blocks. To construct a desired digital system, FPGA's internal logic can be programmed or reprogrammed owing to the hard-wired programmability. Additionally, FPGA has the ability to execute multiple processes at the same time. This feature makes it possible to speed up the operation of the motion controller. Therefore, the motion controller implemented in FPGA can achieve the shorter execution time than that implemented in a CPU with real-time operating system which can only execute sequential processes.

In this work, the force sensing operation with Kalman-filter-based disturbance observer as well as all of the control algorithm is implemented in FPGA. It is possible to improve the performance of force sensing by shortening the sampling period. The FPGA used in this paper is Stratix II- EP2S60F1020C3 manufactured by Altera . The FPGA board has the clock frequency of 100 MHz.

Fig. 3.3 illustrates the internal architecture of the proposed force sensing based on Kalman-filter-based disturbance observer with multi-sensor implemented in FPGA. The FPGA implementation contains the following modules:

An encoder controller module is designed to detect and calculate the phase-shifted pulses from an incremental linear encoder in order to obtain the position information of the linear motor.

An A/D converter controller module is constructed to acquire the acceleration information. It controls the conversion of a 16-bit A/D converter which is used to transform the analog signal generated by an acceleration sensor into 16-bit binary numbers.

Two floating-point converter modules are used to convert 32-bit integer numbers to floating-point numbers. One is used to convert position signal and the other is used for acceleration signal. Since the force control algorithm employs floating-point arithmetic, it is essential to convert position and acceleration information obtained by the encoder controller and the A/D converter controller from integer to floating-point format. In this paper, the format of the floating-point data is the single-precision floating-point number with 32-bit wide. This floating point format is defined by IEEE standard 754 and composed of 1-bit sign, 8-bit exponent and 23-bit mantissa (fraction part). Fig. 3.4 shows the floating point data format.

A force controller module performs the force control algorithm including the force sensing operation by Kalman-filter-based disturbance observer. The inputs of this module are position and acceleration signals and the output is the motor control current. All of the mathematical calculations in this modules use the floating-point arithmetic.

A D/A converter controller module converts the control output signal of the force controller from floating-point to 16-bit integer numbers. Additionally, the D/A controller

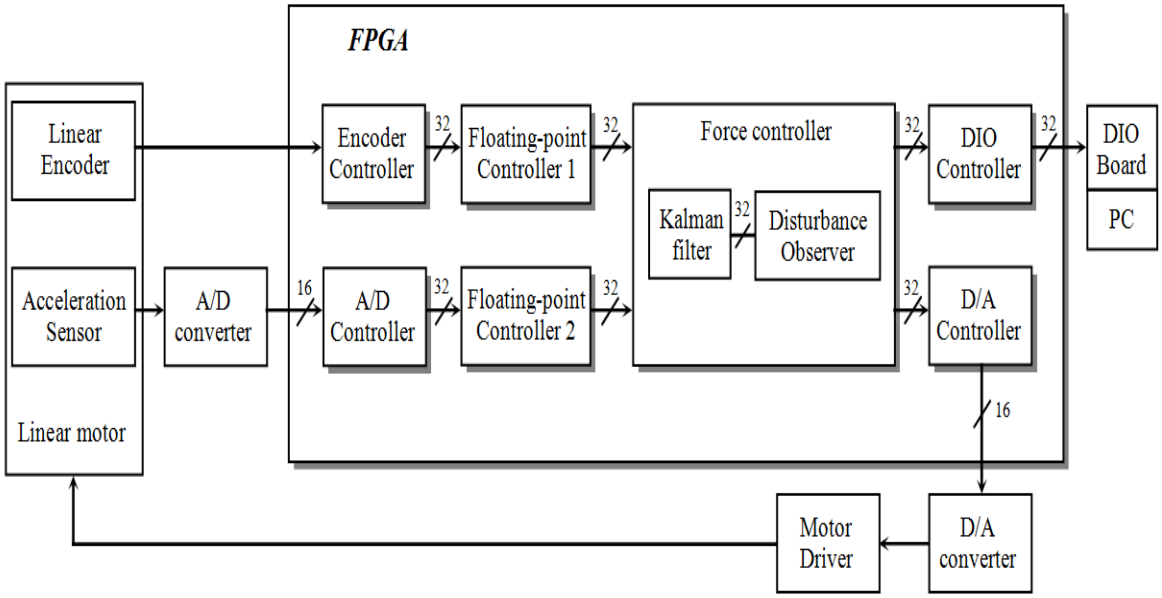

Fig. 3.3. Block diagram of FPGA implementation of the force control with Kalman-filter-based disturbance observer

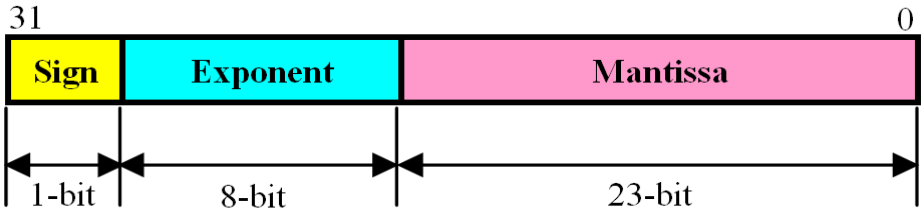

Fig. 3.4. Data format of floating point number

regulates the control signals of an 16-bit D/A converter which is used to transform the motor control signal from digital to analog signal. The output signal of the D/A converter is utilized to operate the servo motor driver.

In order to store data in a PC, a DIO controller module is constructed. The DIO controller converts the floating-point data to 32-bit integer data. It controls the transmission of integer data to a digital input/output (DIO) board using handshake technique.

3.4 Experimental Results

Fig. 3.5 depicts the FPGA board and the linear motor used in the experiments. The FPGA board here adopts Altera Stratix II- EP2S60F1020C3, the linear actuator is a GHC shaftmotor and the motor driver is ADAX3-R5ML2 of Hitachi. An optical incremental linear encoder RGH24Y from Renishaw is mounted on the motor to measure position responses. The acceleration response is attained by an Ono Sokki NP-3211 accelerometer attached to the motor. For the conversion of acceleration signal from analog to digital signal, a 16-bit resolution A/D converter is utilized. Moreover, in order to apply the digital control signal sent out by FPGA to the motor driver, it is necessary to convert the digital signal to analog signal. Thus, a 16-bit D/A converter with ±10 V analog output voltage range is employed in this research. The FPGA configuration for the designed force control system is established using the hardware description language VHDL.

To clarify the effectiveness of the proposed method, the following experiments are conducted .

- Experiments on velocity estimation to compare the velocity response by Kalman-filter using multi-sensor with that by Kalman-filter using only position sensor.
- Experiments on force sensing to compare the performance of the proposed method with that of the position-sensor-based Kalman-filter and disturbance observer (PKFDOB). The experiments are carried out under the same experimental setups as those of the PDOB and PAIDO shown in Fig. 2.4 section 2.1.3 in chapter 2. The bandwidth of the disturbance observer is set to 6280 rad/s and the experimental parameters are shown in table 3.2.
- Experiments on force sensing to investigate the performance of the proposed method when the bandwidth of the disturbance observer is further increased to 62800 rad/s (≈ 10 kHz).

In the experiments, the force command is a constant of 0.5 N and the sampling time is $5\,\mu s$. The linear motor's movements are generated by the human force applied on the motor. The impact motions occur when the motor collides with a rubber piece.

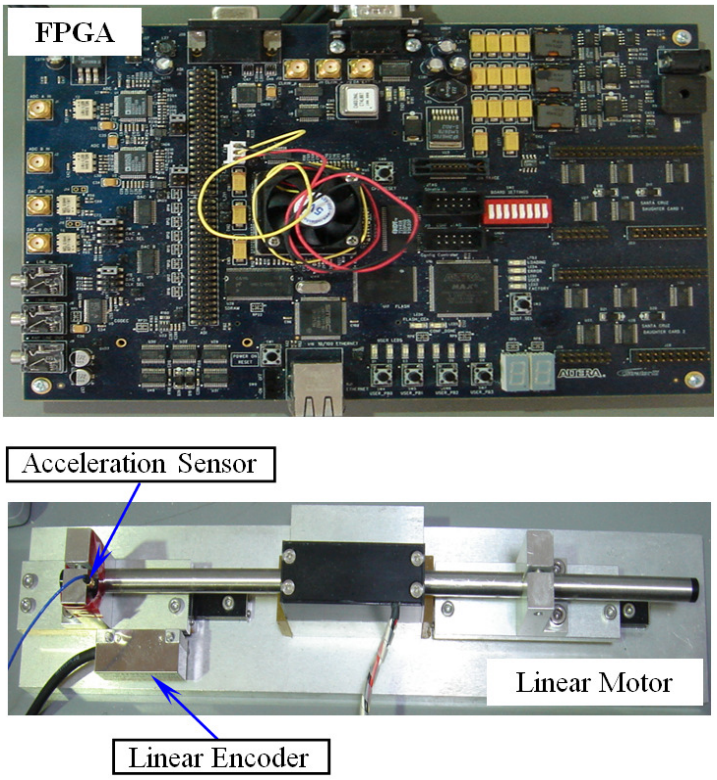

Fig. 3.5. Experimental devices

Table 3.1. FPGA board specifications

Device name	Altera Stratix II- EP2S60F1020C3
DSP block	36
RAM	2,544,192 bits
LEs	60,440
User I/O pin	177

Table 3.2. Parameters used in the experimental set up

Parameters	Value	Unit
Motor mass (M)	0.18	Kg
Force constant (K_t)	3.3	N/A
Encoder resolution	0.1	μm
Encoder mass	11	g
Accelerometer resolution	1.02	$mV/(m/s^2)$
Accelerometer weight	0.5	g
Acceleration bandwidth	10	kHz
Maximum acceleration range	4900	m/s^2
Force command (F_{cmd})	0.5	N
Force control gain (K_f)	5.7	
Sampling time	5	μs

The first experiment is carried out to compare the velocity estimation of the Kalman-filter using multi-sensor with that of the Kalman-filter using only encoder. Fig. 3.6 shows the experimental results of velocity estimation. The blue line is the velocity response estimated by the Kalman-filter using only encoder, and the red line is the velocity response estimated by the Kalman-filter with multi-sensor. It turns out that each velocity response estimated by both methods is coincident except for the contact motion response.

Fig. 3.6 (b) shows the magnification of impact motion velocity response. During the impact motion with high acceleration, the velocity response estimated by Kalman-filter with multi-sensor is much improved. These results confirm the advantage of acceleration measurement to obtain the accurate velocity estimation by Kalman-filter. It is how accurately the velocity is estimated that determines the performance of force sensing by the disturbance observer.

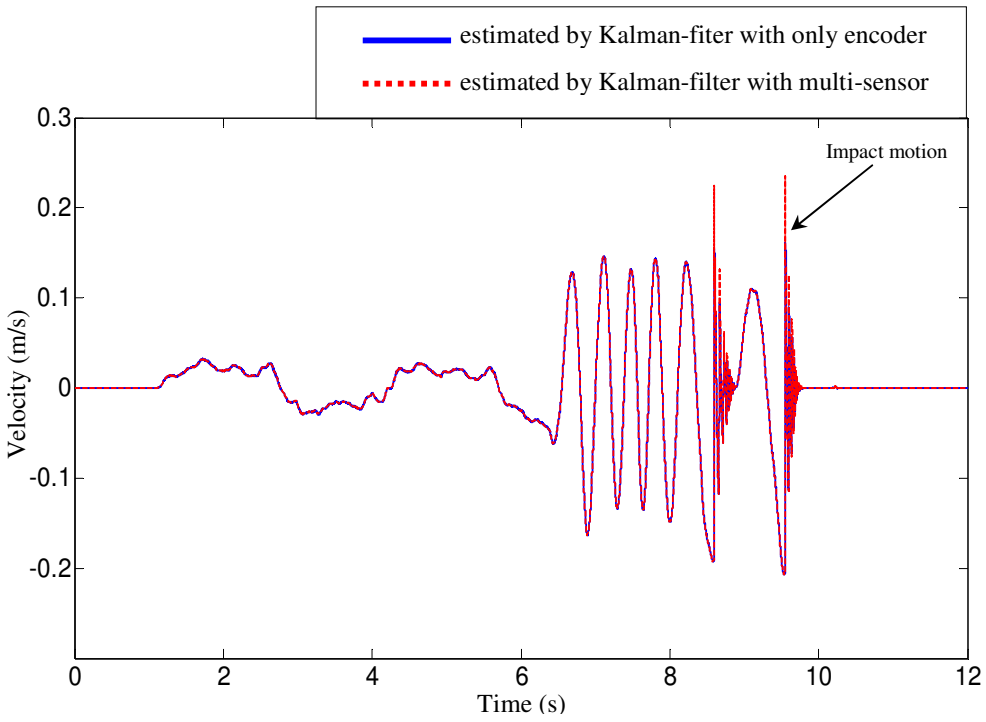

(a) Velocity responses

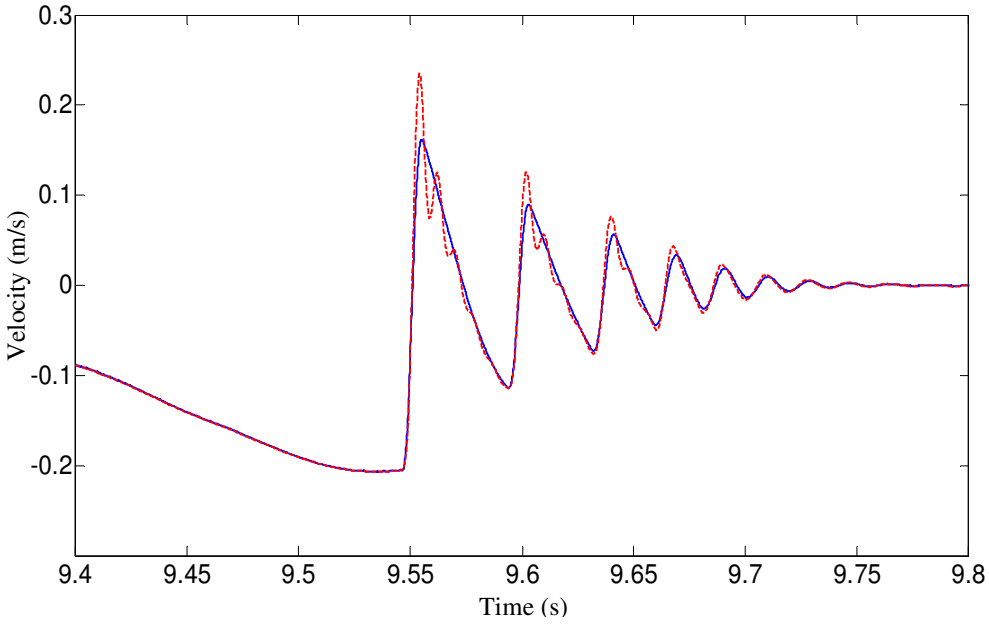

(b) Magnification of impact motion in (a)

Fig. 3.6. Experimental results of velocity estimation

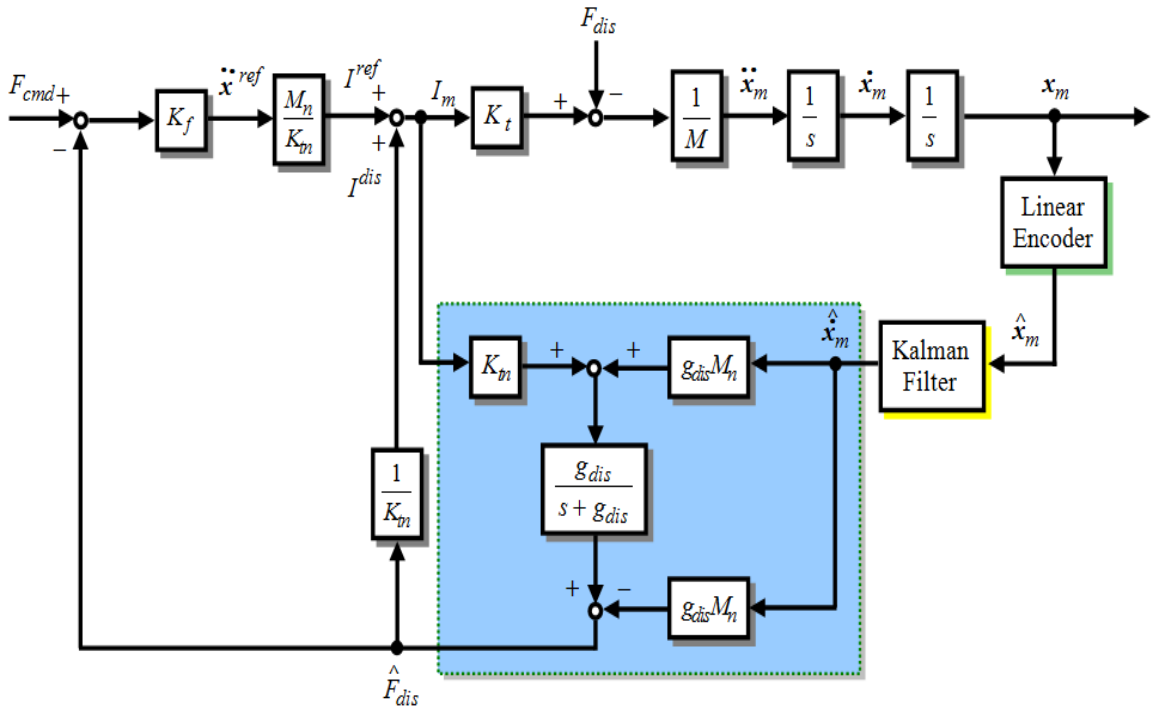

Fig. 3.7. Block diagram of force control with PKFDOB

The second experiments are conducted on the force control to investigate the force sensing performance of the proposed method in comparison with that of the position-sensor-based Kalman-filter and disturbance observer (PKFDOB). The block diagram of the proposed method is shown in Fig. 3.2 and the block diagram of the PKFDOB is shown in Fig. 3.7. In the experiments, the bandwidth of force sensing g_{dis} is set to 6280 rad/s.

Fig. 3.8 displays the force responses at the force sensing bandwidth of 6280 rad/s. The results show that both the proposed method and the PKFDOB obtain the smooth force responses with very low peak-to-peak noise level of 0.06 N and 0.07 N, respectively. From these results, it is clear that the proposed method and the PKFDOB provide the good force sensing performance, and are much better than the PAIDO in noise suppression.

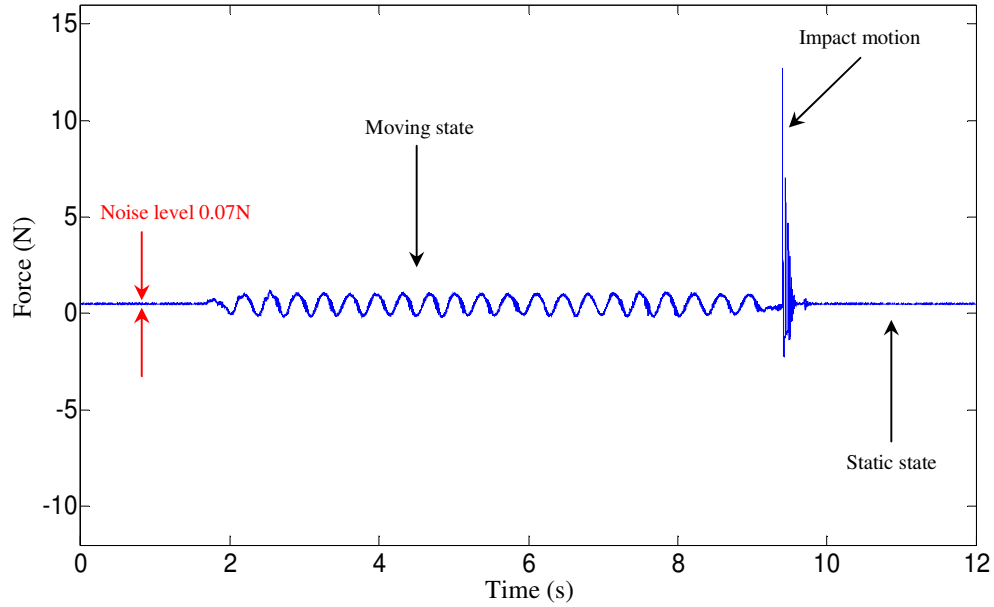

(a) Estimated by Position-sensor-based Kalman-filter and disturbance observer (PKFDOB)

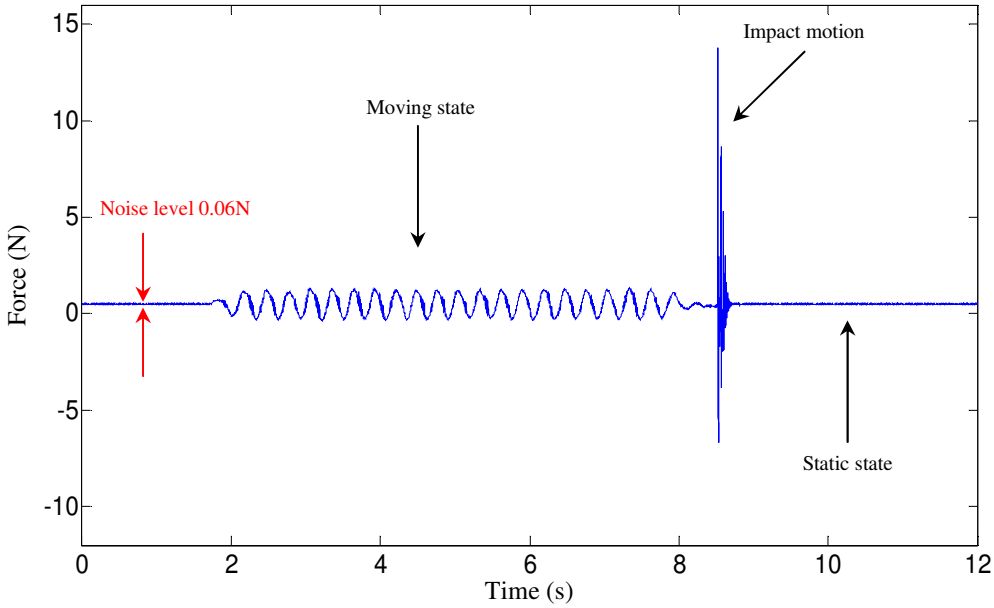

(b) Estimated by Kalman-filter-based disturbance observer with multi-sensor

Fig. 3.8. Force responses at the force sensing bandwidth of 6280 rad/s

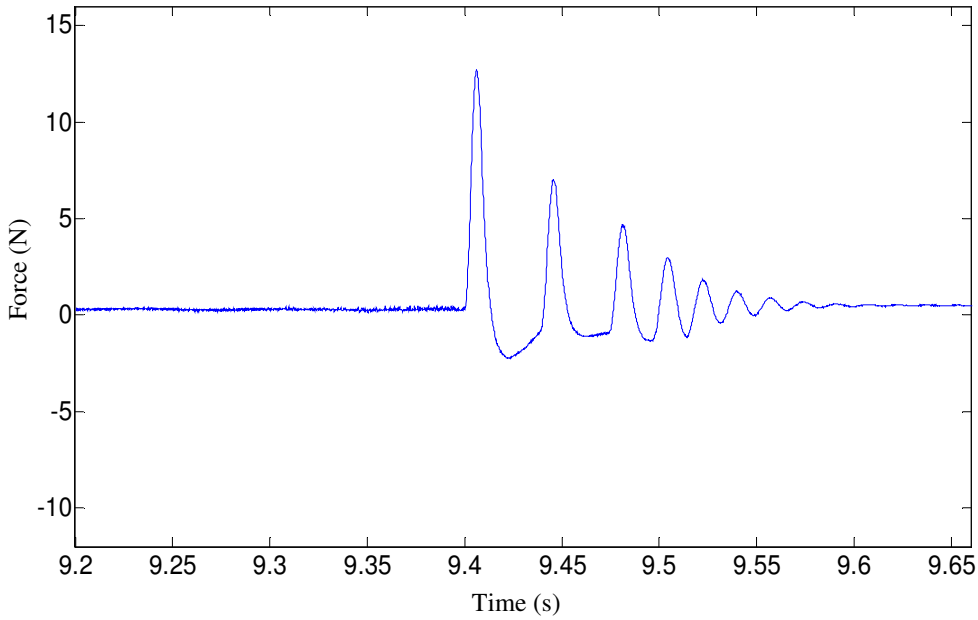

(a) Estimated by Position-sensor-based Kalman-filter and disturbance observer (PKFDOB)

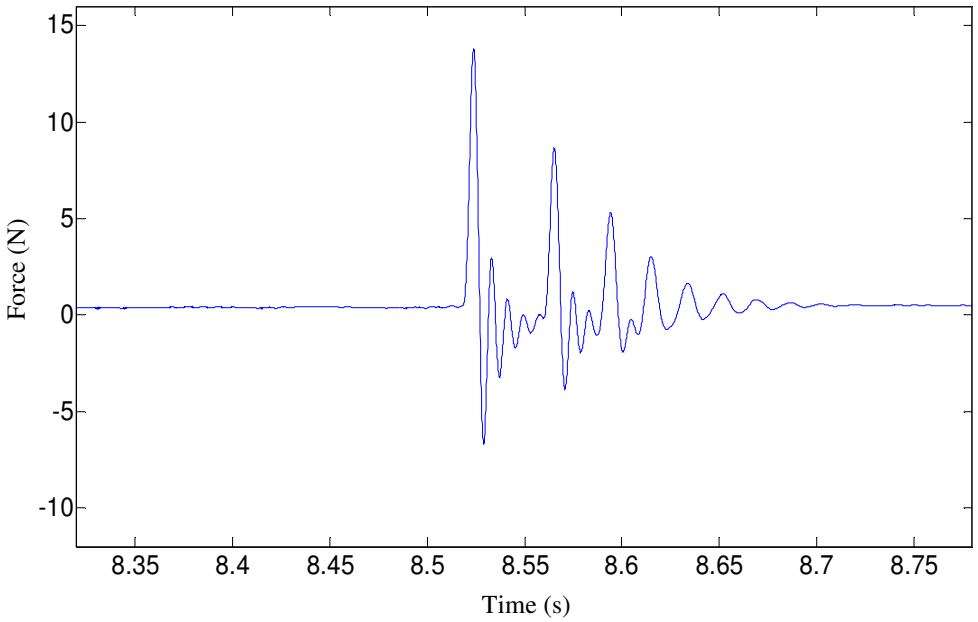

(b) Estimated by Kalman-filter-based disturbance observer with multi-sensor

Fig. 3.9. Magnification of impact force in Fig. 3.8 (a) and (b)

To clarify the effectiveness of the proposed method, the force responses of the impact motion estimated by the proposed method and the PKFDOB are investigated. Fig. 3.9 shows the magnification of the impact force response in Fig. 3.8 (a) and (b). Since the proposed method obtains the accurate velocity estimation during the impact motion by the Kalman-filter with multi-sensor, the impact force response of the proposed method is much more improved as compared with that of the PKFDOB using Kalman-filter with only encoder.

The above results confirm that the force sensing performance of the proposed method is superior to that of the other methods.

Moreover, since the proposed method is implemented in FPGA, a very high sampling rate of $5\,\mu s$ is obtained. Therefore, it is possible to enlarge the bandwidth of force sensing by increasing the cut-off frequency of the disturbance observer to 62800 rad/s (≈ 10 kHz). Fig. 3.10 shows the force response estimated by the proposed method at the force sensing bandwidth of 62800 rad/s. The proposed method still obtains the high force sensing performance with the effective noise suppression and the wide bandwidth force sensing is obtained. The result confirms the enhanced performance force sensing using the proposed method.

The comparison between the proposed method and the other methods is summarized in table 3.3.

Table 3.3. Comparison summary between the proposed method and other methods

Methods	**Peak-to-peak noise level at bandwidth 6280 rad/s**	**Ability to widen force sensing bandwidth to 62800 rad/s**
PDOB	0.9 N	impossible
PAIDO	0.25 N	impossible
PKFDOB	0.07 N	possible
Proposed method	0.06 N	possible

Method	**Accurate impact force estimation**
PKFDOB	impossible
Proposed method	possible

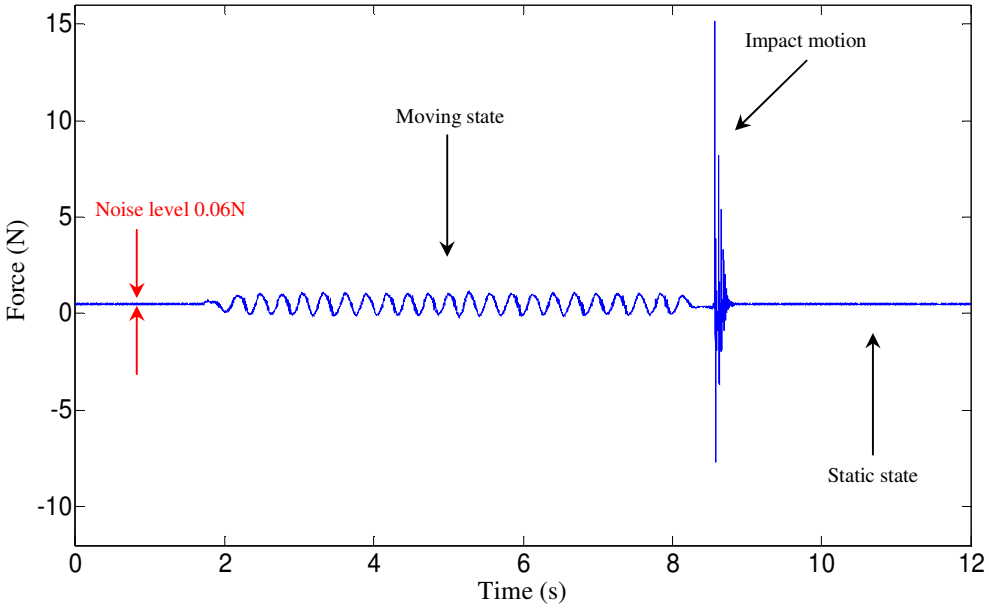

(a) Force response

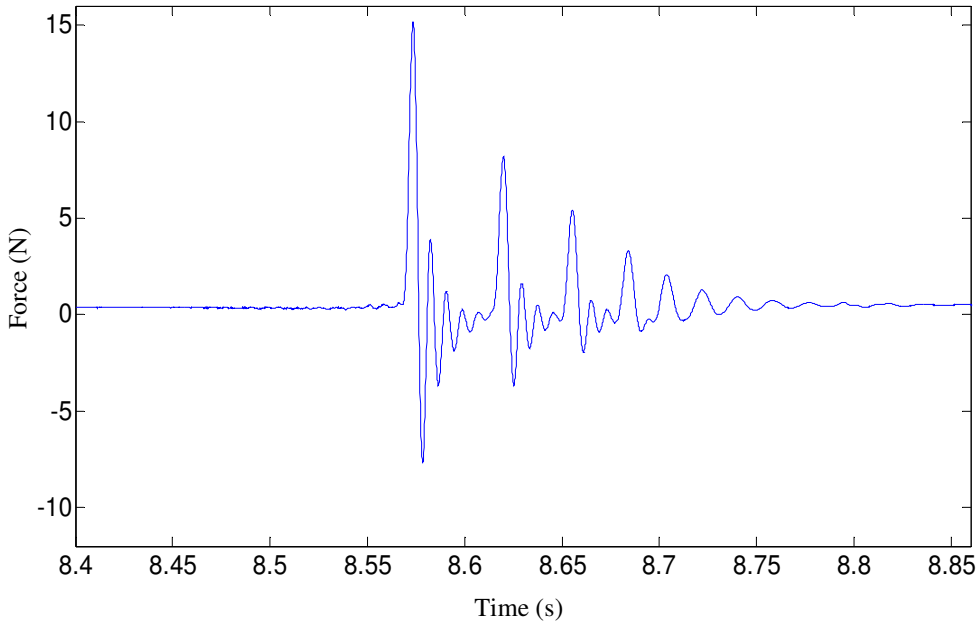

(b) Magnification of impact force in (a)

Fig. 3.10. Force response estimated by the Kalman-filter-based disturbance observer with multi-sensor at the force sensing bandwidth of 62800 rad/s (≈ 10 kHz)

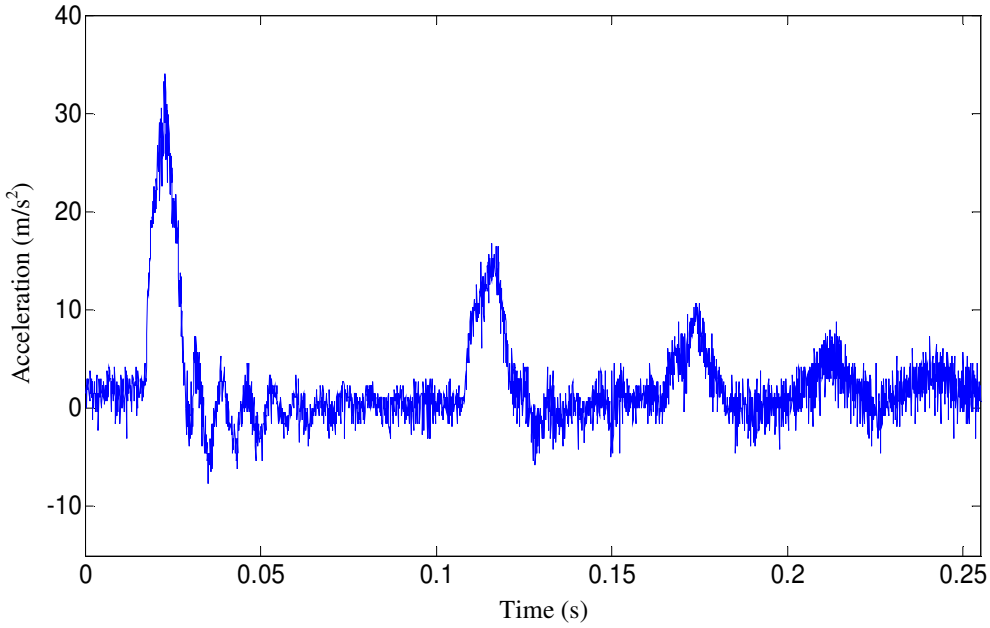

Fig. 3.11. Acceleration measurement of impact motion by acceleration sensor

Additionally, Fig. 3.11 shows the experimental result of acceleration response of impact motion measured by an acceleration sensor. This result confirms the contribution of acceleration signal in the force estimation by the proposed method.

3.5 Conclusions

The research proposes a method to improve the performance of force sensing and widen the bandwidth of force estimation. The force sensing operation is constructed by the Kalman-filter-based disturbance observer with multi-sensor implemented in FPGA. The utilization of FPGA enables the shortening of sampling period of the control algorithm for the enlargement of the disturbance observer bandwidth. The measurement system with multi-sensor Kalman-filter is an effective method to attain the suppression of noise in the force response. The experimental results have verified the efficiency of the proposed method. The shortened sampling time is 5 μs and the force sensing bandwidth is widened to 62800 rad/s (≈ 10 kHz). This bandwidth is superior to human bandwidth of tactile sensation. It is useful for human

support techniques (such as human interfaces, haptic devices, surgical robots, surgical tele-operation, exercising machines) to achieve the high efficiency in haptic information reproduction and transmission with the attained wideband force sensing.

Chapter 4

FPGA-based Wideband Force Control System with Friction-Free and Noise-Free Force Observation

4.1 Introduction

The objective of my research is to construct a wideband force control system with a friction-free and noise-free force observation. The friction compensation method is inspired by the dithering method's simplicity of implementation. A periodic signal is inserted into the control signal to reduce the friction effect on force observation. However, the additional signal generates an oscillatory disturbance that can affect the performance of the control system. The force estimation by the conventional disturbance observer is also influenced by the periodic signal since the effect of the oscillatory disturbance is not taken into account in the conventional method. Therefore, the research proposes a friction-free disturbance observer for force sensing operation and elimination of periodic disturbance in force estimation. The design of the friction-free disturbance observer is motivated by a state-space approach and is applied to a one-mass system. To make the design practical, the problem of noise in the measurement is taken into account. A Kalman filter is used in combination with the friction-free disturbance observer to reduce the effect of noise on the force estimation. The force-sensing bandwidth is significantly improved owing to the effective noise reduction by the Kalman filter. Hence, using a dither signal together with the integration of a friction-free disturbance observer and a Kalman filter provides friction-free and wideband force sensing.

In the research, all control algorithms are implemented in a field-programmable gate array (FPGA). An advantage of using an FPGA is that its very short computation time enables an extremely high rate of sampling of the control cycle. The shortened sampling time

provided by the FPGA can ensure the good performance of the control system when a high-resolution position sensor is adopted, when high-speed controlling is required, or in the case of immense complexity of the control algorithm. Moreover, the high-sampling rate also opens the possibility of enlarging the bandwidth of force sensing. The experimental system consists of a servo motor connected to a ball screw in which friction is always present. The experimental results verify the effectiveness of the proposed method.

4.2 Force Estimation by Conventional Disturbance Observer

Fig. 4.1 shows the block diagram of a force control system using a conventional disturbance observer for force estimation. Here, J_m denotes the motor inertia, K_t denotes the torque coefficient, and the subscript n represents the nominal value. I_m is the motor torque current, θ_m is the angle, and ω_m represents the motor speed. T_m denotes the motor torque, and T_{dis} is the disturbance torque.

The performance of the force control system is determined by how the force is properly detected. However, in practical applications, force estimation by the conventional disturbance observer is affected by friction phenomena. This can degrade the performance of the control system.

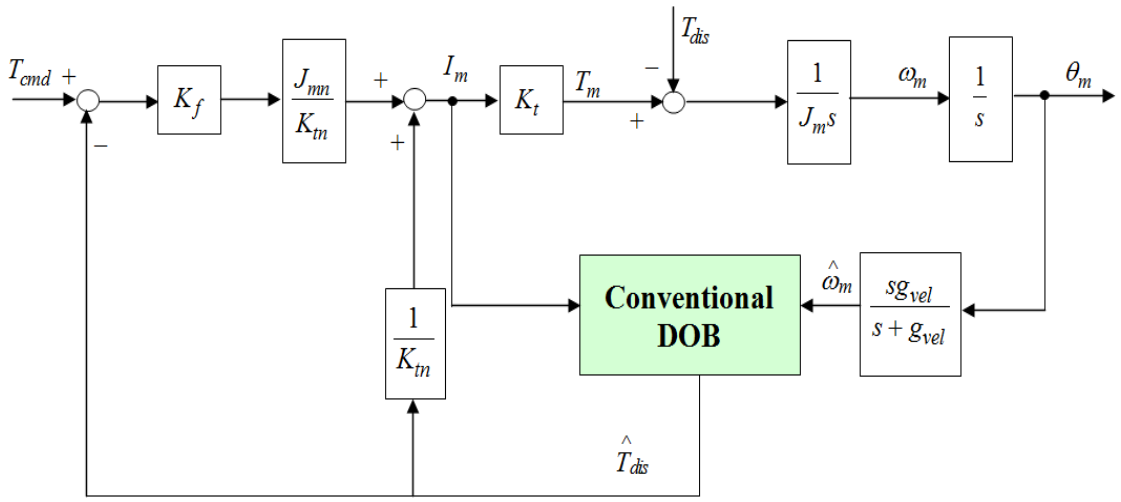

Fig. 4.1. Block diagram of the force control system using the conventional DOB

To present the effect of friction on force estimation in a ball-screw system, the experiment of force control in the ball-screw system was carried out with a constant torque command of 0.1 Nm in condition of constant velocity of 10.5 rad/s. In the research, I use the constant force reference because I would like to visualize the effect of friction on the estimated force so that it can be easily to analyze the friction effect and evaluate the control performance. Here, the conventional DOB performs the force estimation with the observer pole of 300 rad/s. The experimental results of force estimation by conventional DOB is shown in Fig. 4.2. The torque response in Fig. 4.2 is analyzed by fast-Fourier-transform to obtain the frequency components of the estimated torque as shown in Fig. 4.3.

Because the ball-screw system is controlled with a constant torque command, the frequency components in the estimated torque shown in Fig. 4.3 are undesired harmonics. There are several potential causes of these ripples in the torque responses: switching frequency of servo amplifier, mechanical resonant frequency, current measurement error due to current sensor of set or gain deviation, and friction. Normally, the switching frequency of servo amplifier is of 10kHz, and the ball-screw system with high rigidity does not have a low mechanical resonant frequency [62]. Therefore, from Fig. 4.3, it can be interpreted that these two factors are not related to the ripples. Additionally, because the mechanical motor speed of the system is 10.5 rad/s and the pole pair number of motor is of 2, the electrical motor speed is 21 rad/s which is 3.3 Hz. Hence, the current ripple frequency of current sensor offset becomes 3.3 Hz, and that of current sensor gain deviation becomes 6.6 Hz [63, 64]. However, in Fig. 4.3, there is no effect of the frequency components of 3.3 Hz and 6.6 Hz, because the current sensor of servo amplifier is well adjusted, and its current control system has little sensor offset and little sensor gain deviation. Therefore, the ripples in torque response is only caused by friction. As a result of friction, the torque estimated by conventional DOB is deteriorated, having unsmooth waveform, and the peak-to-peak amplitude of torque signal is 0.00545 Nm. Therefore, it is essential to compensate for friction to reduce the effect of undesired frequency components, and consequently, to reduce the peak-to-peak amplitude of torque signal. The friction compensation method is discussed in the next section.

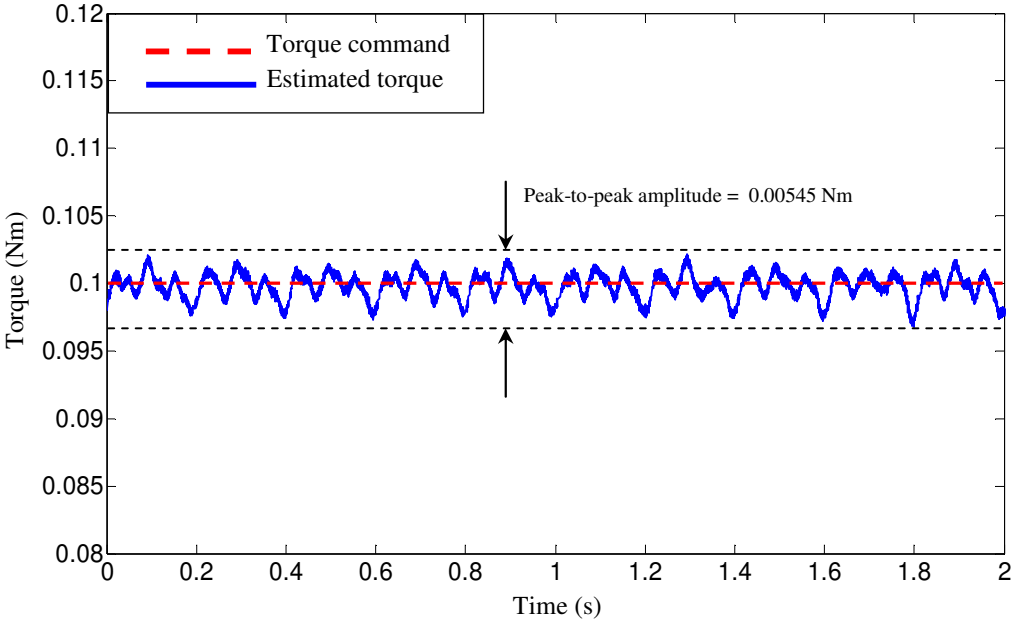

Fig. 4.2. Torque response estimated by conventional DOB distorted by friction

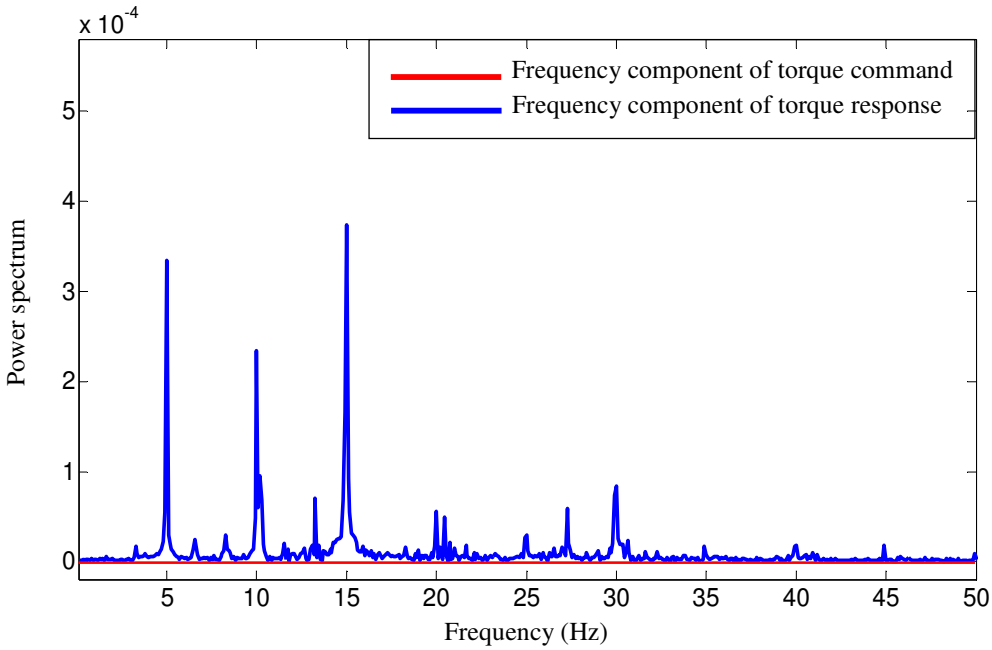

Fig. 4.3. Frequency components of torque response estimated by conventional DOB shown in Fig. 4.2

4.3 Proposed Force Estimation by Friction-Free Disturbance Observer

4.3.1 Friction Compensation Method

As stated in the above section, friction causes undesired force response estimated by conventional DOB. The elimination of friction can improve the force sensing and control performance. In the research, the friction compensation method is motivated by the dithering technique because my aim is to achieve the friction compensation with a simple implementation. Dithering is a technique defined by the addition of a signal with appropriate frequency and amplitude to the desired reference signal. The effect of the dither signal is known as the ability to smooth the discontinuity of friction. Therefore, by using dithering method, I do not consider the friction model in the research.

In the control system, friction characteristics are unknown. To reduce the friction effect, I insert a dither signal to the desired current reference of the control system. The addition of a dither signal with predetermined frequency and amplitude is to generate an artificial disturbance in the force information, and to make the additional signal become the dominant-power signal in the original force signal. When the dither signal is dominant in the force signal, consequently the effect of other undesired frequency components caused by friction is lessened.

On the other hand, dither signal also introduces oscillatory disturbance in force estimation. However, because the characteristics of dither signal are known in advance, we can easily eliminate the oscillatory disturbance. The force estimation by the conventional DOB is affected by oscillatory disturbance because this DOB is designed to estimate the total disturbances applied to the system. Therefore, a force-sensing method capable of eliminating the effect of the oscillatory component in the force information is required. Based upon this reasoning, the research proposes the friction-free disturbance observer with dither signal to perform the force sensing function to reduce friction and oscillatory component in force information. The design of the friction-free DOB is presented in the next section.

4.3.2 Design of Friction-Free Disturbance Observer for Force Estimation

The design of the friction-free DOB requires knowledge of the frequency of the additional signal so that the periodic component in the force information can be eliminated by the friction-free DOB. The dynamics of the oscillatory signal are modeled by a second-order system, and the plant system of the friction-free DOB is shown in Fig. 4.4. Therefore, the oscillatory torque is expressed as shown in (4.1).

$$T_{dis}^{'} = \frac{\omega_0^2}{s^2 + 2\zeta\omega_0 s + \omega_0^2} T_{dis} \tag{4.1}$$

where ω_0 is the predetermined angular frequency of the additional periodic signal and ζ denotes the damping ratio. T_{dis} is the torque signal without the oscillatory component, which is the step function expressed by (4.2). $T_{dis}^{'}$ is the oscillatory torque generated by superimposing of the periodic signal on T_{dis}.

$$\frac{d}{dt} T_{dis} = 0 \tag{4.2}$$

The objective of the friction-free DOB is to estimate the torque signal without the oscillatory component T_{dis}. Therefore, T_{dis} is derived from (4.1) as follows:

$$T_{dis} = \frac{s^2 T_{dis}^{'} + 2\zeta\omega_0 s T_{dis}^{'} + \omega_0^2 T_{dis}^{'}}{\omega_0^2} \tag{4.3}$$

From (4.3), T_{dis} can be represented by transforming multiplication of *s* in the Laplace domain to differentiation in the time domain as shown in (4.4).

$$T_{dis} = \frac{\dddot{T}_{dis}^{'} + 2\zeta\omega_0 \ddot{T}_{dis}^{'} + \omega_0^2 \dot{T}_{dis}^{'}}{\omega_0^2} \tag{4.4}$$

According to (4.4), the friction-free DOB is designed by a state-space approach to estimate $\ddot{T}_{dis}^{'}$, $\dot{T}_{dis}^{'}$, and $T_{dis}^{'}$. Therefore, by using the friction-free DOB, the torque signal without oscillatory component T_{dis} is obtained using the estimated values $\ddot{T}_{dis}^{'}$, $\dot{T}_{dis}^{'}$, and $T_{dis}^{'}$ as expressed in (4.4). The design process of the state-space model of the friction-free DOB is

described as follows.

The model of the friction-free disturbance observer is realized based on the state-space model expressed in (4.5) and (4.6).

$$\dot{x} = \boldsymbol{A}x + \boldsymbol{B}u \tag{4.5}$$

$$y = \boldsymbol{C}x \tag{4.6}$$

where
$$x = \begin{bmatrix} \omega_m \\ \ddot{T}'_{dis} \\ \dot{T}'_{dis} \\ T'_{dis} \end{bmatrix}, \quad u = I_m, \quad y = \omega_m \tag{4.7}$$

The state equations are given by (4.8), (4.9), (4.10), and (4.11).

$$\frac{d}{dt}\omega_m = -\frac{1}{J_m}T'_{dis} + \frac{K_t}{J_m}I_m \tag{4.8}$$

$$\frac{d}{dt}\ddot{T}'_{dis} = -2\zeta\omega_0\ddot{T}'_{dis} - \omega_0^2\dot{T}'_{dis} \tag{4.9}$$

$$\frac{d}{dt}\dot{T}'_{dis} = \ddot{T}'_{dis} \tag{4.10}$$

$$\frac{d}{dt}T'_{dis} = \dot{T}'_{dis} \tag{4.11}$$

From (4.8), (4.9), (4.10), and (4.11), the state matrices $\boldsymbol{A}$, $\boldsymbol{B}$, and $\boldsymbol{C}$ are derived as follows:

$$\boldsymbol{A} = \begin{bmatrix} 0 & 0 & 0 & -1/J_m \\ 0 & -2\zeta\omega_0 & -\omega_0^2 & 0 \\ 0 & 1 & 0 & 0 \\ 0 & 0 & 1 & 0 \end{bmatrix}, \quad \boldsymbol{B} = \begin{bmatrix} K_t/J_m \\ 0 \\ 0 \\ 0 \end{bmatrix},$$

$$\boldsymbol{C} = \begin{bmatrix} 1 & 0 & 0 & 0 \end{bmatrix} \tag{4.12}$$

Since the state variable ω_m is measurable, from the state matrices $\boldsymbol{A}$ and $\boldsymbol{B}$, the friction-free disturbance observer is defined by the minimum-order observer principles and the

Ackermann method [65]. The state equations of the proposed friction-free disturbance observer are obtained as shown in (4.13) and (4.14).

$$\frac{d}{dt}\begin{bmatrix}\eta_1\\ \eta_2\\ \eta_3\end{bmatrix}=\begin{bmatrix}a_0 & a_1 & a_2\\ 1 & 0 & a_3\\ 0 & 1 & a_4\end{bmatrix}\begin{bmatrix}\eta_1\\ \eta_2\\ \eta_3\end{bmatrix}+\begin{bmatrix}b_1\\ b_2\\ b_3\end{bmatrix}\omega_m+\begin{bmatrix}c_1\\ c_2\\ c_3\end{bmatrix}I_m \tag{4.13}$$

$$\begin{bmatrix}\ddot{T}_{dis}^{'}\\ \dot{T}_{dis}^{'}\\ T_{dis}^{'}\end{bmatrix}=\begin{bmatrix}\eta_1\\ \eta_2\\ \eta_3\end{bmatrix}+\begin{bmatrix}k_1\\ k_2\\ k_3\end{bmatrix}\omega_m \tag{4.14}$$

where

$$a_0=-2\zeta\omega_0,\ a_1=-\omega_0^2,\ a_2=\frac{k_1}{J_m},\ a_3=\frac{k_2}{J_m},\ a_4=\frac{k_3}{J_m} \tag{4.15}$$

$$b_1=-2\zeta\omega_0 k_1-\omega_0^2 k_2+\frac{k_1k_3}{J_m} \tag{4.16}$$

$$b_2=k_1+\frac{k_2k_3}{J_m} \tag{4.17}$$

$$b_3=k_2+\frac{k_3^2}{J_m} \tag{4.18}$$

$$c_1=-\frac{K_t k_1}{J_m},\ c_2=-\frac{K_t k_2}{J_m},\ c_3=-\frac{K_t k_3}{J_m} \tag{4.19}$$

where k_1, k_2, and k_3 are the elements of the observer gain matrix K_e which is derived by the Ackermann method and is determined by the observer pole.

The proposed friction-free disturbance observer estimates the disturbance torque by using $\hat{\ddot{T}}_{dis}^{'}$, $\hat{\dot{T}}_{dis}^{'}$, and $\hat{T}_{dis}^{'}$ as shown in (4.20).

$$\hat{T}_{dis}=\frac{\hat{\ddot{T}}_{dis}^{'}+2\zeta\omega_0\hat{\dot{T}}_{dis}^{'}+\omega_0^2\hat{T}_{dis}^{'}}{\omega_0^2} \tag{4.20}$$

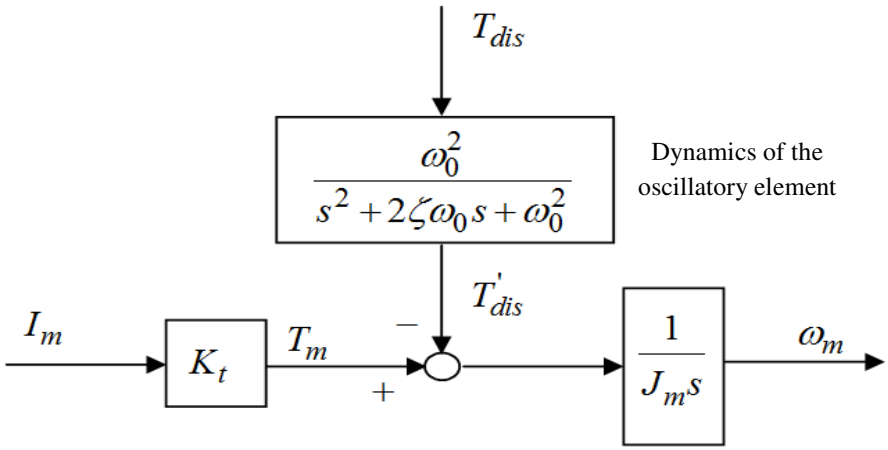

Fig. 4.4. Plant system of the friction-free disturbance observer

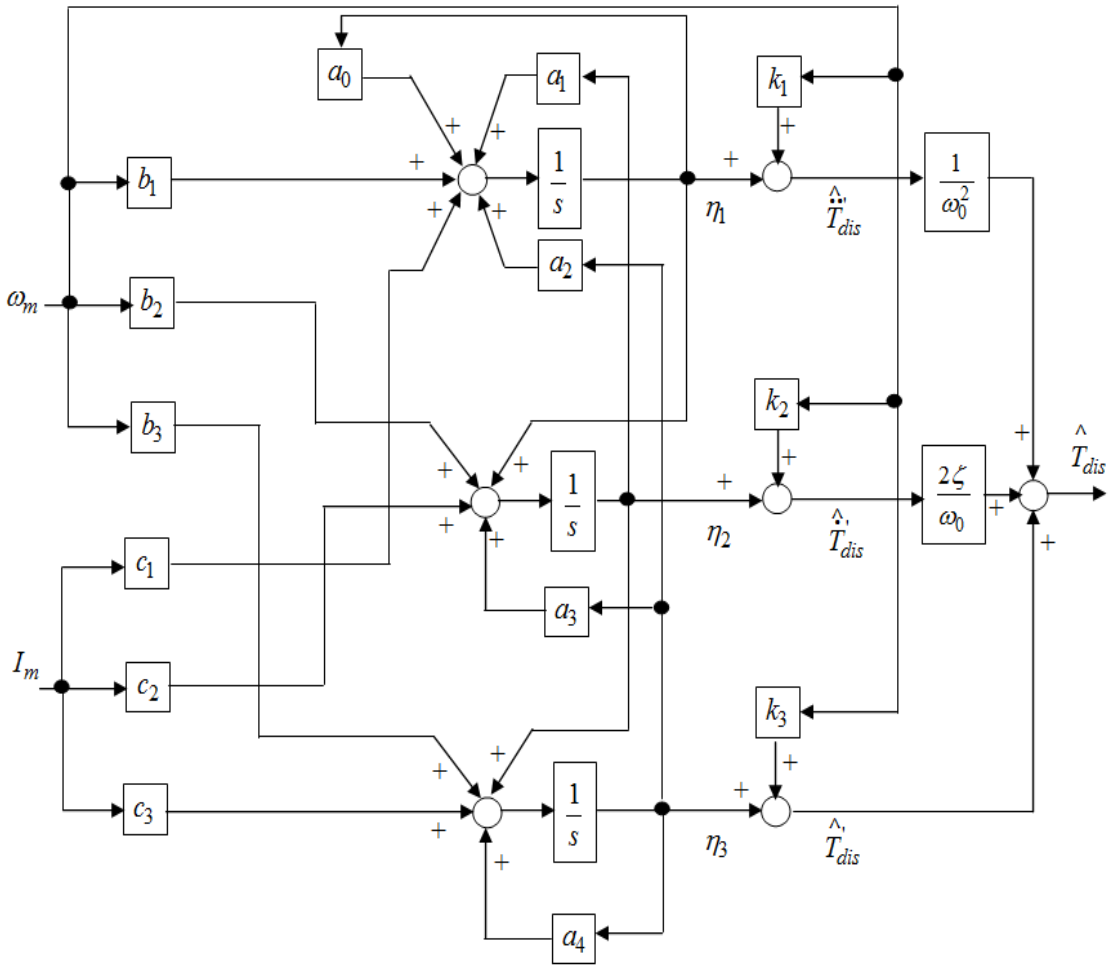

Fig. 4.5. Structure of the friction-free disturbance observer

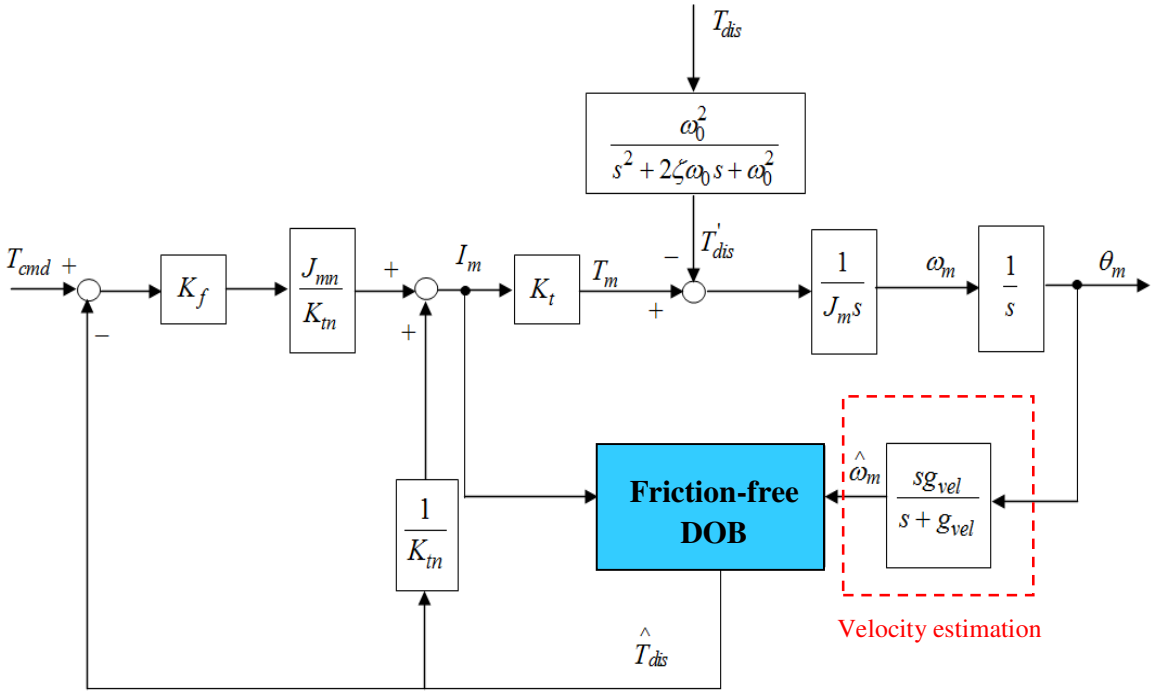

Fig. 4.6. Block diagram of force control using the friction-free DOB with conventional velocity estimation

The structure of the friction-free disturbance observer is illustrated in Fig. 4.5. Fig. 4.6 shows the block diagram of the force control using the friction-free disturbance observer with conventional velocity estimation. Here, the motor speed ω_m is estimated based on the derivative of the angular signal θ_m with respect to time. The angular information is simply obtained from an encoder. The estimated speed is shown in (4.21).

$$\hat{\omega}_m = \frac{s g_{vel}}{s + g_{vel}} \theta_m \tag{4.21}$$

where g_{vel} denotes the cut-off frequency of the low-pass filter which is used to suppress the high-frequency noise.

The design of dither signal is presented as follows. The amplitude of dither signal is determined experimentally so that it does not cause vibration in the control system, and is based on the peak-to-peak amplitude of torque signal deteriorated by friction (ΔT). Here, the

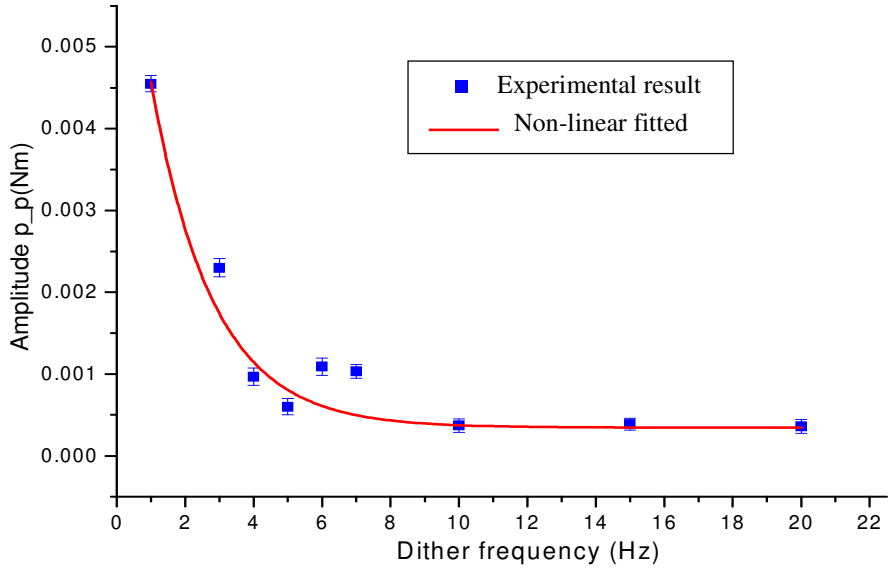

Fig. 4.7. Experimental results of relationship between dither frequency and peak-to-peak amplitude of torque estimated by friction-free DOB

peak-to-peak amplitude of torque signal is 0.00545 Nm as shown in Fig. 4.2. Hence, the corresponding current value is $\Delta I = \Delta T / K_t = 0.011$ A, with $K_t = 0.498$ Nm/A. The amplitude of dither signal is selected with a value higher than ΔI so that the effect of friction can be reduced provided that it does not generate system vibration.

For determination of dither frequency, experiments of force control with different frequencies of dither signal are conducted, also under conditions of constant torque command of 0.1 Nm and constant velocity of 10.5 rad/s. Here, the friction-free DOB with dither signal performs the force estimation with the observer pole of 300 rad/s. The research investigates the relationship between the dither frequency and the peak-to-peak amplitude of torque signal estimated by friction-free DOB. The experimental results are shown in Fig. 4.7.

The results show that the peak-to-peak amplitude of torque signal significantly decreases at dither frequency of 5Hz, then continues to a little decrease and reaches the saturation state at dither frequencies 10Hz, 15Hz, and 20Hz. These results indicate that friction in force estimation is effectively reduced by selecting dither signal with frequency of 5Hz or of higher value. Therefore, in the proposed method, I determine to use the 5Hz-dither signal with friction-free DOB for the force control of ball-screw system.

4.3.3 Experimental Results of Friction-Free Disturbance Observer Using Conventional Velocity Estimation

The effectiveness of the friction-free disturbance observer is illustrated by the experimental results in Fig. 4.8. In this experiment, the observer poles of the conventional DOB and friction-free DOB are 100 rad/s; the friction-free DOB here uses conventional velocity estimation with a cut-off frequency of 100 rad/s, and the additional periodic signal inserted into the desired reference signal has a frequency of 5 Hz. The force control scheme using the conventional DOB and the force control scheme using the friction-free DOB are shown in Figs. 4.1 and 4.6, respectively. The force control algorithms are also implemented in the FPGA with a sampling time of 5 μs.

In Fig. 4.9, the red curve is the torque response estimated by the friction-free DOB. As the force estimation principle of the friction-free DOB is realized by (4.4) together with the knowledge of the frequency of the oscillatory disturbance, the oscillatory disturbance in the estimated torque is reduced significantly using the friction-free DOB. In addition, it is apparent that, together with the effectively periodic component reduction, the friction-free DOB also obtains the torque response without discontinuities in contrast with the conventional DOB in the absence of periodic signal. This indicates that the force-sensing performance of the friction-free DOB overcomes the problems of oscillatory disturbance and friction. The FFT analyses of torque responses in Fig. 4.9 also confirm the performance of the friction-free DOB. This proves that the periodic component of 5 Hz is significantly eliminated by using the friction-free disturbance observer.

However, in this case, the force-sensing bandwidth is only 100 rad/s, which is a narrow bandwidth. To improve the force-sensing performance, a wider force-sensing bandwidth is required. Therefore, I increased the force-sensing bandwidth to 1000 rad/s and investigated the performance of the friction-free DOB using conventional velocity estimation in the presence of the additional periodic signal at 5 Hz. The observer pole and cut-off frequency of the conventional velocity estimation are set to 1000 rad/s. The force control scheme is illustrated in Fig. 4.6.

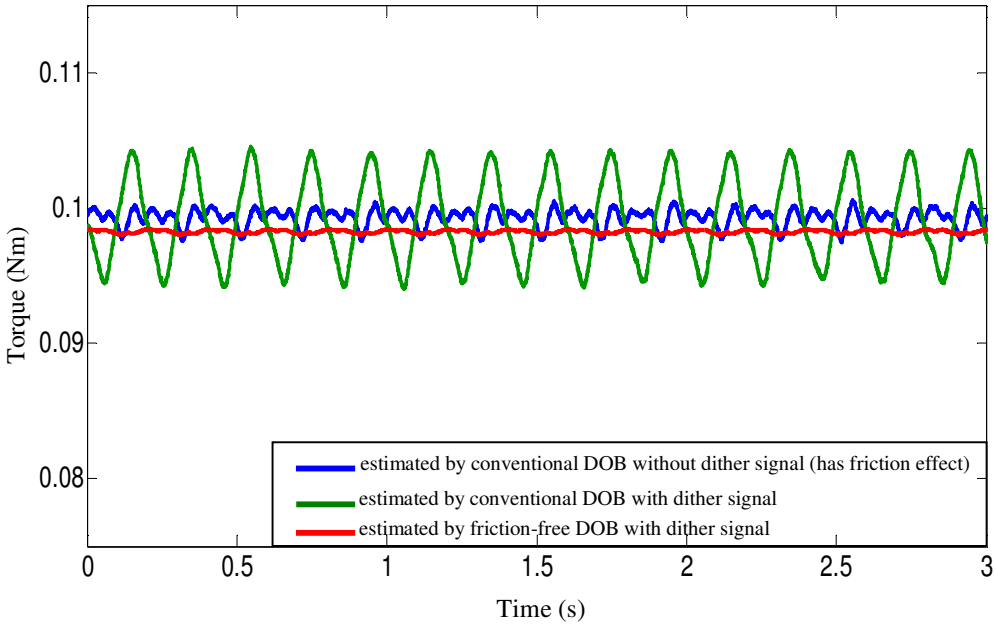

Fig. 4.8. Torque responses with observer pole at 100 rad/s

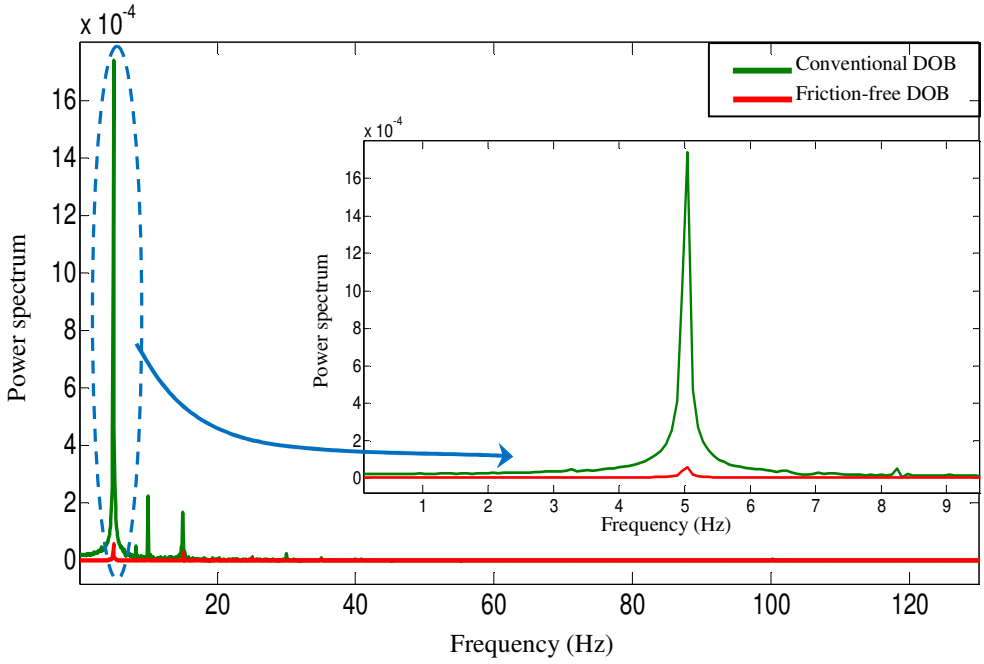

Fig. 4.9. FFT of torque responses in Fig. 4.8 corresponding to conventional DOB and friction-free DOB using conventional velocity estimation under condition of additional periodic signal 5 Hz

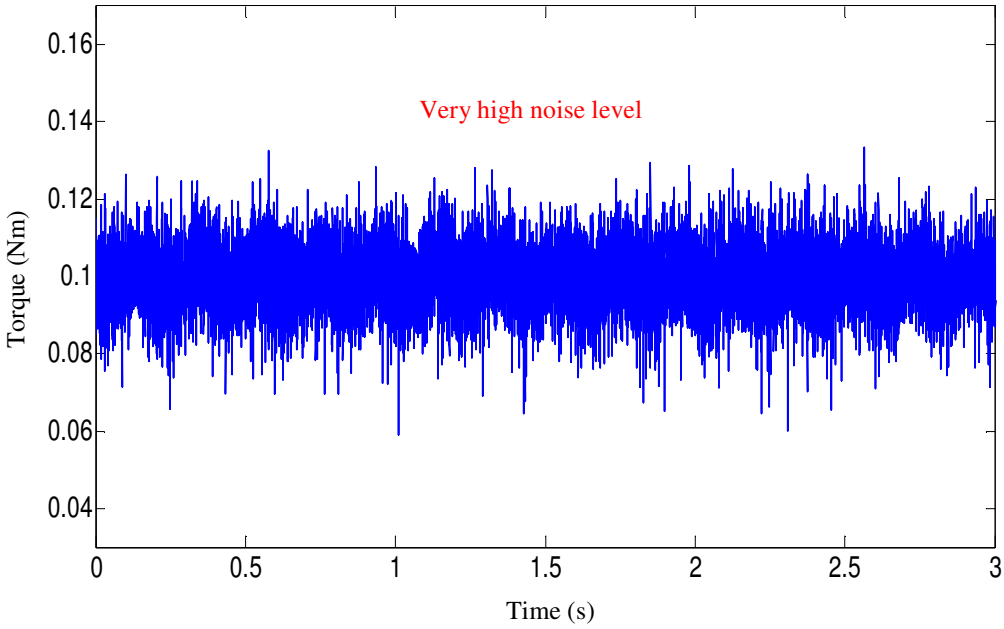

Fig. 4.10. Torque response estimated by friction-free DOB using conventional velocity estimation with observer pole at 1000 rad/s

Fig. 4.10 shows the experimental result of the torque response estimated by the friction-free DOB using conventional velocity estimation with the observer pole at 1000 rad/s. Since the conventional velocity estimation uses the derivative of the position signal, it is affected by the noise problem. Therefore, when the force-sensing bandwidth is increased to 1000 rad/s, the torque response estimated by the friction-free DOB using conventional velocity estimation is totally corrupted by noise. Apparently, the signal-to-noise ratio (SNR) of the HDOB using conventional velocity estimation becomes worse than that of the HDOB using conventional velocity estimation (the red signal) at a force-sensing bandwidth of 100 rad/s in Fig. 4.8. Therefore, it is impossible for the friction-freDOB using conventional velocity estimation to perform the force-sensing operation at a force-sensing bandwidth of 1000 rad/s.

In order to improve the force-sensing performance by suppressing the noise effect and widening the bandwidth of force sensing using the friction-free DOB, the research proposes force control based on the friction-free DOB and a Kalman filter. The proposed method is introduced in the next section.

4.4 Proposed Force Control Based on Friction-Free Disturbance Observer and Kalman Filtering

4.4.1 Kalman Filter Implementation for Velocity Estimation

The performance of force estimation using the friction-free DOB is related to how the velocity is properly estimated. However, since conventional velocity estimation, which is achieved by the derivative of position information, is susceptible to the effect of noise, the force-sensing performance of the friction-free DOB is also degraded by the noise problem.

Therefore, to address the noise problem, a Kalman filter is exploited for velocity estimation [66]. Kalman filter is widely used in motion control applications and is a powerful solution to estimate the state of a process by minimizing the mean of the squared error [67-75]. Using the Kalman filter, we can reduce the noise of the measurement system effectively. As a result, the performance of the control system and the force-sensing bandwidth can be improved.

In the research, velocity estimation by Kalman filtering is based on the angular information measured by an encoder. The Kalman filter estimates the state of the measuring process, formulated in the following equations.

$$x_{(k+1)} = \boldsymbol{A}x_{(k)} + \boldsymbol{B}u_{(k)} + w_{(k)} \tag{4.22}$$

$$z_{(k)} = \boldsymbol{H}x_{(k)} + v_{(k)} \tag{4.23}$$

where

$$\boldsymbol{A} = \begin{bmatrix} 1 & T_s & 0.5T_s^2 \\ 0 & 1 & T_s \\ 0 & 0 & 1 \end{bmatrix}, \boldsymbol{B} = \begin{bmatrix} 0 \\ 0 \\ 0 \end{bmatrix}, \boldsymbol{H} = \begin{bmatrix} 1 & 0 & 0 \end{bmatrix} \tag{4.24}$$

Here, $x_{(k)}$ is the vector of the estimated states, including the angular position θ_m, angular velocity $\dot{\omega}_m$, and acceleration ω_m; $z_{(k)}$ is the measured angular information, which is corrupted by noise; and $u_{(k)}$ is the known input to the system. The random variables $w_{(k)}$ and

$v_{(k)}$ represent the process noise and the measurement noise, respectively. T_s is the sampling time of the control system, and k is the sampling time index.

In the state-space representation shown in (4.22) and (4.23), both the process noise $w_{(k)}$ and the measurement noise $v_{(k)}$ are assumed to be uncorrelated zero-mean Gaussian white noise with the covariance matrix of process noise, $\boldsymbol{Q}$, and the covariance matrix of measurement noise, $\boldsymbol{R}$. The values of $\boldsymbol{Q}$ and $\boldsymbol{R}$ are used for tuning the accuracy of the filter, and the susceptibility of the Kalman filter to measurement noise depends on $\boldsymbol{Q}$ and $\boldsymbol{R}$. The covariance matrices $\boldsymbol{Q}$ and $\boldsymbol{R}$ are defined as follows.

$$\boldsymbol{Q} = E\left[ww^T \right] = \begin{bmatrix} Q_{11} & 0 & 0 \\ 0 & Q_{22} & 0 \\ 0 & 0 & Q_{33} \end{bmatrix} \tag{4.25}$$

$$\boldsymbol{R} = E\left[vv^T \right] = R_{11} \tag{4.26}$$

where $\boldsymbol{Q}$ and $\boldsymbol{R}$ are nonnegative definite matrices and $E[\ ]$ denotes the expected value. Elements of $\boldsymbol{Q}$ and $\boldsymbol{R}$ are defined as follows.

$$R_{11} = Var\left[\Delta\theta_m\right] \tag{4.27}$$

$$Q_{11} = Var\left[\Delta\theta_e\right] \tag{4.28}$$

$$Q_{22} = Var\left[\Delta\omega_e\right] \tag{4.29}$$

$$Q_{33} = Var\left[\Delta\dot{\omega}_e\right] \tag{4.30}$$

where $Var[\ ]$ denotes variance, $\Delta\theta_m$ is the difference between the measured position and the desired position, $\Delta\theta_e$, $\Delta\omega_e$ and $\Delta\dot{\omega}_e$ are the differences between the predicted values of position, velocity, and acceleration, and the desired values of position, velocity and acceleration, respectively. $\Delta\theta_m$ is calculated from the sets of position data measured by an encoder. $\Delta\theta_e$, $\Delta\omega_e$ and $\Delta\dot{\omega}_e$ are calculated from the sets of filter's predicted values of position, velocity, and acceleration, given the corresponding sets of sample data of position measured by encoder. Variances of $\Delta\theta_m$, $\Delta\theta_e$, $\Delta\omega_e$ and $\Delta\dot{\omega}_e$ are computed as follows.

$$Var[X] = \frac{|X_1 - \mu|^2 + ... + |X_n - \mu|^2}{n} \tag{4.31}$$

where

$$\mu = \frac{X_1 + X_2 + ... + X_n}{n} \tag{4.32}$$

X stands for $\Delta\theta_m$, $\Delta\theta_e$, $\Delta\omega_e$ or $\Delta\dot{\omega}_e$, and n is the data number of the sample data set.

The value of matrix $\boldsymbol{R}$ can be easily determined based on the available measured position data, and equations (4.27), (4.31) and (4.32). The values of matrix $\boldsymbol{Q}$ are selected by trial and error. The trial and error process is carried out by fixing $\boldsymbol{R}$ value, running Kalman filter offline with the data set of measured position, obtaining the data sets of predicted values, calculating $\boldsymbol{Q}$ values based on (4.28), (4.29), (4.30), (4.31) and (4.32), and running filter again. The selected values of $\boldsymbol{Q}$ are those enabling the estimated state of filter to achieve the proper values.

To operate Kalman filter, the initial value of the state and the estimation error covariance must be provided. These initial conditions are usually chosen arbitrarily and affect the results of how the filter operates. If the filter is given poor initial conditions, it is possible for the filter to get the poor initial estimate of the state or fail to converge to the true value of the state. In the research, the initial of the state is chosen to be zero, and the process noise covariance is used for the initial estimation error covariance.

The algorithm of the Kalman filter is described in section 3.3.1 in chapter 3. The updated velocity estimation by Kalman filtering is applied to the friction-free DOB to obtain force information as shown in Fig. 4.11. A block diagram of the proposed force control using the friction-free DOB and the Kalman filter is shown in Fig. 4.11. Based on the torque variation between the torque command and the estimated torque, the proportional controller is formulated as follows.

$$I_m = (T_{cmd} - \hat{T}_{dis}) K_f \frac{J_{mn}}{K_{tn}} + \hat{T}_{dis} \frac{1}{K_{tn}} \tag{4.33}$$

where T_{cmd} and K_f are the torque command and force control gain, respectively.

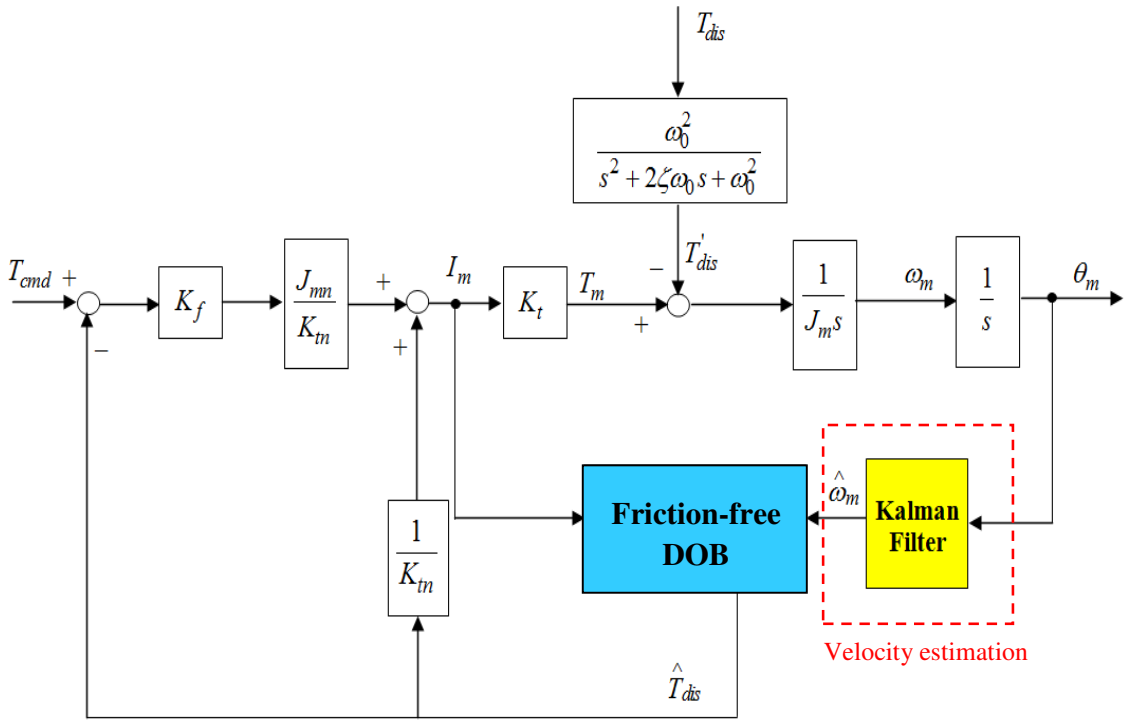

Fig. 4.11. Block diagram of the proposed force control based on the friction-free DOB and the Kalman filter

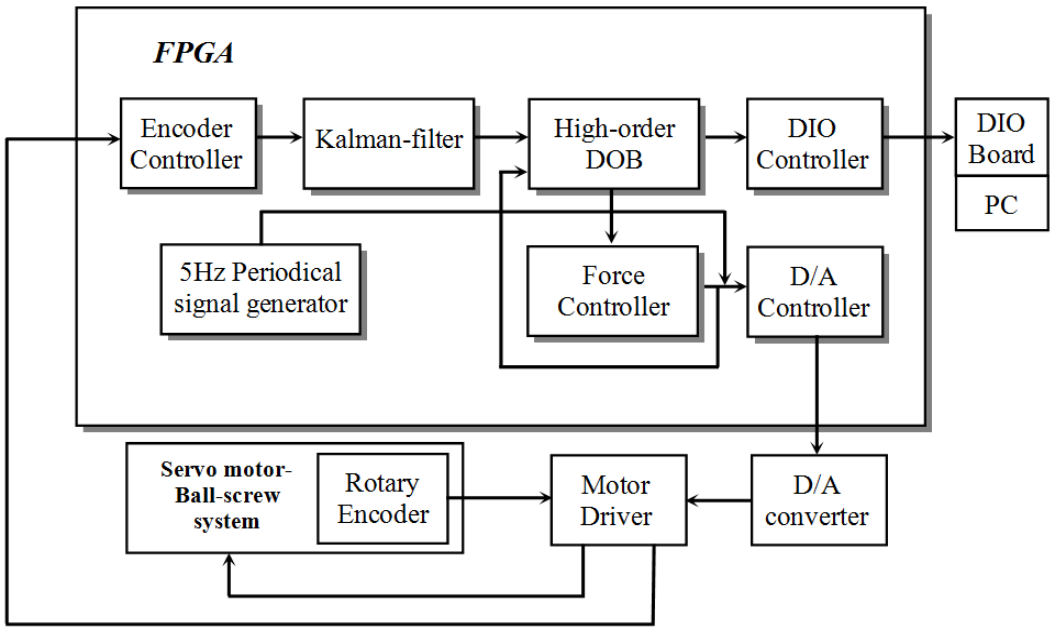

Fig. 4.12. Block diagram of FPGA implementation of the force control based on friction-free DOB and Kalman filter

4.4.2 FPGA Implementation of Force Control

Since the proposed method has a complex algorithm, the FPGA implementation is to achieve the short sampling period of the control cycle and widen force sensing bandwidth. All of the algorithms of force control using friction-free DOB with dither method and Kalman filter are configured as FPGA hardware architecture. The algorithms are constructed with arithmetic fixed point to create the hardware-based controller in FPGA. In the research, the fixed point format has 42-bit length with 1 sign bit, 28 bits of integer part, and 13 bits of fractional part. The FPGA configuration for the proposed force control was established using the hardware description language VHDL. Even the control algorithm is very complicated, the system achieves the short sampling time of control system of $5\,\mu s$ that is difficult for CPU-based or DSP-based controllers to achieve such a short sampling period. The sampling time of $5\,\mu s$ is the minimum sampling period that ensures the proper performance of the force controller. Here, although the friction compensation based on dither signal is not new, the implementation of all techniques of dither, friction-free DOB, Kalman filter and force control in FPGA to achieve high sampling rate makes the proposed method unique. The FPGA used in this paper is the Stratix II-EP2S60 manufactured by Altera. The FPGA board has a clock frequency of 100 MHz.

Fig. 4.12 illustrates the FPGA internal architecture of the proposed force control using friction compensation based on an friction-free DOB and a Kalman filter. The FPGA implementation contains the following modules.

An encoder controller module was designed to detect and calculate angular information from incremental pulses derived from a rotary encoder.

A Kalman filter module was constructed to estimate velocity information from the angular information provided by the encoder controller module.

A periodic signal generator module was used to create the additional 5-Hz signal to insert into the reference signal for friction compensation.

The friction-free DOB and force controller modules perform the algorithm shown in Fig. 4.11 to generate the motor control current.

A digital-to-analog (D/A) converter controller module was used to regulate the control signals of a 16-bit D/A converter, which is used to transform the motor control signal from a digital signal to an analog signal. The output signal of the D/A converter was utilized to operate the servo motor driver.

For data acquisition in a PC, a digital input/output (DIO) controller module was constructed. It controls the transmission of integer data to a DIO board using a handshake technique.

4.5 Experimental Results

Fig. 4.13 depicts the experimental devices used in the research. The FPGA board used here is the Altera Stratix II-EP2S60F1020C3, the actuator is a THK SKR-type ball screw, and the servo motor is the SGMAH of Yaskawa. Table 4.1 shows the parameters used in the experiments.

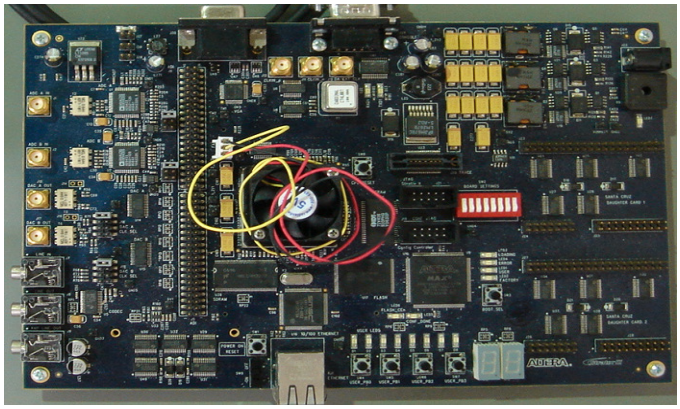

(a) FPGA board

(b) Servo motor with a ball screw

Fig. 4.13. Experimental devices

Table 4.1. Experimental parameters

ζ	0
f_0	5 Hz
$\omega_0 = 2\pi f_0$	31.4 rad/s
Motor inertia J_m	$0.173 \times 10^{-4} kgm^2$
Torque coefficient K_t	0.498 Nm/A
Motor pole pair number	2
Torque command	0.1 Nm
Sampling time	$5\mu s$

To verify the effectiveness of the proposed method, the force control experiments are conducted with the ball-screw system. In the experiments, the control system performs the torque tracking with a constant torque command of 0.1 Nm under a constant velocity of 10.5 rad/s; the sampling period of the FPGA-based force control system is 5 μs.

The first experiment is carried out to investigate the force-sensing performance of the proposed friction-free disturbance observer using the Kalman filter. In this experiment, the force estimation by the friction-free DOB using the Kalman filter is examined in comparison with that by the friction-free DOB using conventional velocity estimation and that by the conventional DOB in the presence of an additional periodic signal. The observer poles of the friction-free DOB and the conventional DOB and the cut-off frequency of the conventional velocity estimation are all set to 100 rad/s. The force control scheme based on the friction-free DOB and the Kalman filter is shown in Fig. 4.11, and the force control scheme using the friction-free DOB with conventional velocity estimation is displayed in Fig. 4.6. The experimental results are shown in Fig. 4.14.

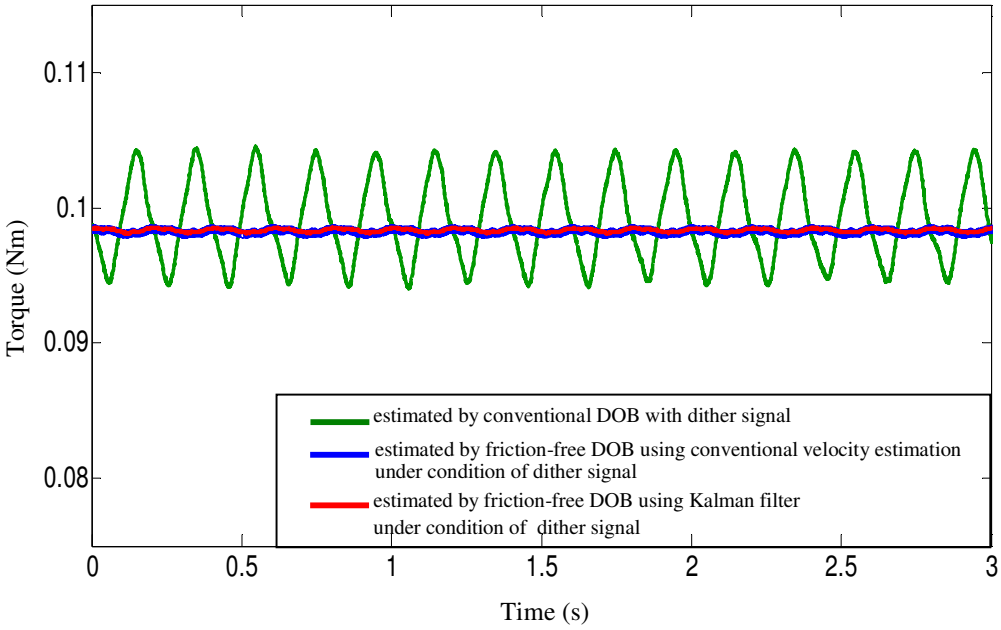

Fig. 4.14. Torque response estimated by conventional DOB, friction-free DOB using conventional velocity estimation, and friction-free DOB using Kalman filter with observer pole at 100 rad/s

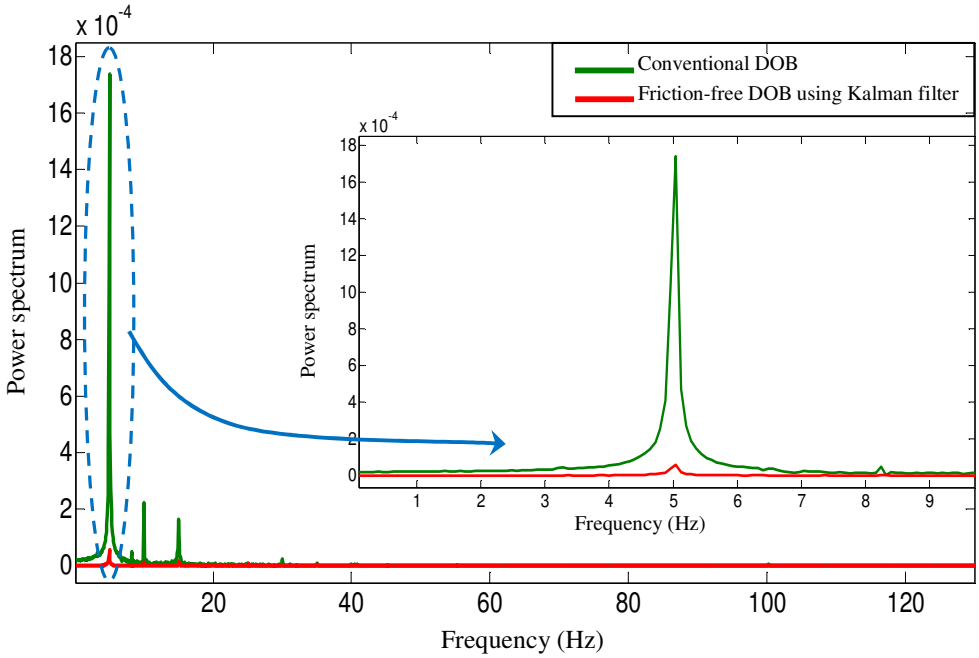

Fig. 4.15. FFT of torque responses in Fig. 4.14 corresponding to conventional DOB and friction-free DOB using Kalman filter under condition of additional periodic signal of 5 Hz and observer pole at 100 rad/s

The results in Fig. 4.14 indicate that, at a force-sensing bandwidth of 100 rad/s, the force-sensing performances of both the friction-free DOB using the Kalman filter and the friction-free DOB using conventional velocity estimation obtain almost the same torque responses with an effective oscillatory disturbance rejection when compared to the torque estimated by the conventional DOB in the presence of an additional periodic signal of 5 Hz. Obviously, the SNR of the signal estimated by the friction-free DOB with the Kalman filter (the red signal) and the SNR of the signal estimated by the friction-free DOB without the Kalman filter (the blue signal) are almost the same. These results ensure the effectiveness of the proposed force sensing based on the friction-free DOB and the Kalman filter in the case of periodic signal exclusion and friction reduction. The FFT analyses in Fig. 4.15 provide more evidence of efficient periodic component elimination for the friction-free DOB using Kalman filter.

However, similar to the case in Fig. 4.8, in this case, the force-sensing bandwidth is only 100 rad/s, which is a narrow bandwidth. To improve the force-sensing performance, a wider force-sensing bandwidth is required. Therefore, to further clarify the effectiveness of the proposed method, the research increases the force-sensing bandwidth to 1000 rad/s and investigated the performance of the proposed friction-free DOB using the Kalman filter, the friction-free DOB using conventional velocity estimation, and the conventional DOB, all in the presence of a dither signal of 5 Hz.

The force-sensing bandwidth is determined by the observer pole. Increasing the force-sensing bandwidth is achieved by increasing the observer pole. The cut-off frequency of the conventional velocity estimation is also set to 1000 rad/s. The force control schemes corresponding to the three methods are illustrated in Figs. 4.11, 4.6, and 4.1, respectively. The experimental results are shown in Figs. 4.16 and 4.17.

Fig. 4.16 displays the experimental result of the torque response estimated by the conventional DOB in the presence of the 5-Hz additional periodic signal with an observer pole of 1000 rad/s. The estimated torque with the conventional DOB is oscillatory and is affected by the high noise level. Obviously, the SNR of the signal in this case is worse than those of the signals in Fig. 4.14 at a bandwidth of 100 rad/s.

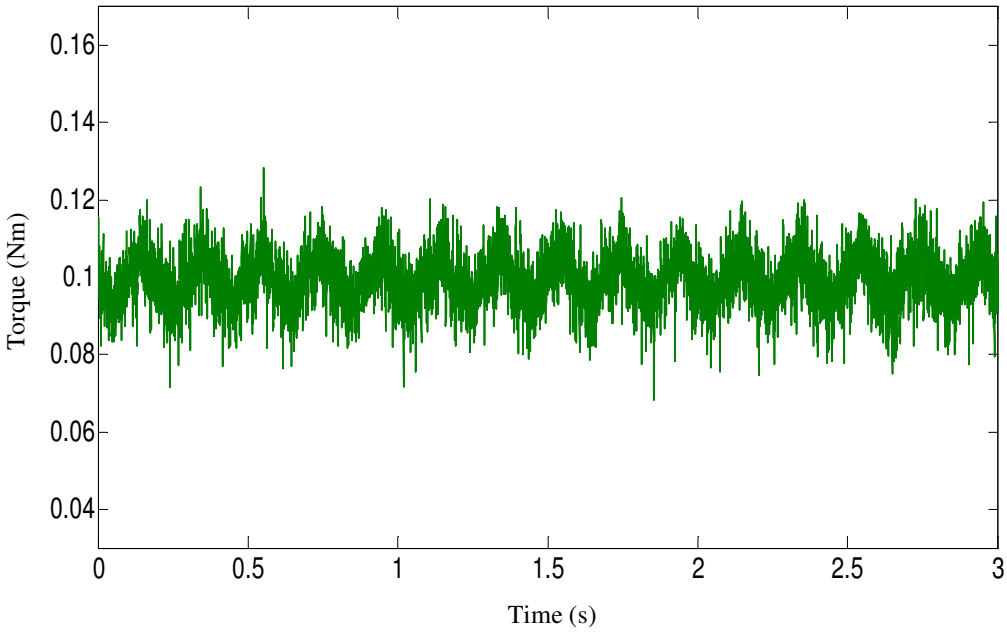

Fig. 4.16. Torque response estimated by conventional DOB under condition of 5-Hz dither with observer pole 1000 rad/s

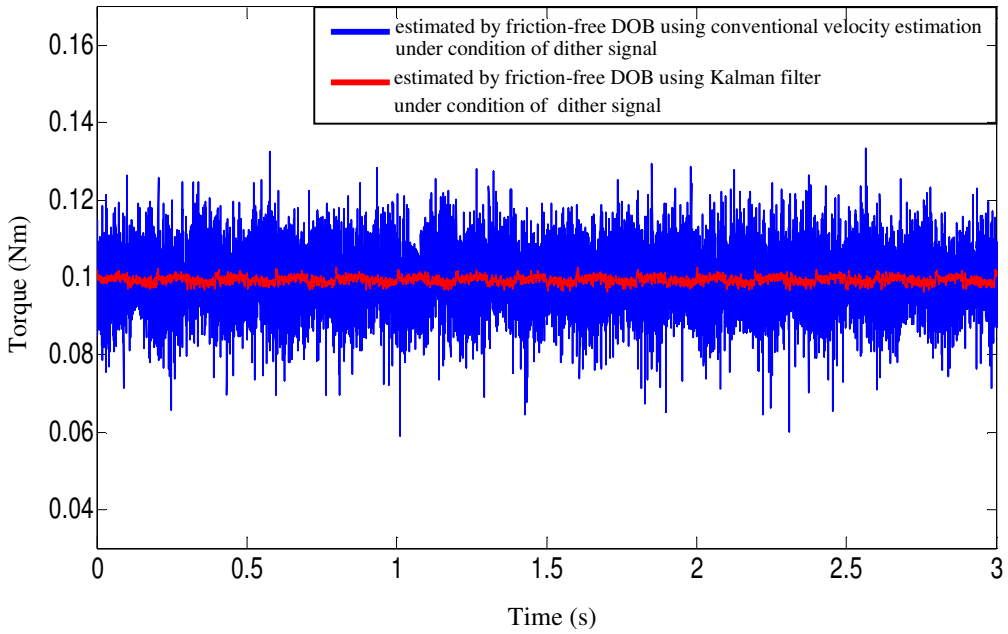

Fig. 4.17. Torque responses estimated by friction-free DOB using Kalman filter and friction-free DOB using conventional velocity estimation with observer pole at 1000 rad/s

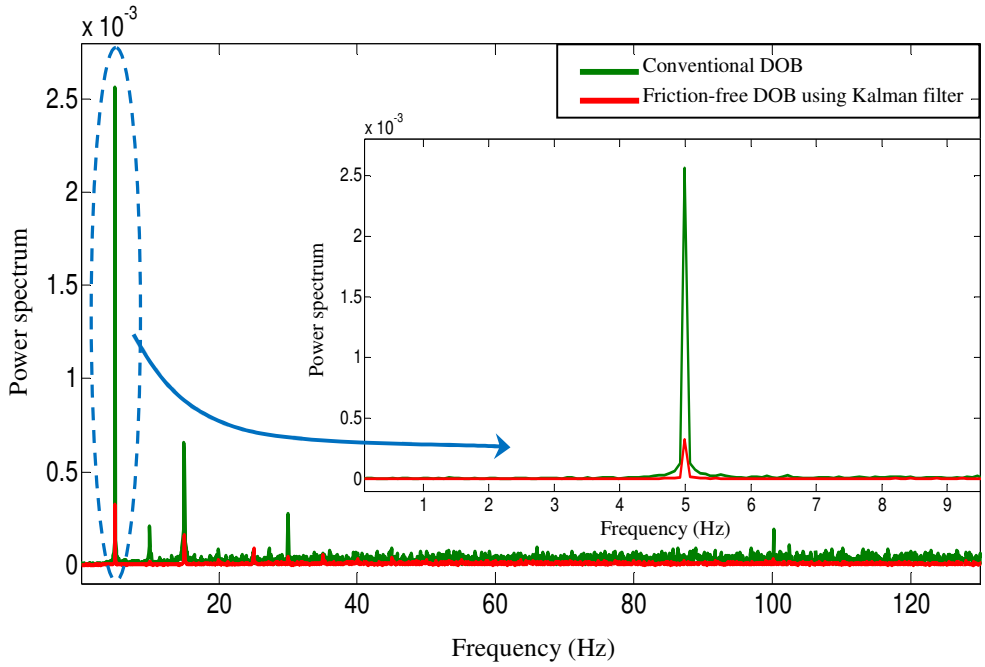

Fig. 4.18. FFT of torque responses corresponding to conventional DOB and friction-free DOB using Kalman filter under condition of additional dither signal 5Hz and observer pole at 1000 rad/s

Fig. 4.17 shows the experimental results of the torque responses estimated by the proposed friction-free DOB using the Kalman filter and by the friction-free DOB using conventional velocity estimation in the presence of an dither signal of 5 Hz when the force-sensing bandwidth is increased to 1000 rad/s. The signal estimated by the friction-free DOB without the Kalman filter (the blue signal) is strongly corrupted by the very high noise level. However, the signal estimated by the friction-free DOB using the Kalman filter (the red signal) is radically improved because the noise in the estimated torque is suppressed effectively and the oscillatory disturbance is also reduced. Apparently, the SNR of the signal estimated by the friction-free DOB using the Kalman filter is improved compared to that of the signal estimated by the friction-free DOB without the Kalman filter. The FFT analyses of the torque responses in Fig. 4.18 clarify the proposed method's efficiency in suppressing the 5-Hz periodic component.

From the above experimental results, it is confirmed that the proposed force control using the friction-free DOB and the Kalman filter achieves high-performance force sensing with a widened bandwidth of 1000 rad/s based on the friction-free and noise-free force observation.

To evaluate how much the performance is improved by our method, the research compares the signal-to-noise ratio (SNR) of the signals estimated by the friction-free DOB using the Kalman filter and the friction-free DOB using conventional velocity estimation in Figs. 4.14 and 4.17. Table 4.2 shows the comparison of the SNRs.

The comparison in Table 4.2 shows that the SNRs of the friction-free DOB using the Kalman filter and the friction-free DOB using conventional velocity estimation are almost similar at the force-sensing bandwidth of 100 rad/s. However, when the force-sensing bandwidth is increased to 1000 rad/s, the SNR of the proposed method (the friction-free DOB with the Kalman filter) is improved to 842.8% compared to that of the friction-free DOB without the Kalman filter.

In Fig. 4.14, there is a steady-state error in the torque estimated by the friction-free DOB with the observer pole at 100 rad/s. The investigation of the relationship between the steady-state error and the observer pole of the friction-free DOB using the Kalman filter is conducted experimentally at different observer pole positions of 50 rad/s, 100 rad/s, 200 rad/s, 300 rad/s, and 1000 rad/s, and the results are shown in Fig. 4.19.

Table 4.2. Comparison of signal-to-noise ratios (SNRs)

Force sensing bandwidth	**100 rad/s**	**1000 rad/s**
SNR of friction-free DOB without Kalman filter ($SNR_{withoutKM}$)	869	14
SNR of friction-free DOB with Kalman filter (SNR_{withKM})	862	118
SNR_{withKM}/ $SNR_{withoutKM}$ (%)	99.2%	842.8%

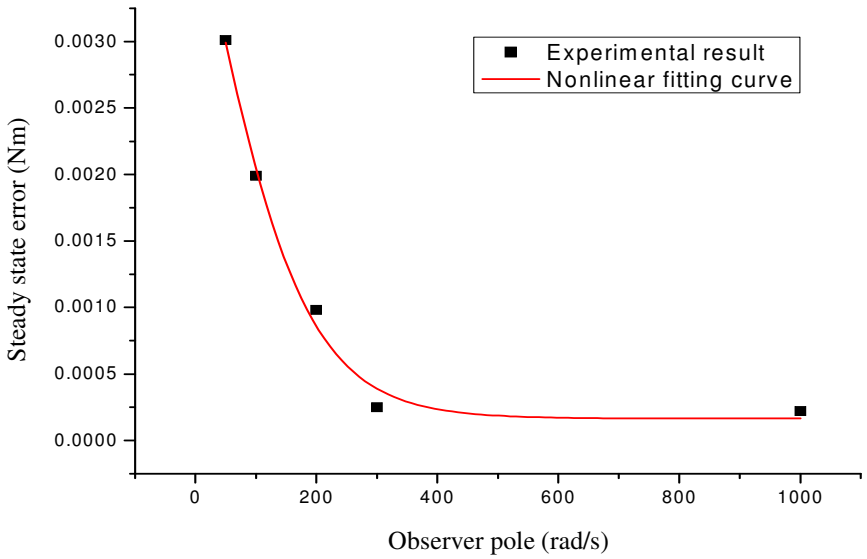

Fig. 4.19. Experimental result of the relationship between the steady-state error and the observer pole of the friction-free DOB using Kalman filter

The experimental result in Fig. 4.19 shows that at observer poles of 300 rad/s and 1000 rad/s, the steady-state error in the estimated torque is minimum. In the proposed method, the friction-free DOB using the Kalman filter operates with an observer pole at 1000 rad/s, achieving high-performance force sensing, and at this observer pole position, the effect of the steady-state error can be neglected.

To further verify the effectiveness of the proposed method, the research conducted the following experiments.

First, the research investigated the force-sensing performance of the conventional DOB without a dither signal at force-sensing bandwidths of 100 rad/s and 1000 rad/s. In these experiments, torque responses are estimated by the conventional DOB in two cases: without the Kalman filter (only using conventional velocity estimation) and with the Kalman filter for velocity estimation. Figs. 4.20 and 4.21 show torque responses estimated by the conventional DOB without a dither signal at bandwidths of 100 rad/s and 1000 rad/s, respectively.

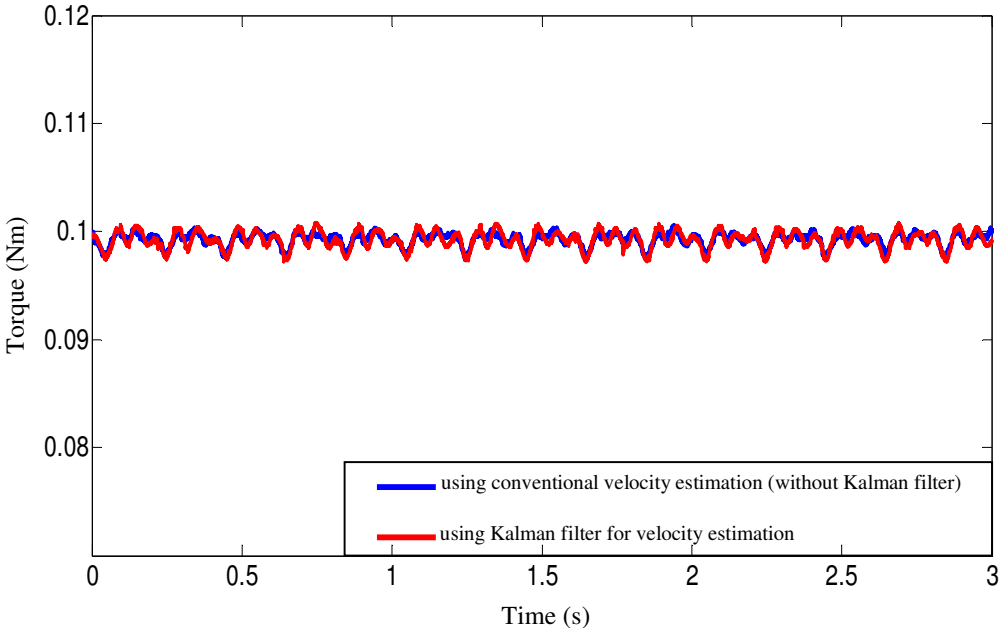

Fig. 4.20. Torque responses estimated by conventional DOB without dither signal for observer pole at 100 rad/s

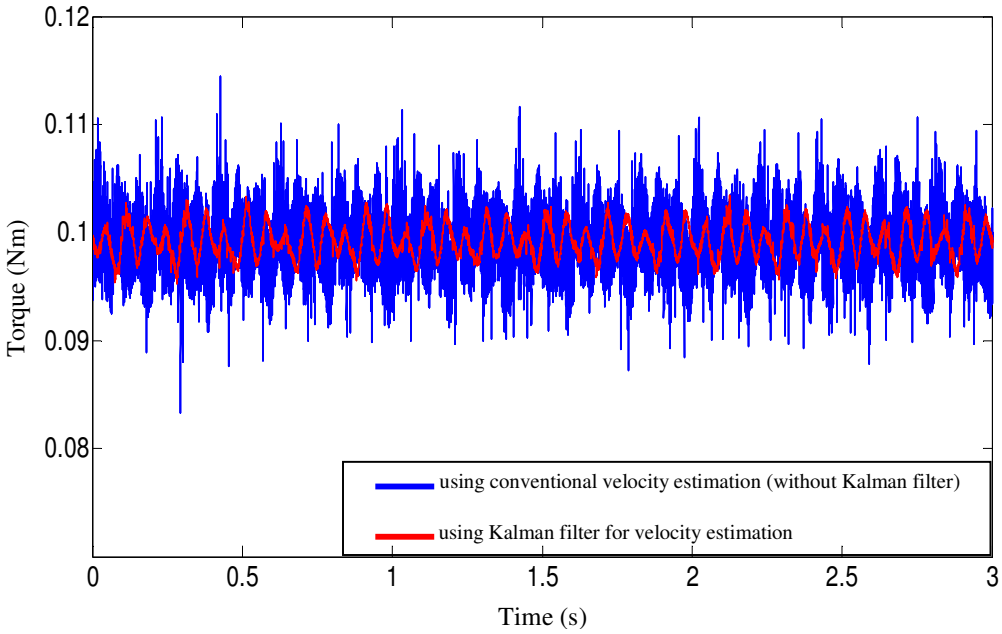

Fig. 4.21. Torque responses estimated by conventional DOB without dither signal for observer pole at 1000 rad/s

In Fig. 4.20, both the conventional DOB without Kalman filtering and conventional DOB with Kalman filtering obtain similar unsmooth torque responses (shown by the blue and red signals in the figure, respectively) due to the effect of friction. It is also obvious that the SNRs of the signals estimated by both methods are almost the same at the force-sensing bandwidth of 100 rad/s.

In Fig. 4.21, when the force-sensing bandwidth is increased to 1000 rad/s, the SNR of the signal estimated by the conventional DOB without the Kalman filter (the blue signal) becomes worse than that of the signal estimated by the conventional DOB with the Kalman filter (the red signal). In this result, applying the Kalman filter to the conventional DOB can only effectively reduce noise in the estimated torque and improve the bandwidth of force sensing; however, the friction still affects the force estimation and also results in an unsmooth torque response (the red signal).

Next, the research compares the force-sensing performance of the conventional DOB using the Kalman filter without the dither signal and the friction-free DOB using the Kalman filter with the dither signal with the observer pole at 1000 rad/s. The experimental results are shown in Fig. 4.22.

In Fig. 4.22 (a), the impact torque responses occur when the ball screw contacts the iron environment. The results in Fig. 4.22 show that the noise problem in the estimated torque is reduced by both force-sensing methods owing to the employment of the Kalman filter. Fig. 4.22 (c) and (d) indicates that the estimated torque responses of the static state and of the impact motion by the two methods are also similar. However, using the conventional DOB with the Kalman filter and without the dither signal, the estimated torque response still shows the effect of friction during the moving state as shown in Fig. 4.22 (b). Using the friction-free DOB with the Kalman filter and with the dither signal, the oscillatory component is decreased, and the effect of friction in the estimated torque response of the moving state is also reduced as shown in Fig. 4.22 (b). The results in Fig. 4.22 prove that the proposed method is superior to the conventional method.

Therefore, to improve the performance of force sensing by reducing the effect of friction on force estimation and increasing the force-sensing bandwidth, application of the dither signal and using the friction-free DOB with a Kalman filter is an effective method.

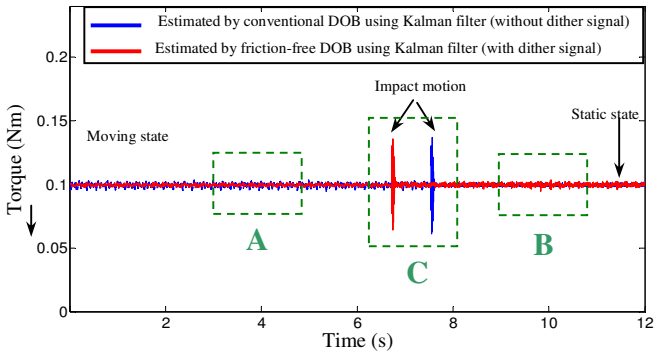

(a) Torque responses of moving state, static state and impact motion with observer pole at 1000 rad/s.

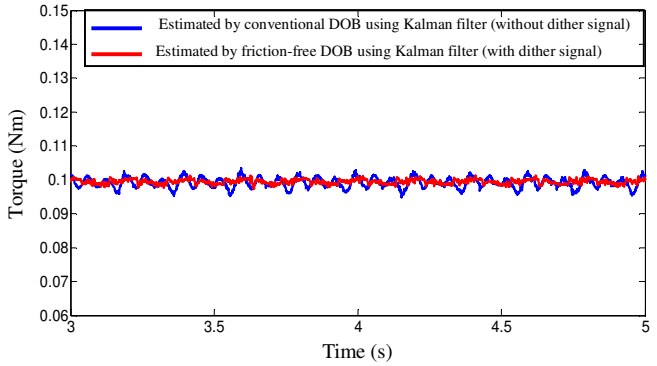

(b) Magnification of torque responses of **A** area (moving state) in Fig. 4.22 (a).

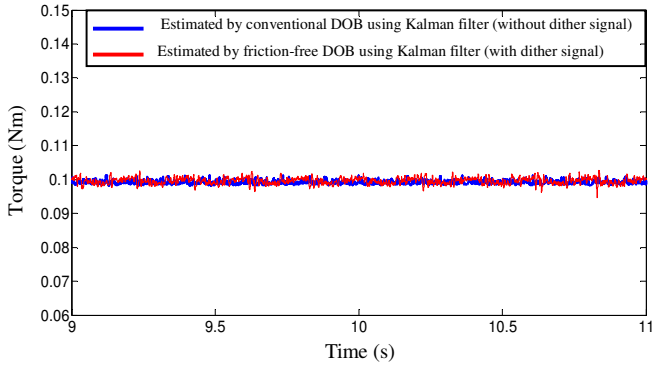

(c) Magnification of torque responses of **B** area (static state) in Fig. 4.22 (a).

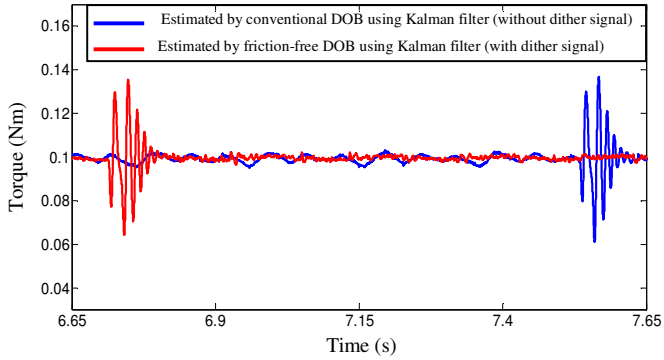

(d) Magnification of torque responses of **C** area (impact motion) in Fig. 4.22 (a).

Fig. 4.22. Torque responses estimated by conventional DOB using Kalman filter (without dither signal) and friction-free DOB using Kalman filter (with dither signal) at bandwidth of 1000 rad/s

Additionally, to investigate the effect of the additional periodic signal on the stability of the control system, an experiment was carried out to measure the acceleration with an acceleration sensor. In this experiment, the acceleration sensor is mounted on the moving part of a ball-screw system. The force control scheme implemented in the ball-screw system here utilizes the proposed friction-free DOB and the Kalman filter as shown in Fig. 4.11. The frequency and amplitude of the additional periodic signal are the same as in the previous experiments. The experimental setup of the acceleration measurement is shown in Fig. 4.23, and the experimental result of the acceleration response is displayed in Fig. 4.24. The experimental result in Fig. 4.24 corresponds to the three states of the acceleration response: the moving state, the static state, and the impact motion. The impact acceleration response occurs when the moving part of the ball-screw system collides with an iron bar.

The acceleration response in Fig. 4.24 shows that during the operation of force control of the ball-screw system, the acceleration signals of the moving state and static state of the ball screw have no observed vibration. This result indicates that the additional periodic signal does not affect the system stability. The validity of the proposed method is confirmed by this experimental result.

4.6 Conclusions

The research proposes a method to achieve a wideband force control system based on friction-free and noise-free force observation. The friction compensation in the force estimation is carried out by adding a periodic signal into the control system. The force-sensing operation is performed by the combination of a friction-free disturbance observer and a Kalman filter. The influence of the periodic signal on force estimation is rejected by the friction-free disturbance observer. The force-sensing bandwidth is widened to 1000 rad/s due to the effective noise suppression by using a Kalman filter. The utilization of an FPGA to implement all of the control algorithms provides the fast sampling time of 5 μs that also contributes to the ability to widen the force-sensing bandwidth and ensure the performance of the control system with a highly complex computation algorithm. The experimental results have verified the effectiveness of the proposed method. The proposed method is useful for applications such as robots, machine tools, and bilateral control systems.

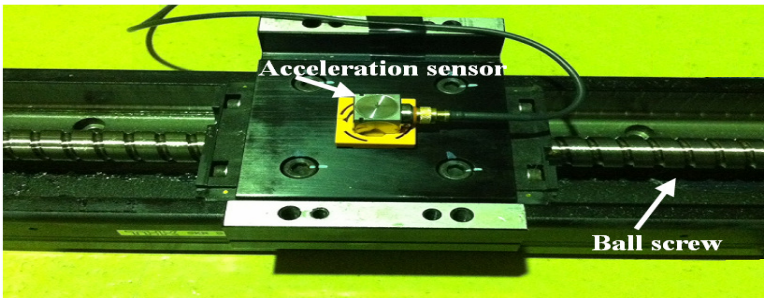

(a) Ball-screw system in free motion condition

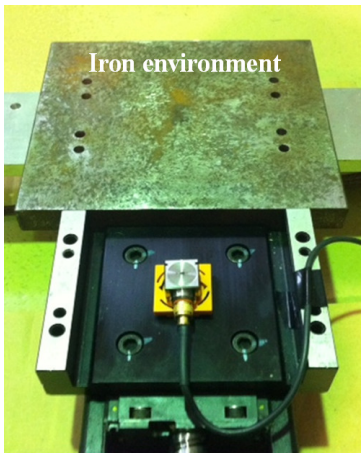

(b) Ball-screw system contacts environment

Fig. 4.23. Experimental setup of acceleration measurement

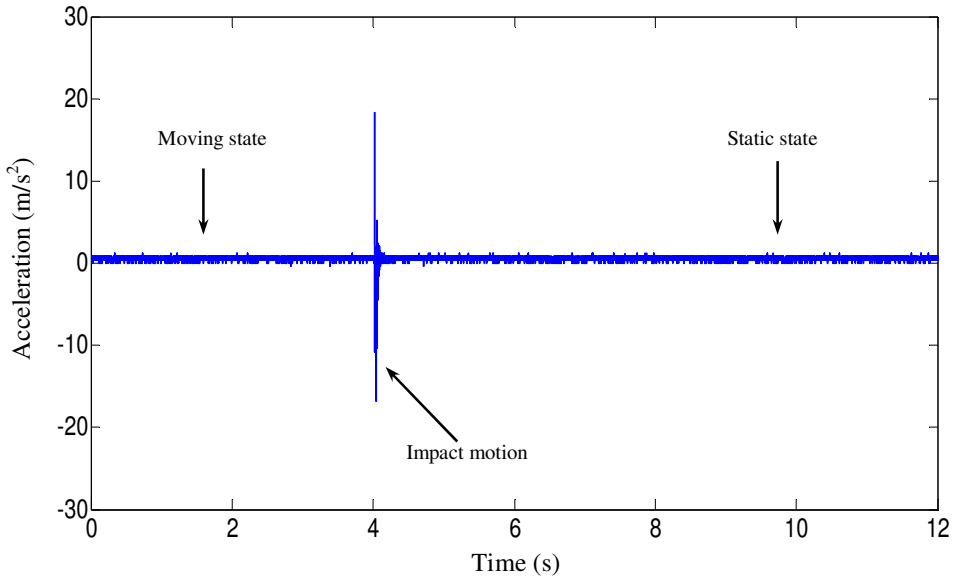

Fig. 4.24. Experimental result of acceleration response of control system using the proposed method

Chapter 5

High Performance Power Assisted Bilateral Control System of Different Configurations Based on Friction-Free Force Observer

5.1 Introduction

Recently, bilateral control has undergone considerable development for haptics and human–robot interaction applications [76-79]. In a bilateral control system, human operator is in contact with the master device and the slave device is in contact with the environment. Human operator manipulates the master device to assign tasks to the slave side. The slave device senses the interaction force with the environment and transmits force to the master side so that the operator can perceive the task operation as if he/she directly contacts the remote environment. Force information acquisition and transmission in a bilateral control system is very important because it directly affects control performance. Considerable research on bilateral control has been proposed to obtain tactile feedback from the remote environment. However, a large number of bilateral control systems are made up of master and slave devices with matching structures. For applications requiring high loading ability and high stiffness of the slave side while assisting human operators to manipulate flexibly with low operational power through the master manipulator, the master and the slave system should have different structures.

Therefore, in my research, I propose a bilateral control system with differing mechanisms for the master and the slave sides operating as a power-assisted control system. A linear shaft motor and a ball screw perform the roles of the master and the slave, respectively. The use of a frictionless mechanism as the master while the slave mechanism is affected by high friction,

together with an appropriate force scaling ratio between the master and the slave, reduces the effect of friction and enhances the manual capability of the human operator while still allowing the user to perceive the interaction between the slave and the environment. However, the force-sensing performance of the bilateral control system can be degraded because of the friction effect of the ball screw.

In Chapter 4, the thesis has verified the effectiveness of using a friction-free DOB with a dither signal to achieve the high-performance force control of a ball-screw system. Therefore, to improve the force-sensing performance of the bilateral control system, the research implemented a dither signal and a friction-free DOB for force sensing on the slave side. The proposed bilateral control is based on acceleration control and consists of a conventional DOB and a friction-free DOB for the master and the slave, respectively. All the control algorithms are also implemented in the FPGA to achieve a high sampling rate for the control cycle, which enables the force-sensing bandwidth to be widened.

5.2 Bilateral Control with the Same Master and Slave Mechanisms Using Conventional DOB

In bilateral control, position and force matching is important to reproduce environmental impedance. Hence, the objective of bilateral control is described as follows:

$$x_m - x_s = 0 \tag{5.1}$$

$$F_m + F_s = 0 \tag{5.2}$$

where x_m and x_s are the positions of the master and the slave, respectively, and F_m and F_s denote the operational force and reaction force from the environment, respectively. Equations (5.1) and (5.2) denote that both position and force of the bilateral control system should be controlled simultaneously. However, it is impossible to realize position and force control in one axis concurrently because they have opposing control stiffnesses. Therefore, (5.1) and (5.2) are transformed into the dimension of acceleration as follows:

$$\ddot{x}_m - \ddot{x}_s \to 0 \tag{5.3}$$

$$\ddot{x}_m + \ddot{x}_s = 0 \tag{5.4}$$

In the acceleration dimension, (5.3) and (5.4) are rewritten using an orthogonal coordinate transformation in (5.5).

$$\begin{bmatrix} \ddot{x}_c \\ \ddot{x}_d \end{bmatrix} = \begin{bmatrix} 1 & 1 \\ 1 & -1 \end{bmatrix} \begin{bmatrix} \ddot{x}_m \\ \ddot{x}_s \end{bmatrix} \tag{5.5}$$

where x_d denotes the acceleration response of the differential mode and x_c denotes the acceleration response of the common mode. To satisfy (5.3) and (5.4), the acceleration references of the common mode and the differential mode are described as follows:

$$\ddot{x}_c^{ref} = -K_f (F_m + F_s) \tag{5.6}$$

$$\ddot{x}_d^{ref} = -(K_p + sK_v)(x_m - x_s) \tag{5.7}$$

where K_f is the force control gain, K_p is the position control gain, and K_v is the velocity control gain.

Acceleration references of the master and the slave are transformed from the acceleration references of the common mode and the differential mode using a second-order inverse Hadamard matrix, as expressed in (5.8).

$$\begin{bmatrix} \ddot{x}_m^{ref} \\ \ddot{x}_s^{ref} \end{bmatrix} = \frac{1}{2} \begin{bmatrix} 1 & 1 \\ 1 & -1 \end{bmatrix} \begin{bmatrix} \ddot{x}_c^{ref} \\ \ddot{x}_d^{ref} \end{bmatrix} \tag{5.8}$$

The block diagram of bilateral control based on acceleration control is shown in Fig. 5.1. The bilateral control system is configured by the same mechanisms of the master and the slave. The force sensation is performed by the conventional disturbance observer.

However, for applications requiring high loading ability and high stiffness of the slave side while assisting human operators to manipulate flexibly with low operational power through the master manipulator, the master and the slave system should have different structures. Therefore, in my research, I propose a bilateral control system with differing mechanisms for the master and the slave sides operating as a power-assisted control system. The bilateral control system with differing mechanisms is described in the next section.

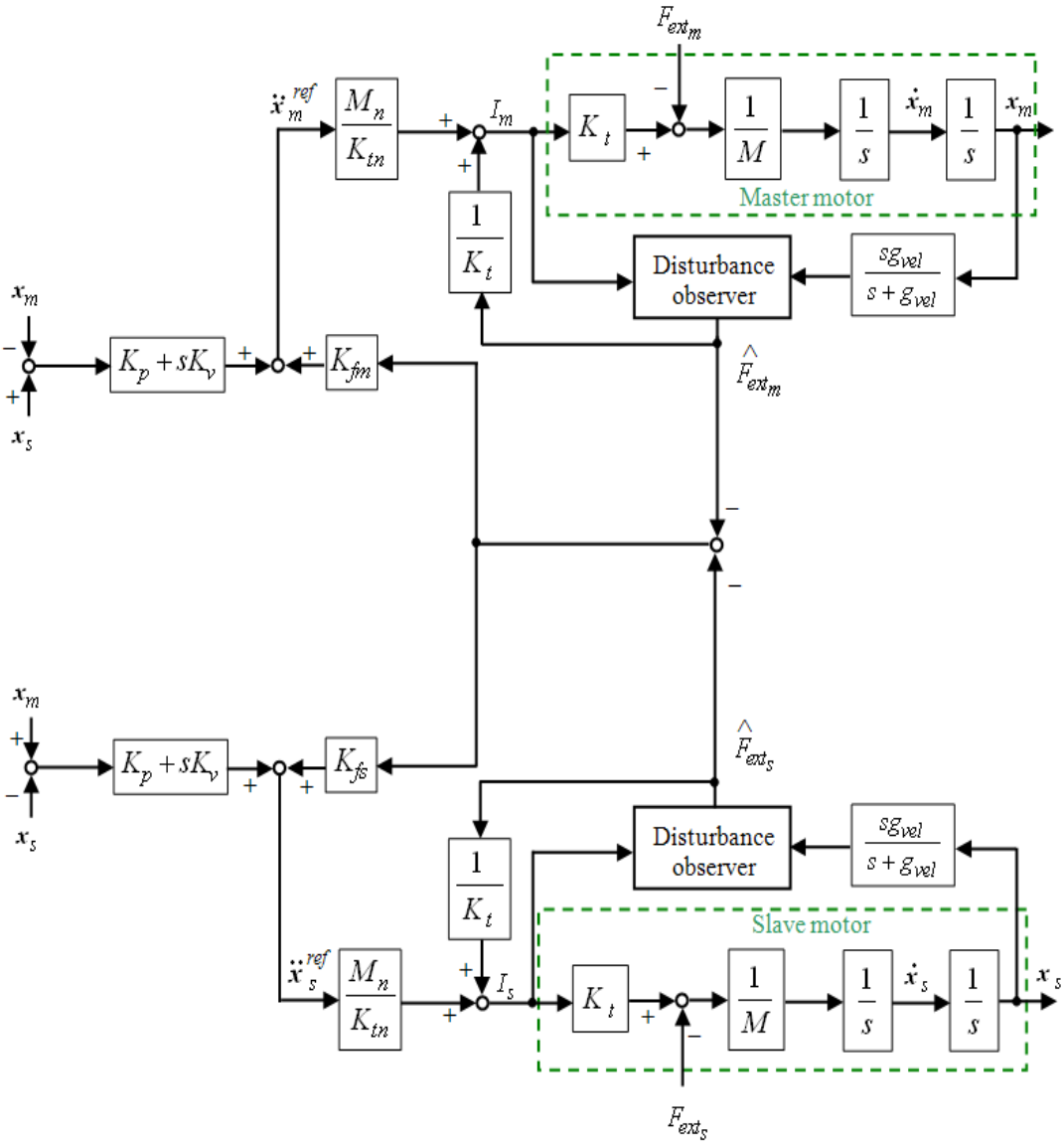

Fig. 5.1. Block diagram of bilateral control with the same master and slave mechanisms using conventional disturbance observer

5.3 Bilateral Control with Different Master and Slave Mechanisms Using Conventional DOB

Fig. 5.2 shows the block diagram of bilateral control based on acceleration control with different mechanisms of the master and the slave. The bilateral control system is configured by a linear motor system as the master and a ball screw system as the slave. The force sensation is performed by the conventional disturbance observer.

In Fig. 5.2, subscripts m and s denote master and slave, respectively. x is the linear distance, θ is the angular distance, $x_s = \alpha\theta_s$, where α is the ratio between the angular distance and the linear distance. K_{fm} denotes the force control gain of the master, and K_{fs} denotes the force control gain of the slave. β is the force scaling ratio between the master and the slave. Here, the master and the slave are differ in terms of their mechanism: the slave system exhibits high friction, and the master is a frictionless system. Therefore, in order to assist the human operator, the scaling factor between the operational force and the reaction force must be taken into account, and the force control gain of the slave is set to a high value. The force scaling ratio β is related to how the operator feels the device. The value of β is determined experimentally to compensate for friction and so that, for the operator, the device is lighter and easier to manipulate.

In the bilateral control system, the measurement of force is very important since the accuracy of the force measurement directly affects the performance of the control system. Some of the problems of force sensing techniques are the effects of friction and harmonic disturbances in force estimation. Friction and harmonic disturbances can degrade the accuracy of motion control system by deteriorating the force measurement performance. The effects of harmonics and harmonics suppression have been considerably addressed in a lot of research [80], [81]. Therefore, it is essential to reduce the effects of friction and residual harmonics on force estimation to improve the control performance. These problems of friction and harmonic disturbances are not addressed by the conventional DOB. Hence, this research proposed the friction-free DOB for the bilateral control with different mechanism of the master and the slave to reduce the effects of friction and harmonic disturbances.

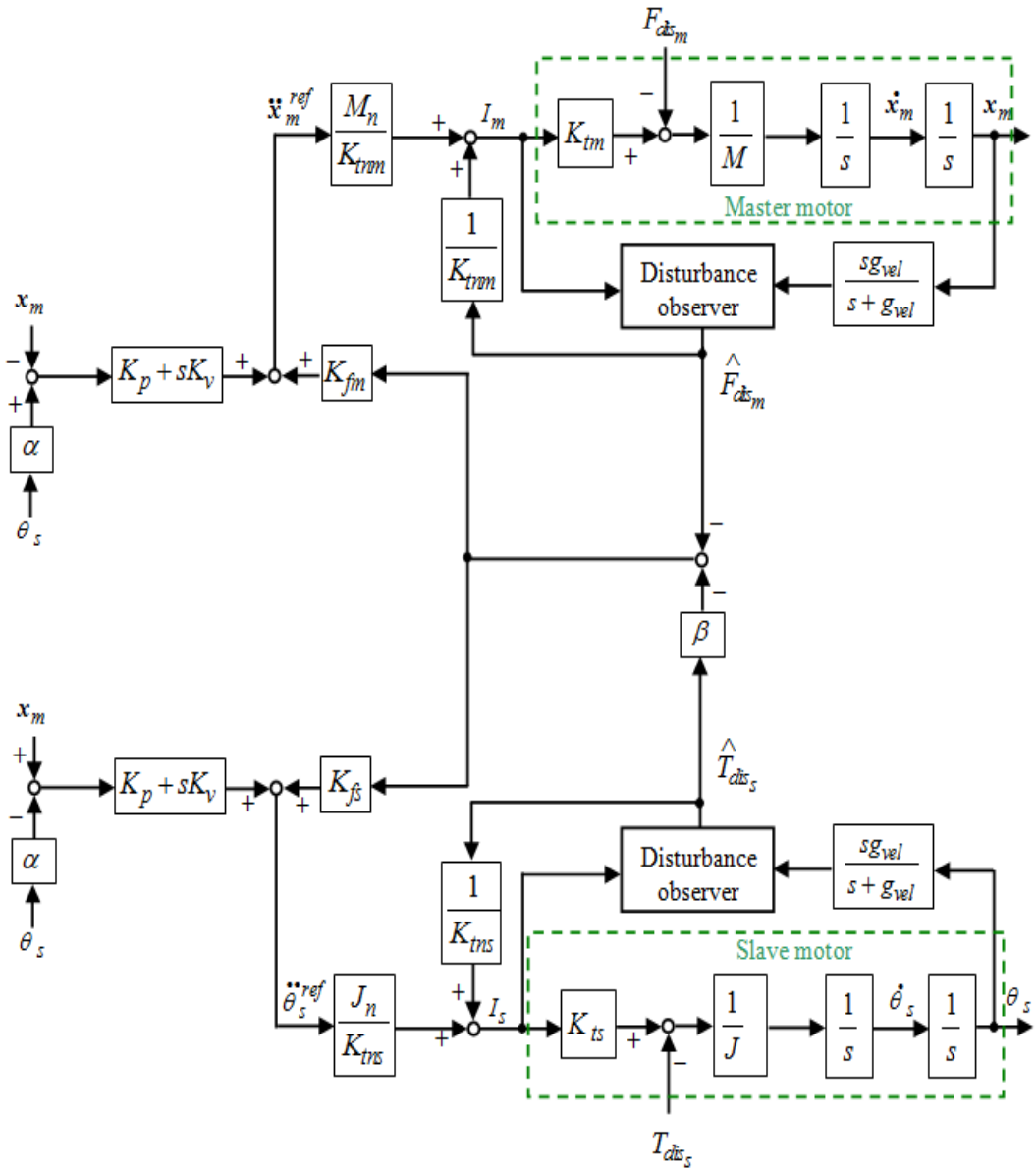

Fig. 5.2. Block diagram of bilateral control with different master and slave mechanisms using conventional disturbance observer

5.4 Proposed Bilateral Control with Different Master and Slave Mechanisms Using Friction-Free Disturbance Observer

Since the bilateral control system employs a ball screw as the slave, force estimation by the conventional DOB is affected by friction. Therefore, to improve the performance of the bilateral control system, the research implemented a dither signal and a friction-free DOB for force sensing on the slave side. Moreover, the friction-free DOB has a great advantage of effectively suppressing harmonic disturbances in force estimation. Therefore, the friction-free DOB can improve force sensing performance by reducing the harmonic distortion. In the proposed method, the conventional DOB is used for force sensing on the master side and the friction-free DOB is employed for force estimation on the slave side. The design and the effectiveness of the friction-free DOB in friction reduction are described in Chapter 4. The block diagram of the bilateral control system with different master and slave mechanisms using the proposed friction-free DOB is shown in Fig. 5.3.

All the control algorithms are also implemented in the FPGA. Because the proposed method has a complex algorithm, the FPGA implementation is to achieve the short sampling period of the control cycle and widen force sensing bandwidth. All of the algorithms of force control using friction-free DOB with dither method, as well as the bilateral control of different mechanism are configured as FPGA hardware architecture. This implementation also makes the proposed method unique.

The algorithms are constructed with arithmetic fixed point to create a hardware-based controller in the FPGA. The FPGA configuration for the proposed control system is established using the hardware description language VHDL. Using a complex control algorithm, the control system achieves a short sampling time of $5\,\mu s$ of the control cycle, which is difficult for conventional CPU-based or DSP-based controllers. The FPGA used in this research is the Stratix IV manufactured by Altera. The FPGA board has a clock frequency of 100 MHz. Fig. 5.4 illustrates the FPGA's internal architecture for the proposed bilateral control system utilizing the friction-free DOB.

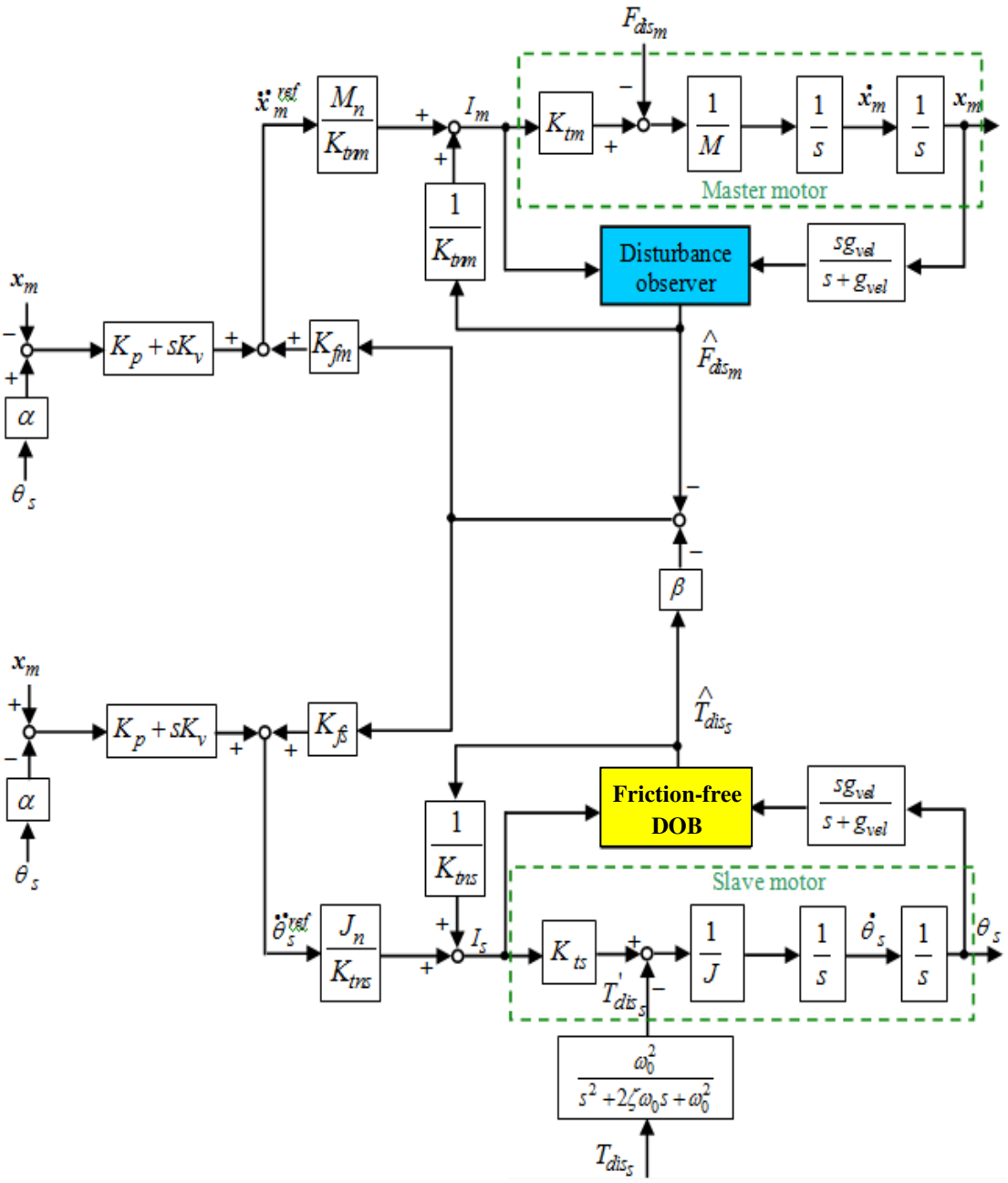

Fig. 5.3. Block diagram of bilateral control with different master and slave mechanisms using friction-free DOB

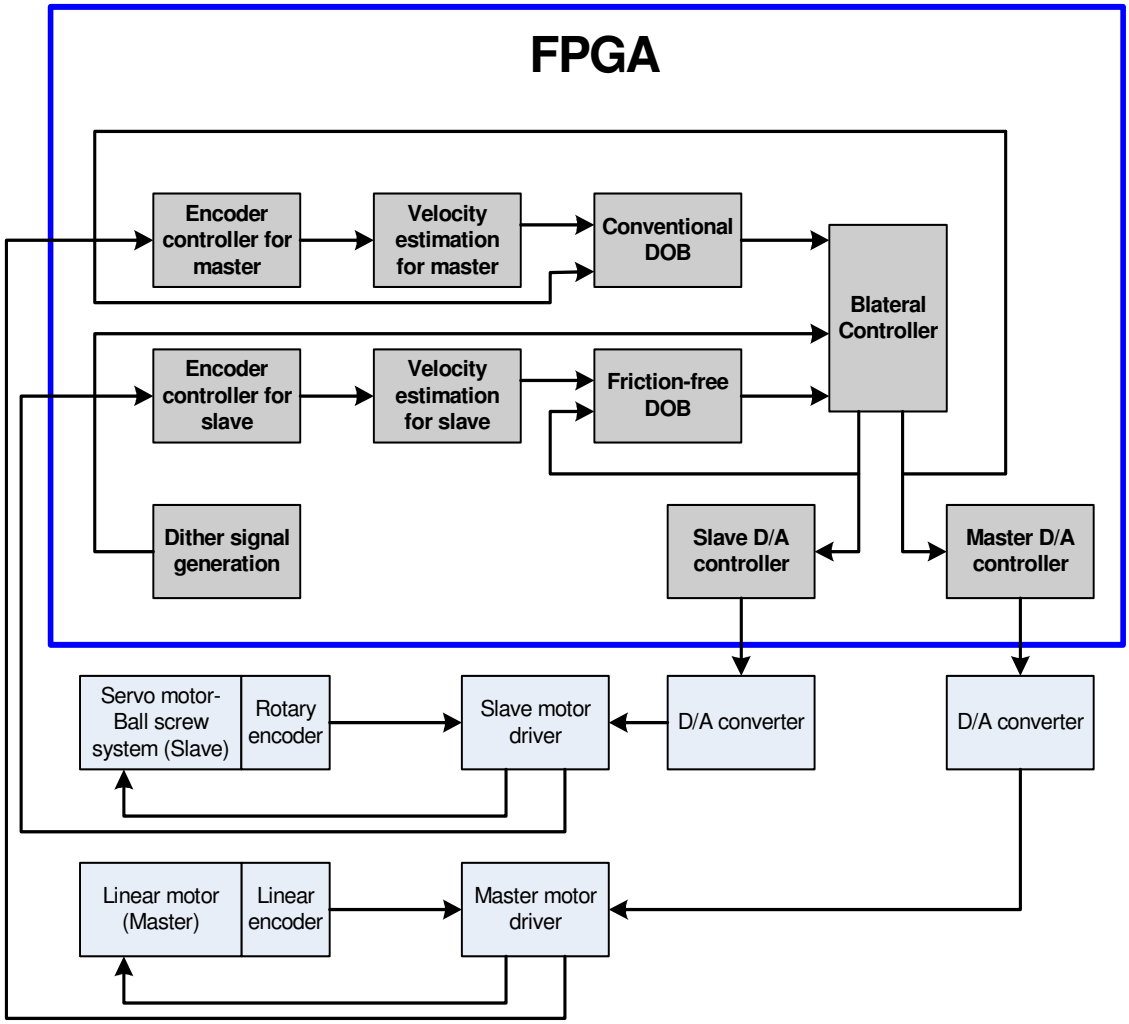

Fig. 5.4. Block diagram of FPGA implementation of bilateral control with different master and slave mechanisms using friction-free DOB

5.5 Experimental Results

To verify the effectiveness of the proposed method, this section describes the experimental results of the bilateral control of a different master–slave mechanism. Figs. 5.5 and 5.6 depict the experimental system. The FPGA used in the experiments is an Altera Stratix IV with a clock frequency of 100 MHz. Table 5.1 displays the parameters used in the experiments.

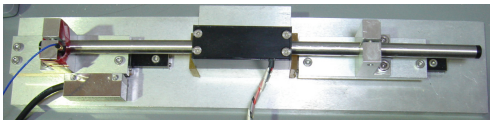

Master device-Shaft linear motor

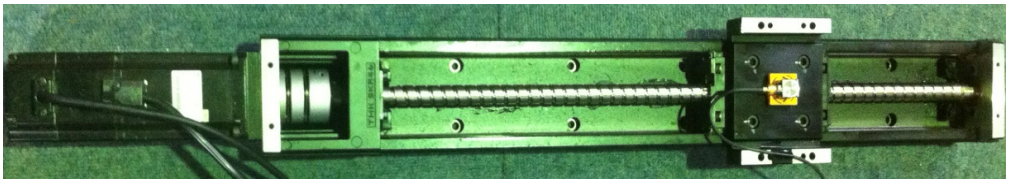

Slave device-Ball screw

Fig. 5.5. Bilateral control system with different master and slave mechanisms

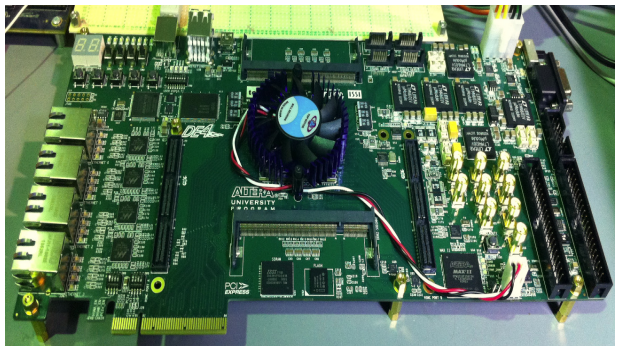

Fig. 5.6. FPGA Stratix IV

Table 5.1. Experimental parameters of bilateral control

Parameters	Values
K_{tm}	3.3 N/A
M	0.18 Kg
K_{ts}	0.498N.m/A
J	0.173×10^{-4} Kg.m^2
K_p	400
K_v	300
K_{fm}	1
K_{fs}	10000
α	0.00159
β	4
Sampling time	5 μs

In the first experiments, the research investigated the performance of the bilateral control system under conditions of a 20-Hz additional periodic signal and an observer pole at 300 rad/s. Because the force control performance of ball-screw system has been investigated with dither frequency of 5Hz in Chapter 4, I would like to confirm the performance of the proposed method with different dither frequency. Therefore, in this case, I select dither frequency of 20Hz. The experiments were conducted to compare the performances of two methods of bilateral control: bilateral control using the conventional DOB for force estimation by both the master and the slave, and the proposed bilateral control using the conventional DOB for force sensing by the master and the friction-free DOB for force estimation by the slave. The bilateral control system is operated by applying human force on the master device.

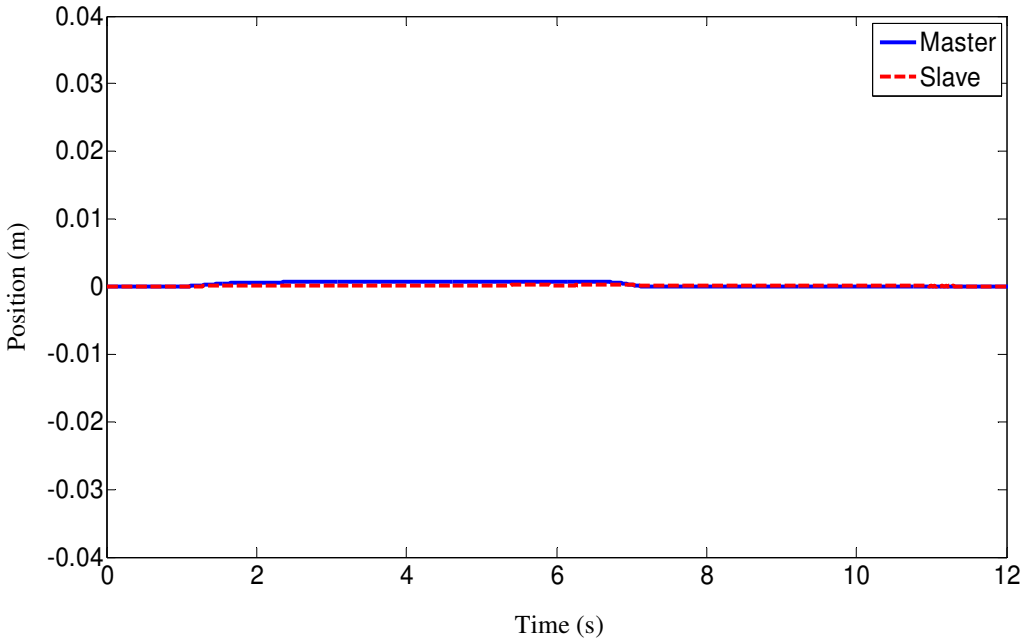

(a) Position responses

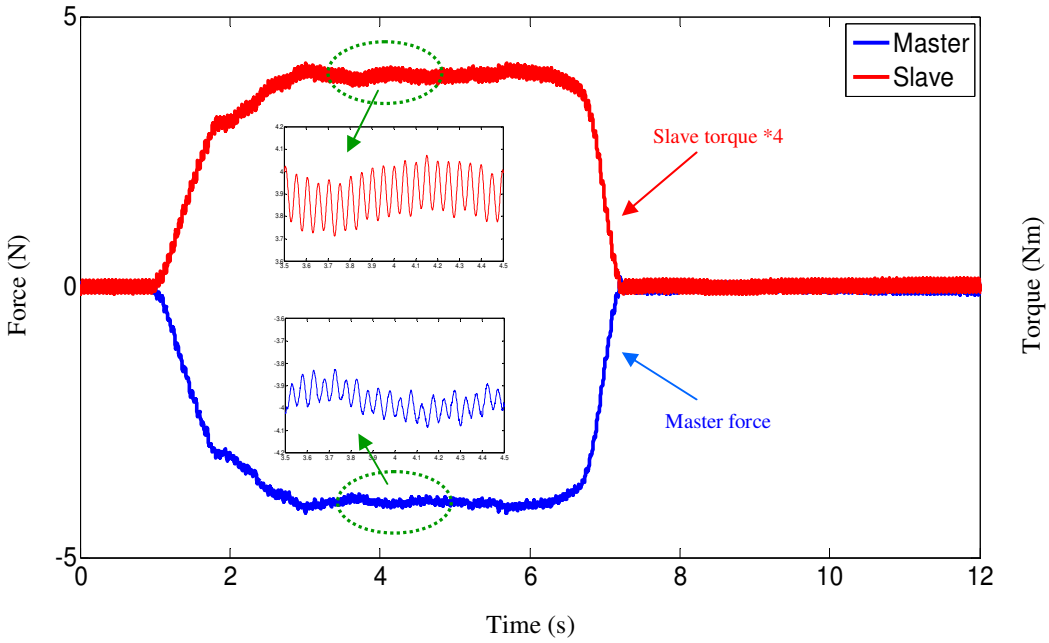

(b) Force responses

Fig. 5.7. Experimental results of pushing of bilateral control using conventional DOBs (20Hz-dither signal)

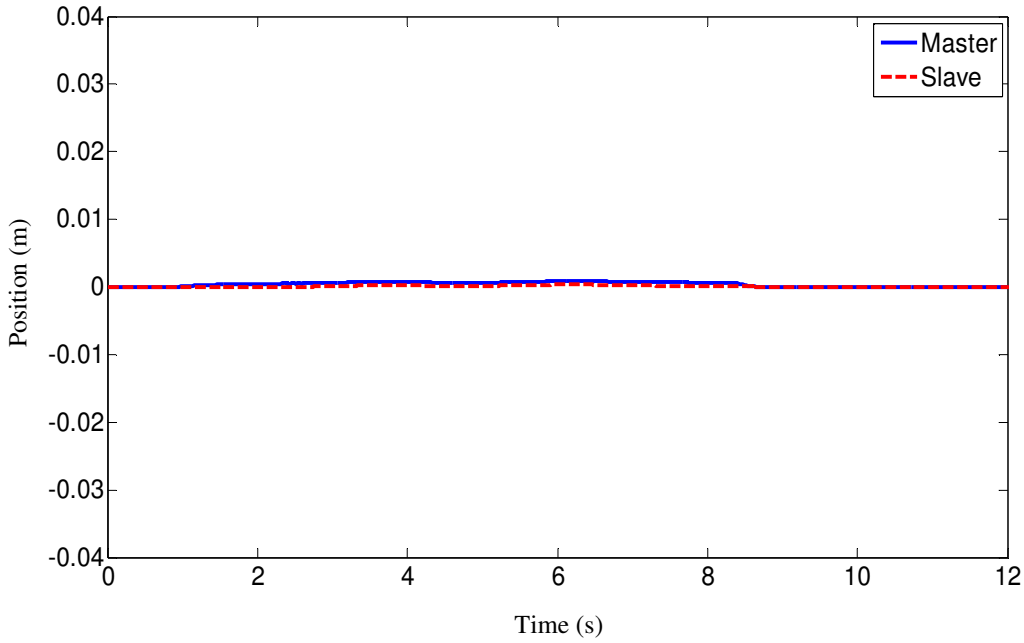

(a) Position responses

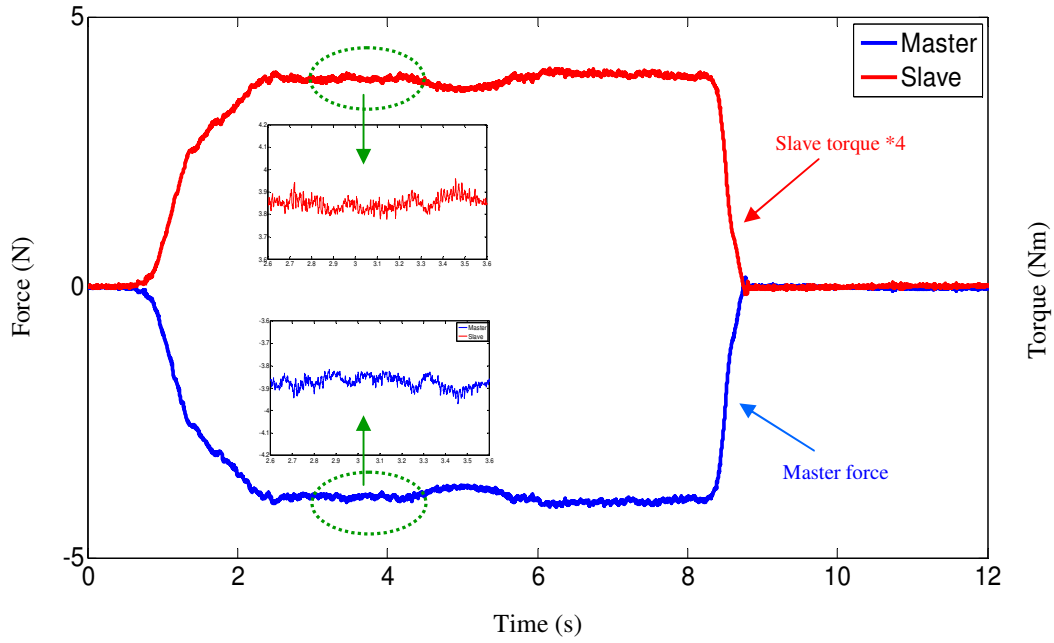

(b) Force responses

Fig. 5.8. Experimental results of pushing of bilateral control using friction-free DOB (20Hz-dither signal)

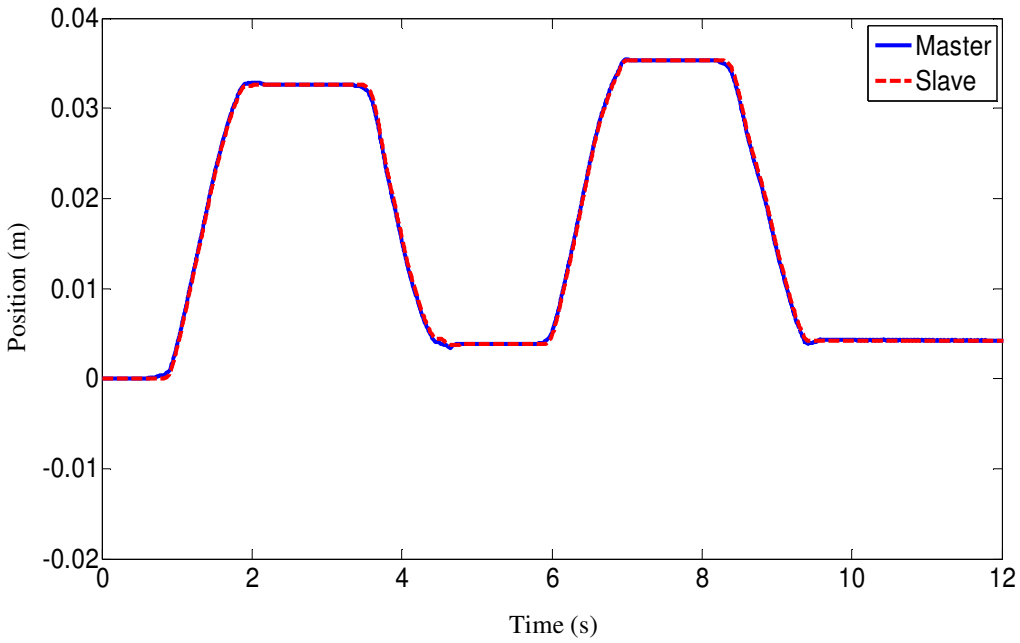

(a) Position responses

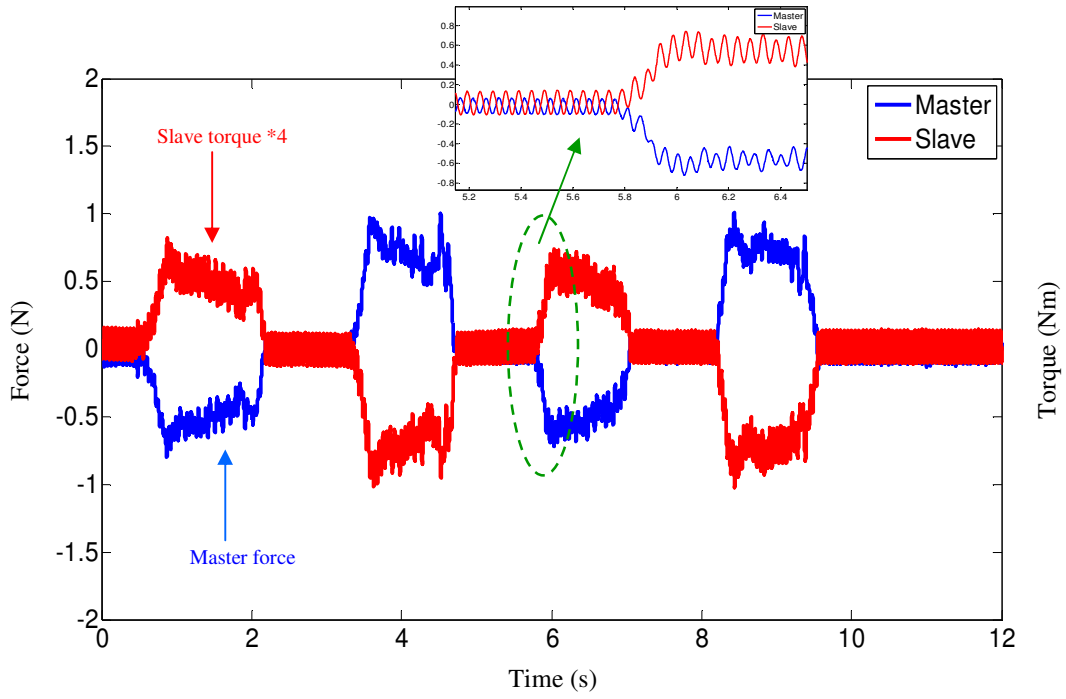

(b) Force responses

Fig. 5.9. Experimental results of free motion of bilateral control using conventional DOBs (20Hz-dither signal)

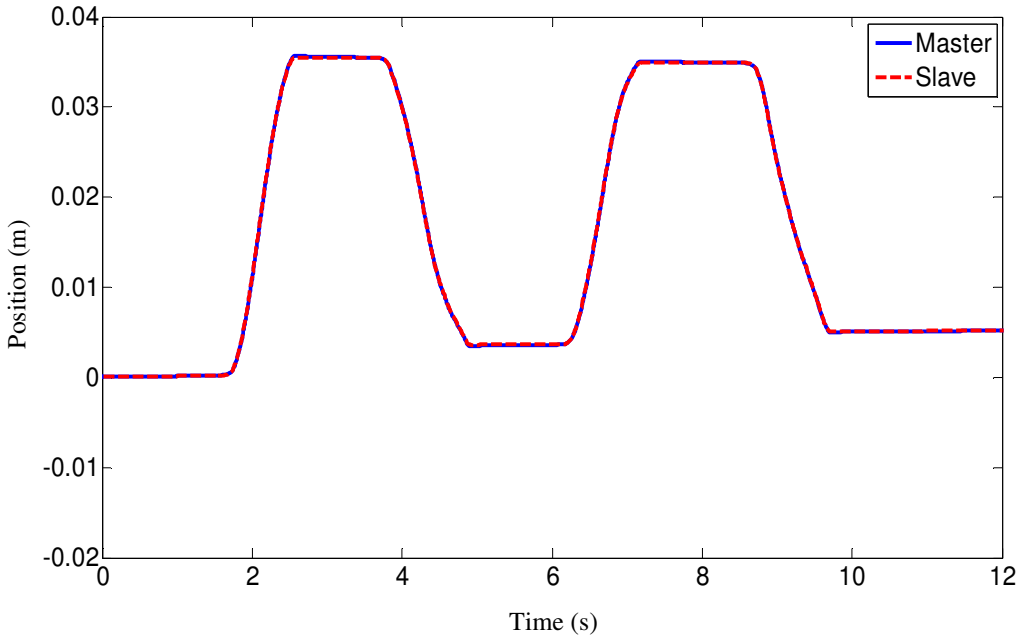

(a) Position responses

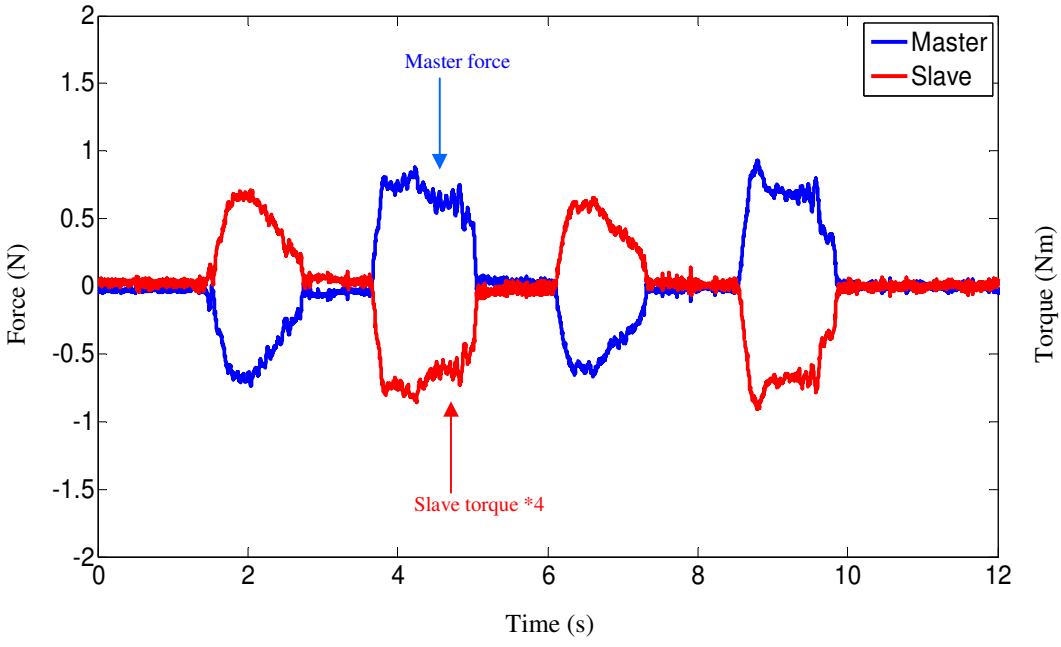

(b) Force responses

Fig. 5.10. Experimental results of free motion of bilateral control using friction-free DOBs (20Hz-dither signal)

Figs. 5.7 and 5.8 show the experimental results of pushing the slave toward an iron bar. Figs. 5.9 and 5.10 show the experimental results of free motion. The results in Figs. 5.7 and 5.9 indicate that in the bilateral control system using the conventional DOB for force sensing, the force responses of the master and the slave become oscillatory under the condition of an additional periodic signal. However, in the case of the proposed bilateral control system with the conventional DOB for force sensing by the master and the friction-free DOB for force sensing by the slave, the oscillatory disturbance in the force responses is reduced effectively on both the master and slave sides, as shown in Figs. 5.8 and 5.10. These results verify that the law of action and reaction is realized between the master and the slave. The experimental results also show that the bilateral control system attains good tracking in the position and force responses of the master and slave devices, even when the mechanisms of the master and the slave differ. Moreover, from the results of free motion, it can be seen that the human operator is assisted in manipulating the device with small operational force, although the slave mechanism is characterized by high friction and therefore requires high operational force in order to directly operate it.

Since the proposed bilateral control is constructed by different mechanism and the force sensing functions of the master and the slave are performed by different types of force observation (conventional DOB for the master, and friction-free DOB with dither signal for the slave), to evaluate the control performance, the force matching between the master and the slave is investigated. Therefore, to evaluate how much the force matching of the master and the slave is, the research investigates the cross correlation of torque responses of the master and the slave. Fig. 5.11 shows the cross correlation of torque responses corresponding to the conventional method in Fig. 5.9. Fig. 5.12 shows the cross correlation of torque responses corresponding to the proposed method in Fig. 5.10. From these results we can see that the cross correlation coefficient of the conventional method is 0.975 and that of the proposed method is 0.991. Therefore, the proposed method achieves almost the same force responses of the master and slave, and better force matching than that of the conventional method. The results confirm that the proposed method achieve good control performance on force matching of the master and the slave.

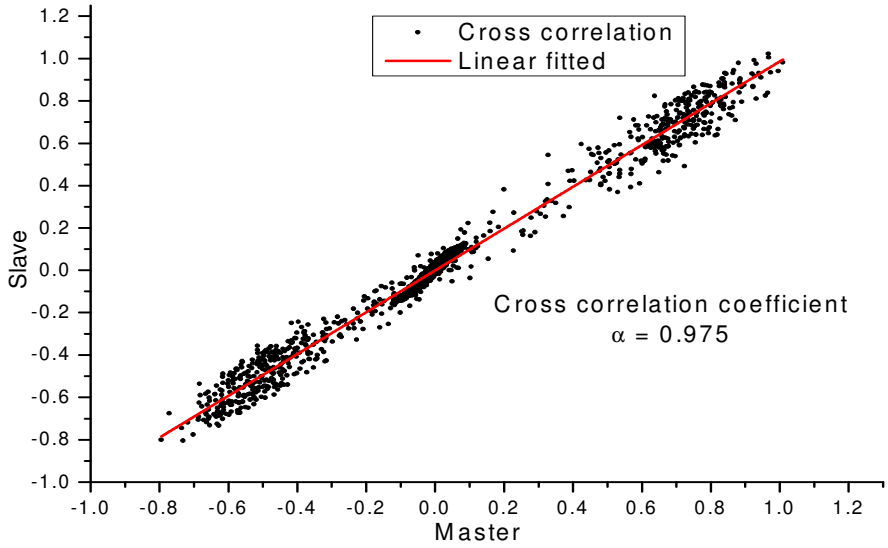

Fig. 5.11. Cross correlation of torque responses of master and slave in the control system using conventional DOB

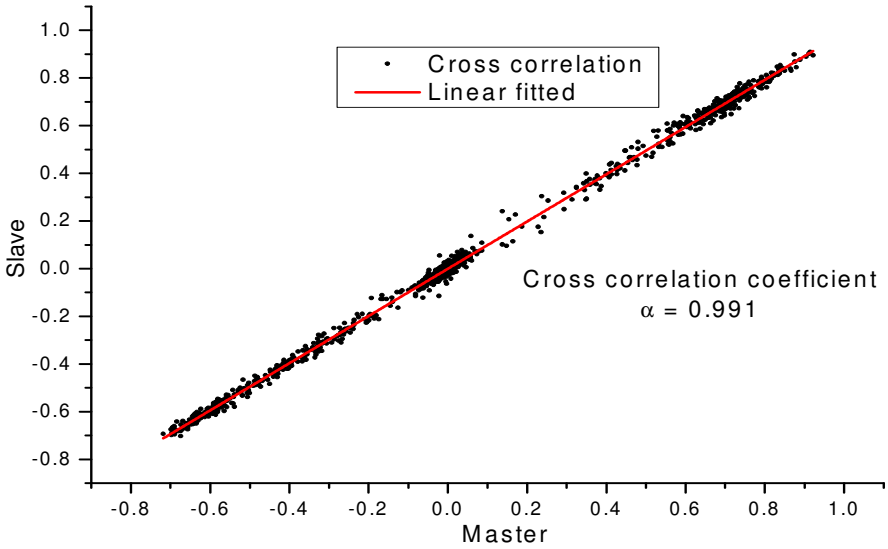

Fig. 5.12. Cross correlation of torque responses of master and slave in the control system using friction-free DOB

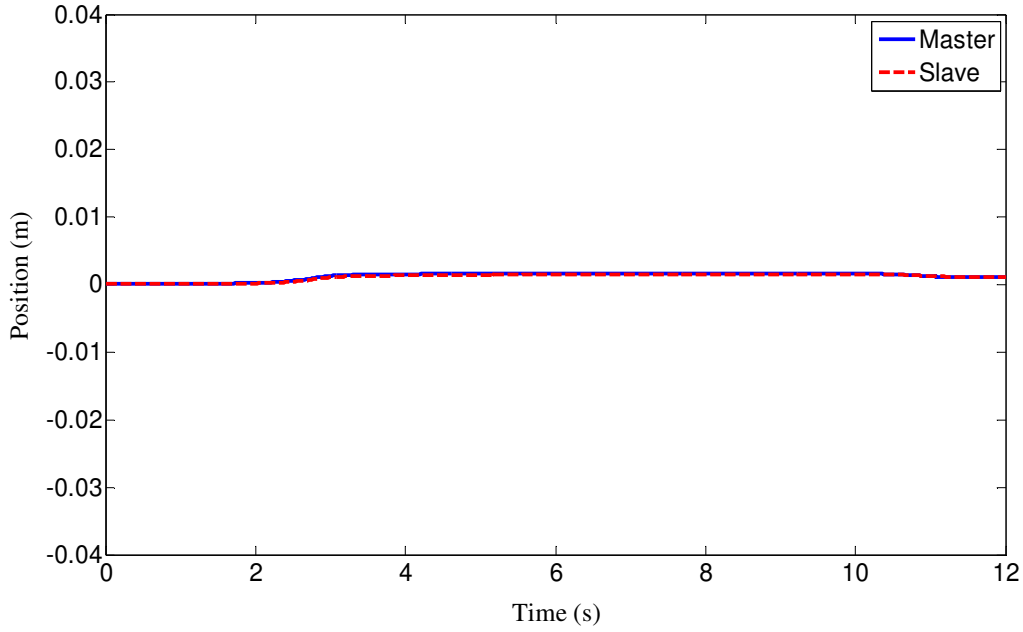

(a) Position responses

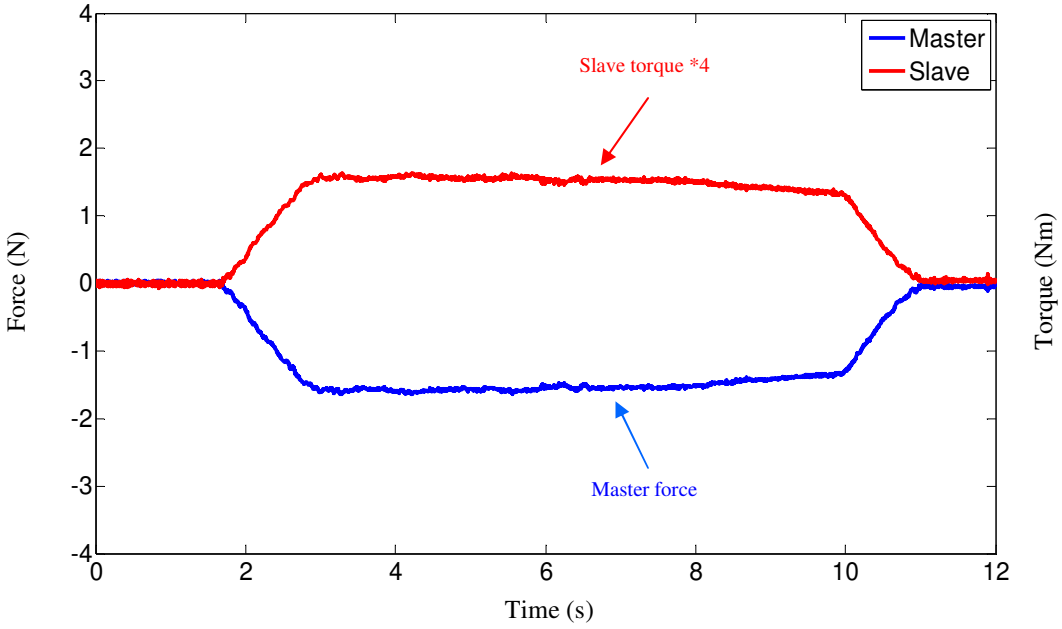

(b) Force responses

Fig. 5.13. Experimental results of pushing of bilateral control using proposed method (rubber environment, 20Hz-dither signal)

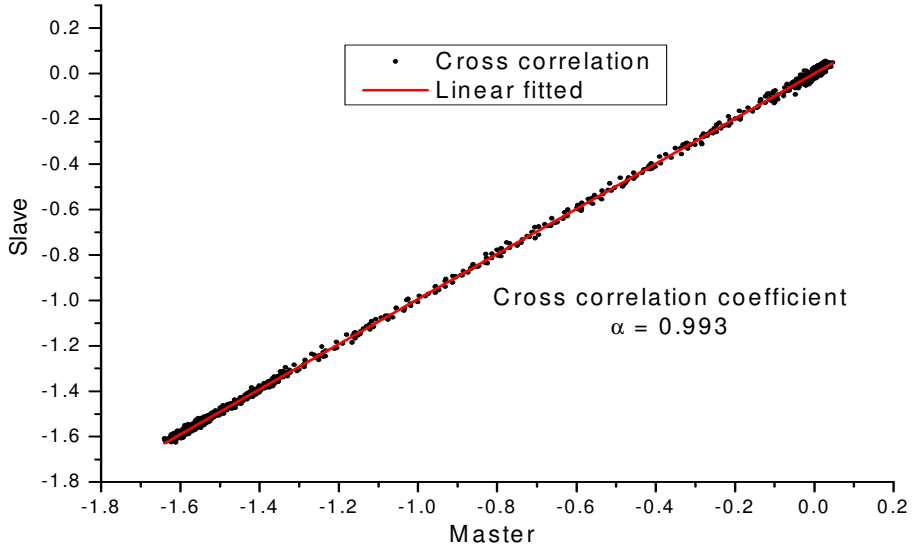

Fig. 5.14. Cross correlation of torque responses of master and slave corresponding to Fig. 5.13

The effectiveness of the proposed bilateral control of pushing toward iron environment in condition of 20Hz-dither signal has been confirmed by the results in Fig. 5.8.

To evaluate the effect of stiffness of contact environment on the control performance as well as dither frequency, the experiment of the proposed bilateral control of pushing toward the rubber environment is carried out. In this experiment, frequency of dither signal is also of 20Hz. The experimental results are shown in Fig. 5.13. To evaluate how much the force matching of the master and the slave is, the cross correlation of torque responses of the master and the slave is shown in Fig. 5.14. The results in Figs. 5.13 and 5.14 clarify that the proposed method still obtains proper force estimation with different contact environment. Hence, it is confirmed that the frequency of dither signal is not affected by stiffness of contact environment.

The above experimental results confirm the effectiveness of the proposed method in force sensing and in the elimination of a periodic component in force information in a bilateral control system.

The next experiments are conducted to clarify the effectiveness of the friction-free DOB in harmonic disturbances suppression. Here, the performances of bilateral control system using conventional DOB and friction-free DOB are investigated under conditions of 200rad/s observer pole and 10Hz dither signal. The motion of the bilateral control system is generated by a force command inserted to the master side as shown in Fig. 5.15. In the experiments, the control performance is investigated in two cases of the sinusoidal force command's frequency of 3Hz and 6Hz. The experimental results of bilateral control under condition of 3Hz Fcmd are shown in Figs. 5.16, 5.17, 5.18, and 5.19. The experimental results corresponding to 6Hz Fcmd are shown in Figs. 5.20, 5.21, 5.22, and 5.23.

These results show that there are undesired harmonics appearing in the force responses of both the master and slave devices. These harmonic components depend on the fundamental frequency of the force command. These harmonics cause distortion of the force estimation and their effect is necessary to be reduced. The power spectrum analyses in Figs. 5.18, 5.19, 5.22, and 5.23 clarify that the friction-free DOB effectively suppresses the harmonic disturbances in the force estimation in both the master and slave in comparison to the conventional DOB.

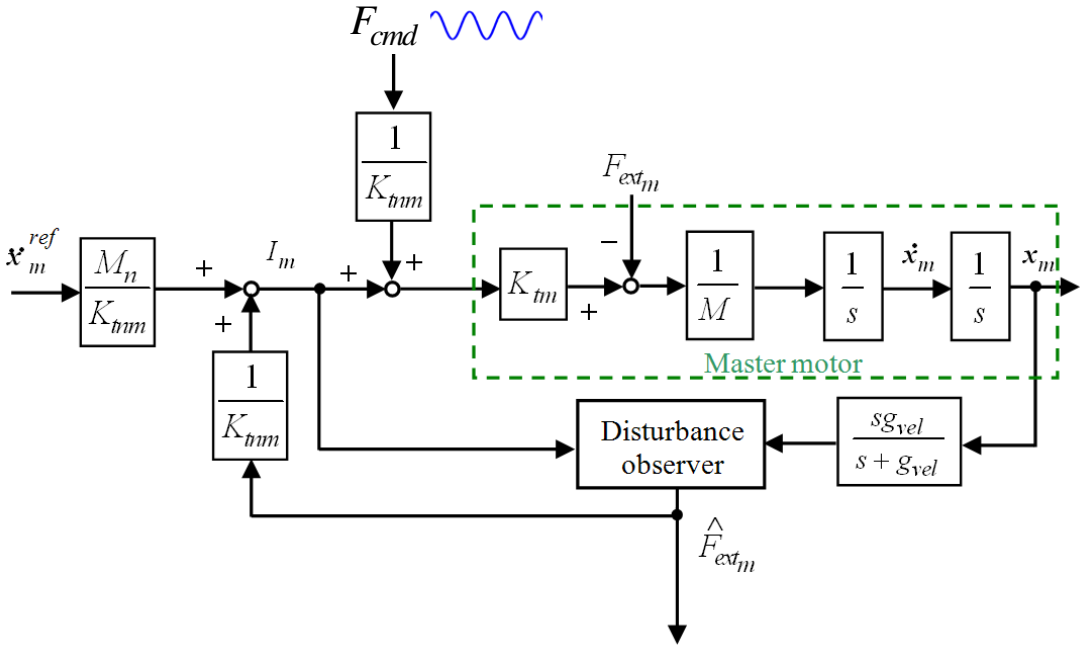

Fig. 5.15. Master actuator with sinusoidal force command to generate motion

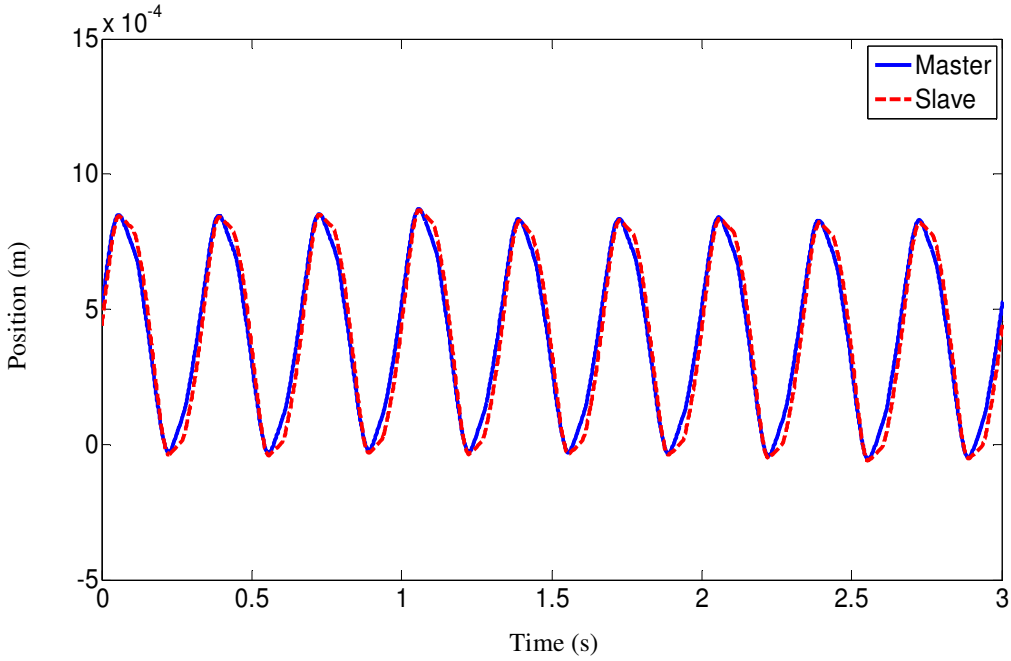

(a) Position responses

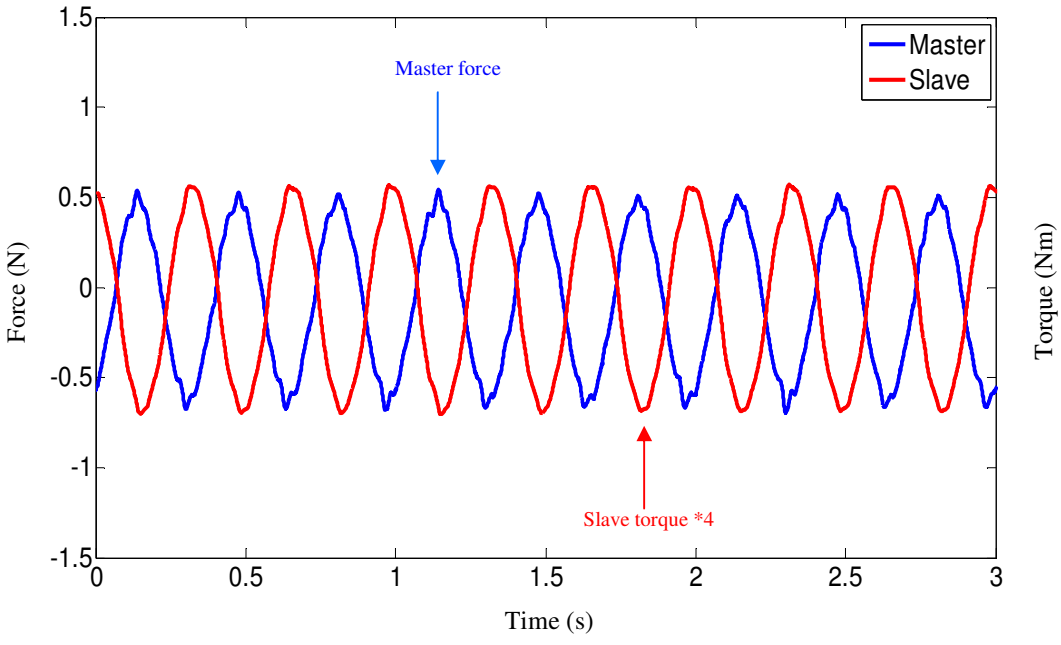

(b) Force responses

Fig. 5.16. Experimental results of bilateral control using conventional DOB with Fcmd 3Hz

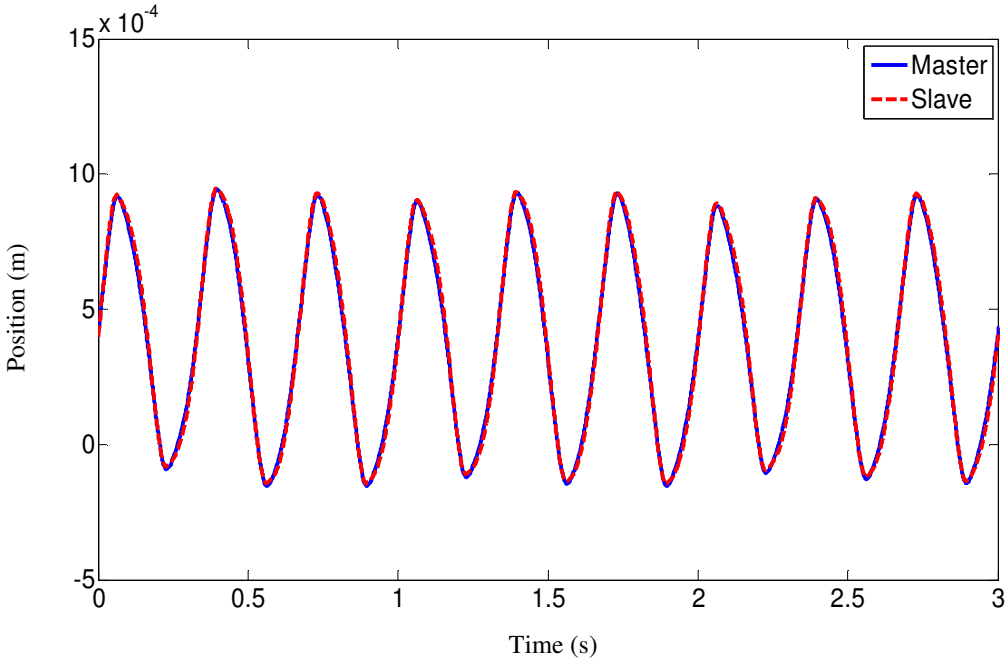

(a) Position responses

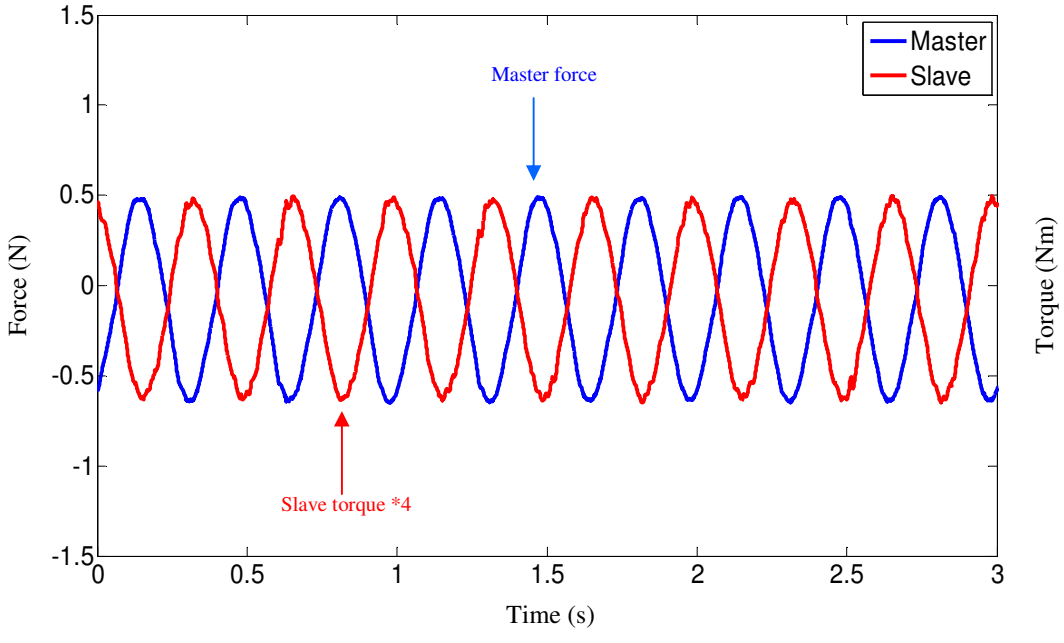

(b) Force responses

Fig. 5.17. Experimental results of bilateral control using friction-free DOB with Fcmd 3Hz

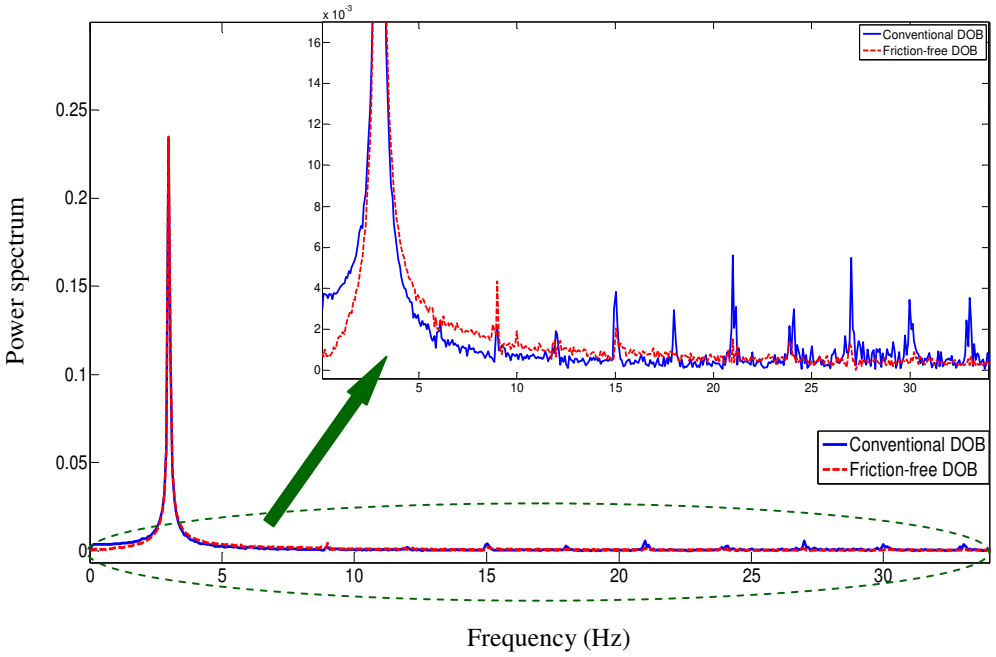

Fig. 5.18. Power spectrum analyses of force responses of the masters using conventional DOB and friction-free DOB with Fcmd 3Hz

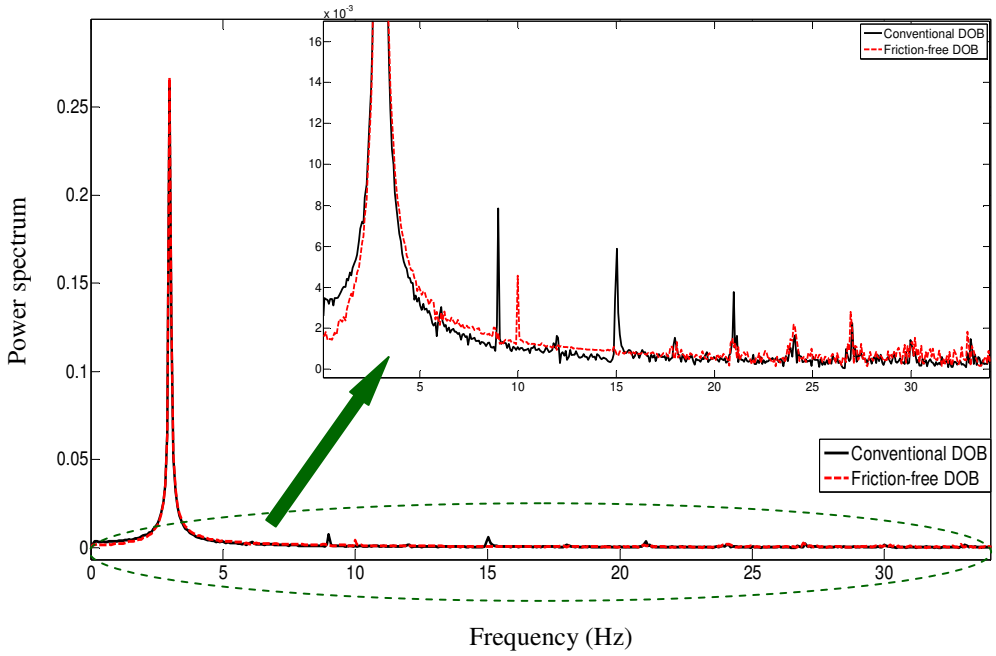

Fig. 5.19. Power spectrum analyses of force responses of the slaves using conventional DOB and friction-free DOB with Fcmd 3Hz

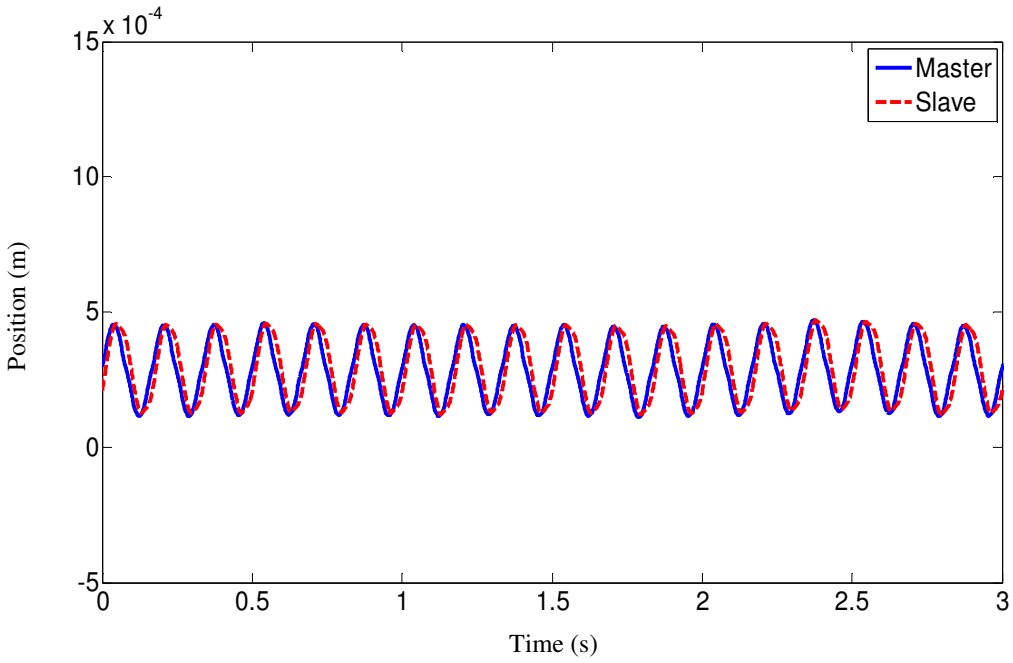

(a) Position responses

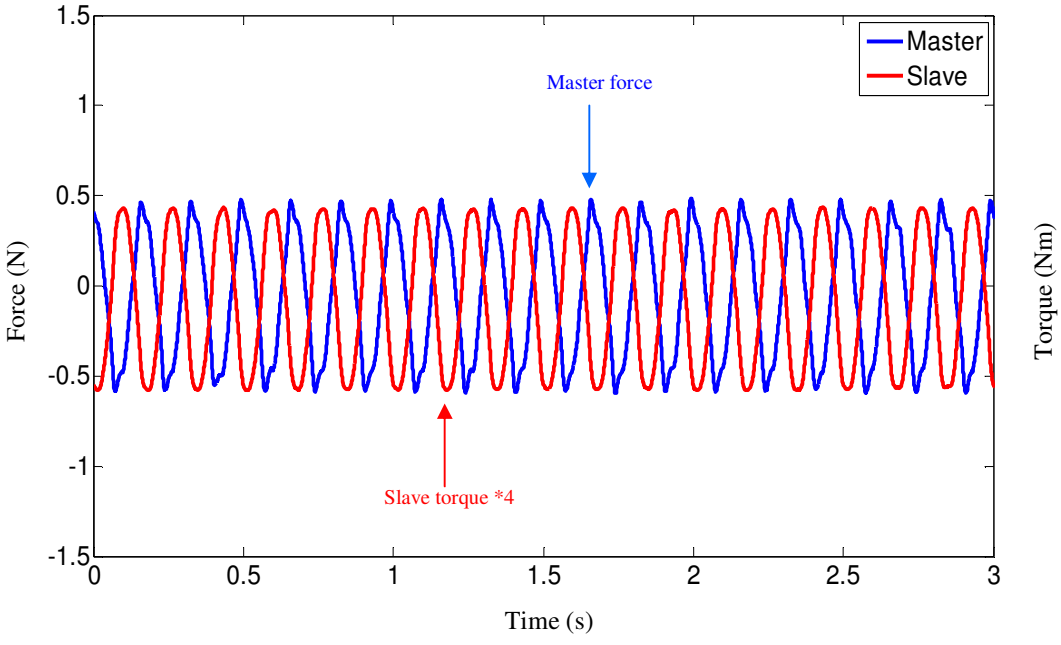

(b) Force responses

Fig. 5.20. Experimental results of bilateral control using conventional DOB with Fcmd 6Hz

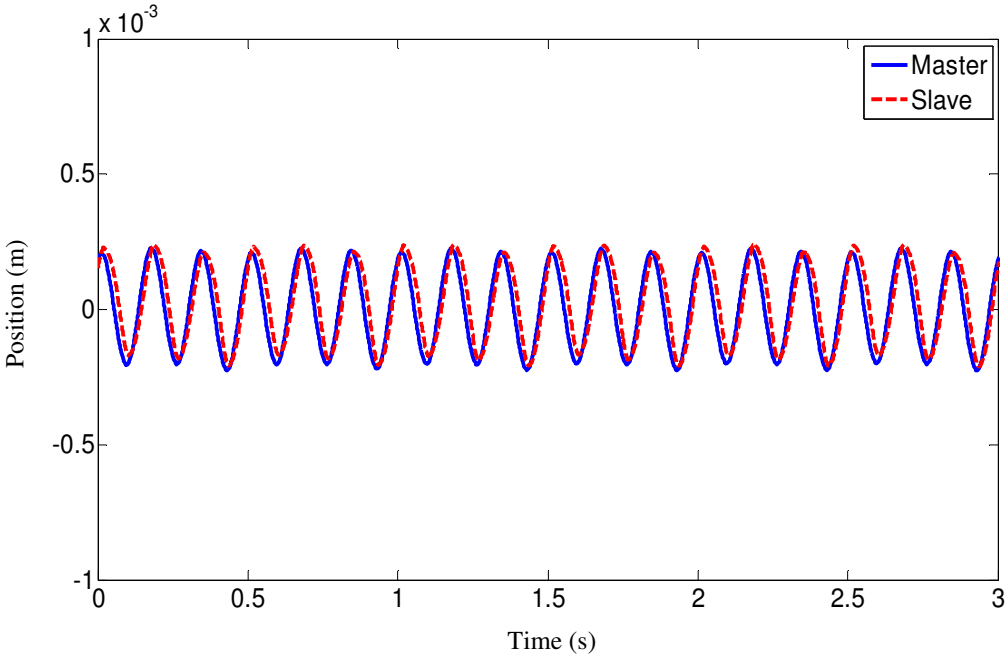

(a) Position responses

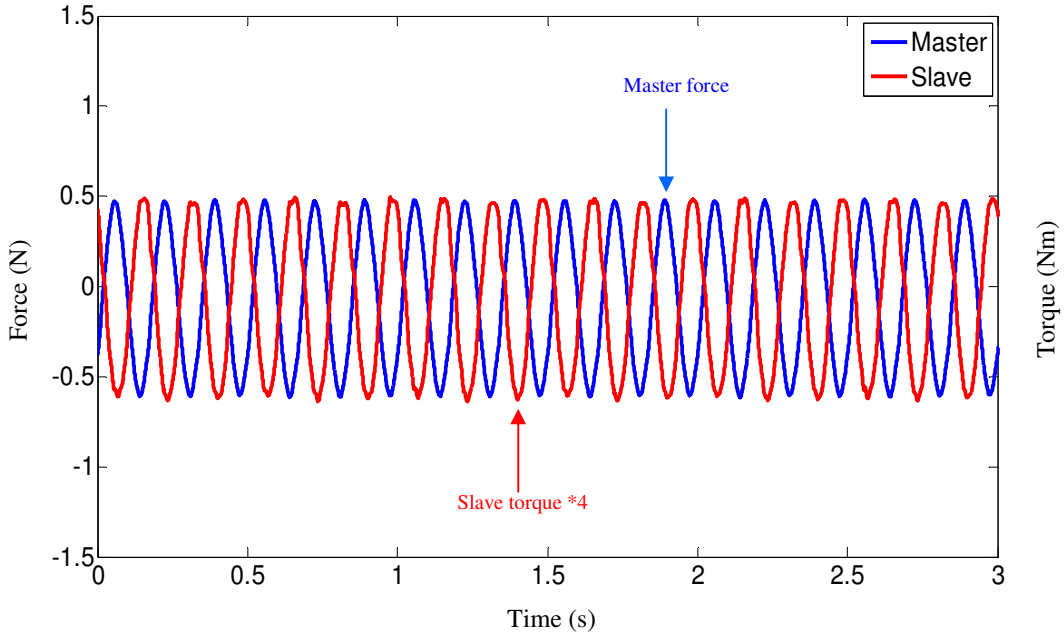

(b) Force responses

Fig. 5.21. Experimental results of bilateral control using friction-free DOB with Fcmd 6Hz

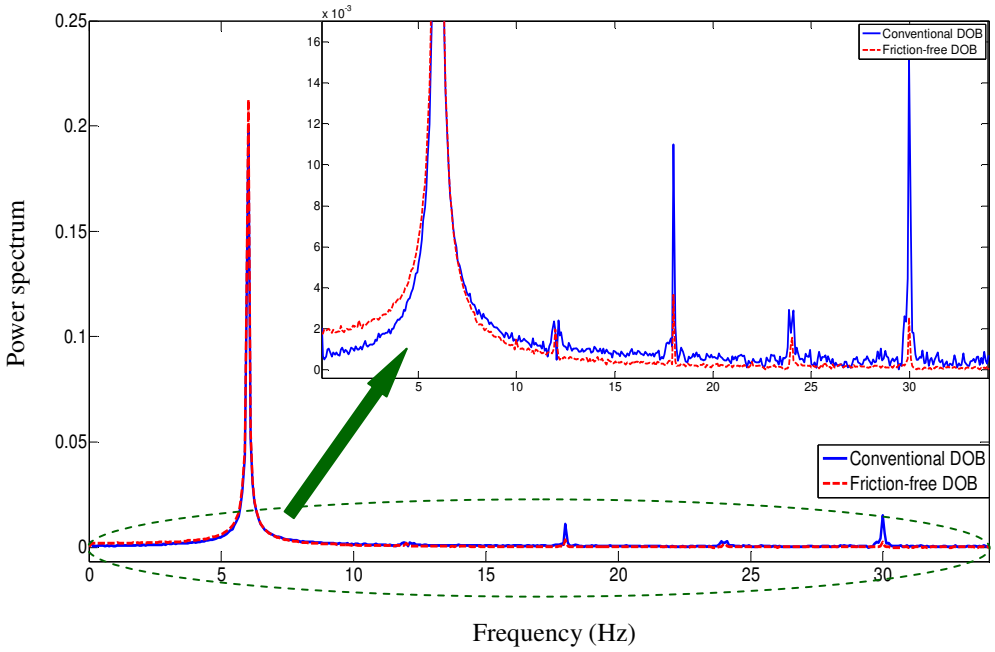

Fig. 5.22. Power spectrum analyses of force responses of the masters using conventional DOB and friction-free DOB with Fcmd 6Hz

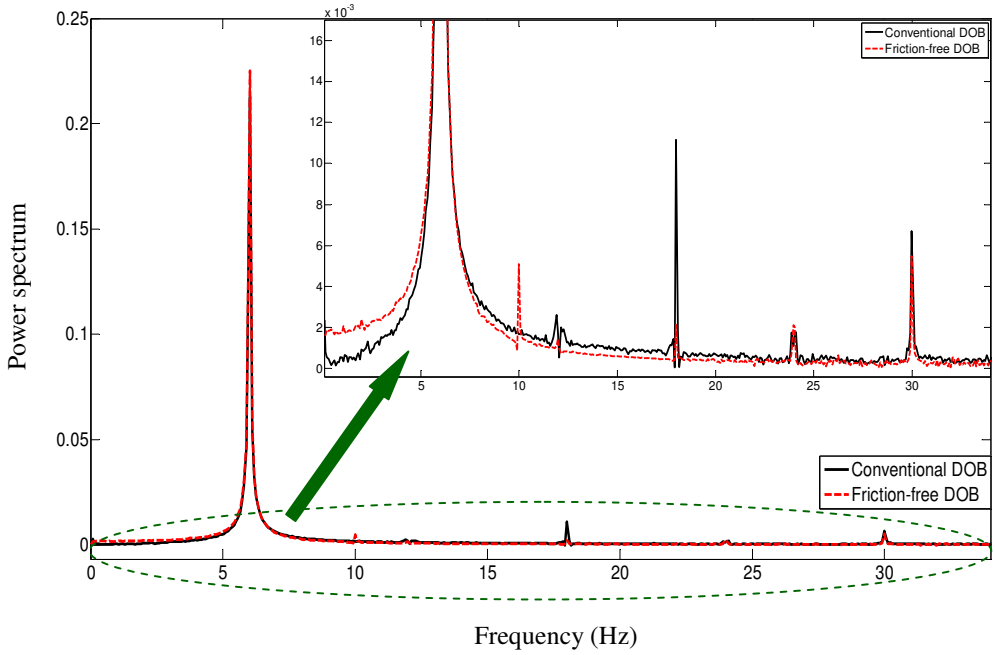

Fig. 5.23. Power spectrum analyses of force responses of the slaves using conventional DOB and friction-free DOB with Fcmd 6Hz

5.6 Conclusions

The research proposes a bilateral control system using a friction-free DOB to improve control performance by reducing the effects of friction, eliminating oscillatory disturbances, and suppress the harmonics in force estimation. The bilateral control system is configured using different mechanisms of the master and slave actuators. The proposed friction-free DOB with a dither signal is used for the force sensing function in the salve. The force sensation of the master is performed by a conventional DOB. All control algorithms are implemented in an FPGA to achieve a high sampling rate for the control cycle. The proposed method has been successfully implemented in a bilateral control system with different master and slave mechanisms and is feasible for application to human assist systems or in industrial applications.

Chapter 6

Summary of the Dissertation

6.1 Conclusions and Evaluations

This thesis presents a methodology to attain the high performance human-robot-interaction control system based on the superior wideband force sensing and the friction-free force observation. Consequently, this thesis has proposed and accomplished the following research work.

- *High performance force control system with wideband force sensing based on Multi-sensor integration in Kalman-filter-based disturbance observer:*

The force sensing operation is constructed by the combination of the Kalman-filter and the disturbance observer. The Kalman-filter is adopted for velocity estimation. An integration between a linear encoder and an acceleration sensor structures the measurement system. The Kalman-filter uses position signals and acceleration signals as its inputs to estimate the velocity. By using Kalman-filter with multi-sensor integration, the noise in velocity estimation is suppressed effectively and the improved velocity information is obtained, especially during the impact motions with high acceleration.

The estimated velocity by Kalman-filter is used by the disturbance observer to obtain the force information. With the employment of improved velocity information, the force estimated by disturbance observer is markedly enhanced. Besides, the robustness of the control system is achieved owing to the realization of acceleration control by disturbance observer.

Additionally, FPGA is adopted to implement all of the control algorithms. Since FPGA is able to execute parallel processes, the sampling time of the control algorithm is shortened to $5\,\mu s$. With this high sampling rate, it is possible to increase to bandwidth of the disturbance observer. As a result, the wide bandwidth of force sensing is obtained.

The experimental results of force sensing confirm the high performance force sensing using the proposed method. The force response has no observation noise due to the noise suppression by Kalman-filter. The performance of force sensing of the proposed method in the case of impact motions is better than that of the conventional disturbance observer. The results also show the ability to increase the bandwidth of the disturbance observer. With the conventional disturbance observer, the force response becomes degraded by noise when the bandwidth of the disturbance observer is increased. However, the proposed method still can obtain the enhanced force response when the cut-off frequency of the disturbance observer is enlarged. The bandwidth of force sensing is widened to 62800 rad/s (≈ 10Khz) using the proposed method. This bandwidth is superior to human bandwidth of tactile sensation and is useful for human support techniques. The proposed method can be employed to achieve the high efficiency in haptic information reproduction and transmission applications.

- *Enhanced force sensing performance based on wideband, friction-free and noise-free force estimation:*

A novel force sensing method named as friction-free disturbance observer is proposed to achieve a wideband force control system with friction-free and noise-free observation. The effect of friction on force observation is eliminated owing to the addition of a dither signal to the desired reference signal. The effect of the dither signal is the ability to smooth the discontinuity of friction. The friction compensation method is inspired by the dithering method because it is simple to implement and the friction indemnification process can be neglected.

The disadvantage of the dithering method is that it generates an oscillatory disturbance that can affect the performance of the control system. As the results, the force estimation by the conventional disturbance observer is also degraded by the periodic signal because the effect of the oscillatory disturbance is not taken into account in the conventional method

The proposed friction-free disturbance observer is designed for force sensing operation and elimination of periodic disturbance in force estimation. To make the design practical, the problem of noise in the measurement is taken into account. A Kalman filter is used in combination with the friction-free disturbance observer to reduce the effect of noise on the force estimation. The influence of the periodic signal on force estimation is rejected by the

friction-free disturbance observer. The force-sensing bandwidth is widened to 1000 rad/s due to the effective noise suppression by using a Kalman filter.

The utilization of an FPGA to implement all of the control algorithms provides the fast sampling time of 5 μs that also contributes to the ability to widen the force-sensing bandwidth and ensure the performance of the control system with a highly complex computation algorithm. The experimental results and analyses in Chapter 4 have verified the effectiveness of the proposed method: Using a dither signal together with the integration of a friction-free disturbance observer and a Kalman filter provides friction-free and wideband force sensing. The proposed method is useful for applications such as robots, machine tools, and bilateral control systems.

- *High performance power assisted bilateral control system of different configurations based on friction-free force observer:*

The research presents a new force sensing approach to improve the performance of a bilateral control system with different mechanisms of the master and the slave sides operating as a power assisted control system. A linear shaft motor and a ball screw perform the roles of the master and the slave, respectively. By using a frictionless mechanism as the master while the slave mechanism is affected by high friction, together with an appropriate force scaling ratio between the master and the slave, the effect of friction is reduced and the manual capability of the human operator is enhanced while he/she still perceives the interaction of the slave and environments.

However, the force sensing performance of bilateral control system is degraded due to the effect of friction and harmonic disturbances in force estimation. Because we have verified the effectiveness of using a friction-free disturbance observer with a dither signal in reducing friction effect on force sensation of a ball-screw system. Therefore, to improve force sensing performance of the bilateral control system, we implement a dither signal and a friction-free disturbance observer for force sensing operation on the slave side.

In our method, to reduce friction effect on force estimation due to ball screw mechanism, a periodic signal is inserted into the control signal of the slave side. However, the addition of periodic signal causes oscillatory force responses on both master and slave sides. Hence, a

friction-free disturbance observer is designed for force sensing operation on the slave side to reduce the effect of oscillatory disturbance on force information. The proposed bilateral control is based on acceleration control and consists of a conventional disturbance observer and a friction-free disturbance observer for the master and slave, respectively.

The experimental results show that the oscillatory disturbance in the force responses is reduced effectively on both master and slave sides. These results prove that the law of action and reaction is achieved between the master and the slave. The experimental results also shows that the bilateral control system obtains the good tracking in the position and force responses of the master and the slave devices, even when the mechanisms of the master and the slave are different. Moreover, from the results, it can be seen that the human operator is assisted to manipulate the device with a small operational force, while still perceiving the impedance of the remote environment. Additionally, the results also clarify that the friction-free DOB effectively suppresses the harmonic disturbances in the force estimation in both the master and slave in comparison to the conventional DOB. The proposed method has been successfully implemented in a bilateral control system with different master and slave mechanisms and is feasible for application to human assist systems or in industrial applications.

6.2 Future Plans

6.2.1 Motion copying system

The proposed methodologies in the thesis are some of the fundamental techniques for haptic sensing devices and human-robot interaction systems, because they overcome the limitations of a force sensor and achieve improved system stability, accurate force information, and wideband force sensation.

Therefore, in the incoming work, the advantages of the research work can be applied to develop a High performance Motion-copying system based on super wideband and friction-free force sensing for broadcasting education, training and communication: The rapid development of motion control technologies has brought up intelligent control systems that can replace human role in medicine, industry, and society. Among them, a motion-copying system is developed to imitate human motions. The motion-copying system preserves and the reproduces the motions of an expert or human operator. The motion-copying system based on bilateral control consists of a motion-saving system and a motion-loading system that mimics the motion of an expert or human operator based on preserved information about its position and force. The motion-saving system is realized by the bilateral control of a master-slave system to record the force and position of the master device in a motion data memory. Using the human motion stored in this data memory, the motion-loading system reproduces the motion without a human operator. In this way, the actuator in a motion-loading system consists of only the slave device, and the regeneration of motion does not require modeling.

The performance of a motion-copying system is strongly dependent on force information recording and reproduction. Therefore, the incoming research work develops the motion-saving and motion-loading systems based on the super wideband and friction-free force sensing in order to achieve the high-performance motion-copying system with very precise motion preservation and motion regeneration, reducing human mistakes during operation, and increasing working efficiency. The proposed high-performance motion-copying system is very useful for applications in broadcasting education and training systems, surgical robots, human assist systems, and industrial robots.

6.2.2 Development of a safe robot motion control system by applying safety technology

Unsafe systems cause serious accidents to human, system, environments, and result in money being lost due to accidents, disruption to production, loss of market share, and degradation of company assets. In many developed countries, system safety is the key technology and is widely implemented in critical safety-related systems of civil aviation, marine industry, railway industry, and nuclear plant. Therefore, how to construct a safe system and develop the safety technology in a system must be addressed in any control system. However, most research about control systems mainly focuses on constructing functionalities without consideration of system safety as a part of the system design. Safety costs money but damage can even be more expensive. Therefore, the incoming research aims at taking into account the safety design of the robot system in order to protect human, robot system, and environment from hazardous situations. With the application of safety technologies, the control system can gain high reliability; thereby is safe for human and working environments, and confidentially to be applied in society.

The following contents introduce some basic concepts and principles of safety technology. Then the tentative conceptual safety function is briefly described.

Safety of machinery

- ***Safety definition:*** Safety is to protect human life, environment, plant property including products from damage.

Safety is needed in many fields in our daily life:

- Process safety (power plant, chemical industry…)
- Machinery safety (manufacturing, industrial robots, machine tool…)
- Traffic safety (airplanes, railways, sea transportation, automotive…) …

Safety costs money but damage can even be more expensive.

Safety needs regulations:

- Product life cycle.
- Reduction of non-tolerable risks.

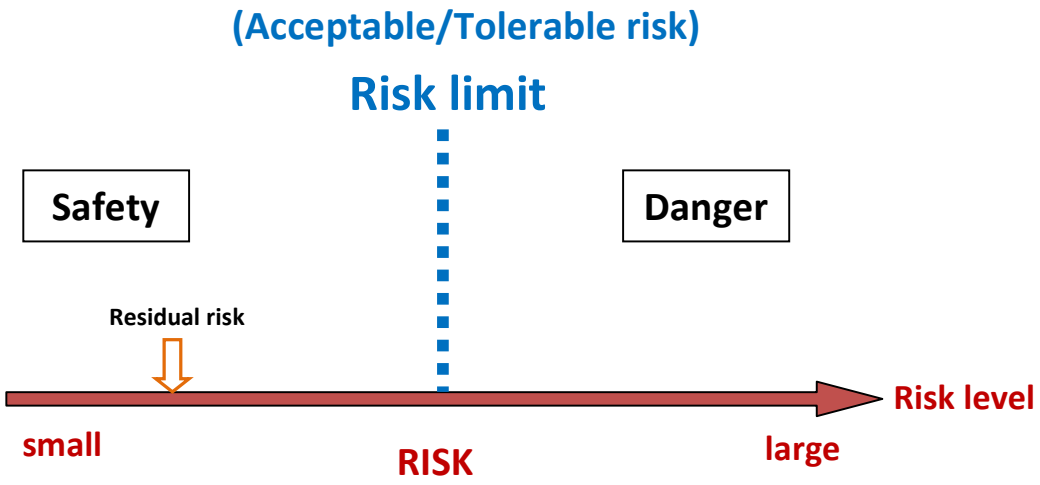

Fig. 6.1. Relationship of risk, safety and danger

- ***Risk assessment and risk reduction:***

To implement risk assessment and risk reduction, the following actions must be taken by the designer in the following order:

- Determine the limits of the machinery, which include the intended use and any reasonably foreseeable misuse.
- Identify the hazards and associated hazardous situations.
- Estimate the risk for each identified hazard and hazardous situation.
- Evaluation the risk and take decisions about the need for risk reduction

The above four steps are related to risk assessment.

- Eliminate the hazard or reduce the risk associated with the hazard by means of protective measures. This step is related to risk reduction.

Risk assessment is a series of logical steps to enable the analysis and evaluation of the risks associated with machinery.

Risk assessment is followed by risk reduction. Iteration of this process can be necessary to eliminate hazards as far as practicable and adequately reduce risks by the implementation of protective measures.

Protective measures are the combination of the measures implemented by the designer and the user as shown in Fig. 6.3. Measures which can be incorporated at the design stage are preferable to those implemented by the user and usually are more effective.

The objective of risk assessment and risk reduction is to achieve the greatest practical risk reduction, taking into account the following factors:

- The safety of the machine during all the phases of its life cycle
- The ability of the machine to perform its function
- The usability of the machine
- The manufacturing, operational and dismantling costs of the machine

The strategy of risk assessment and risk reduction is represented by the flowchart in Fig. 6.2. The process is iterative and several successive applications can be necessary to reduce the risk, making the best use of available technology.

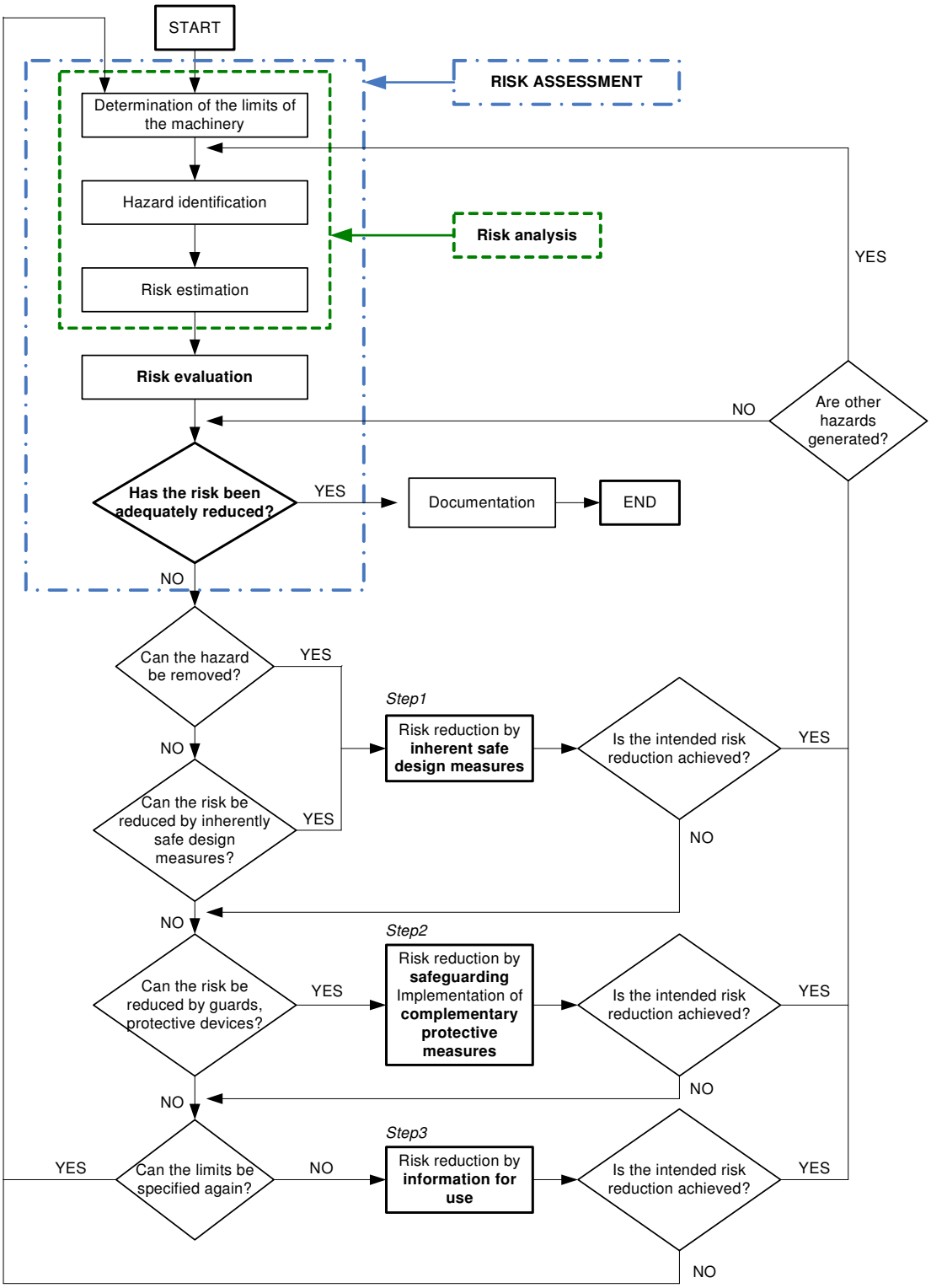

Fig. 6.2. Flowchart of risk reduction process including iterative three-step method

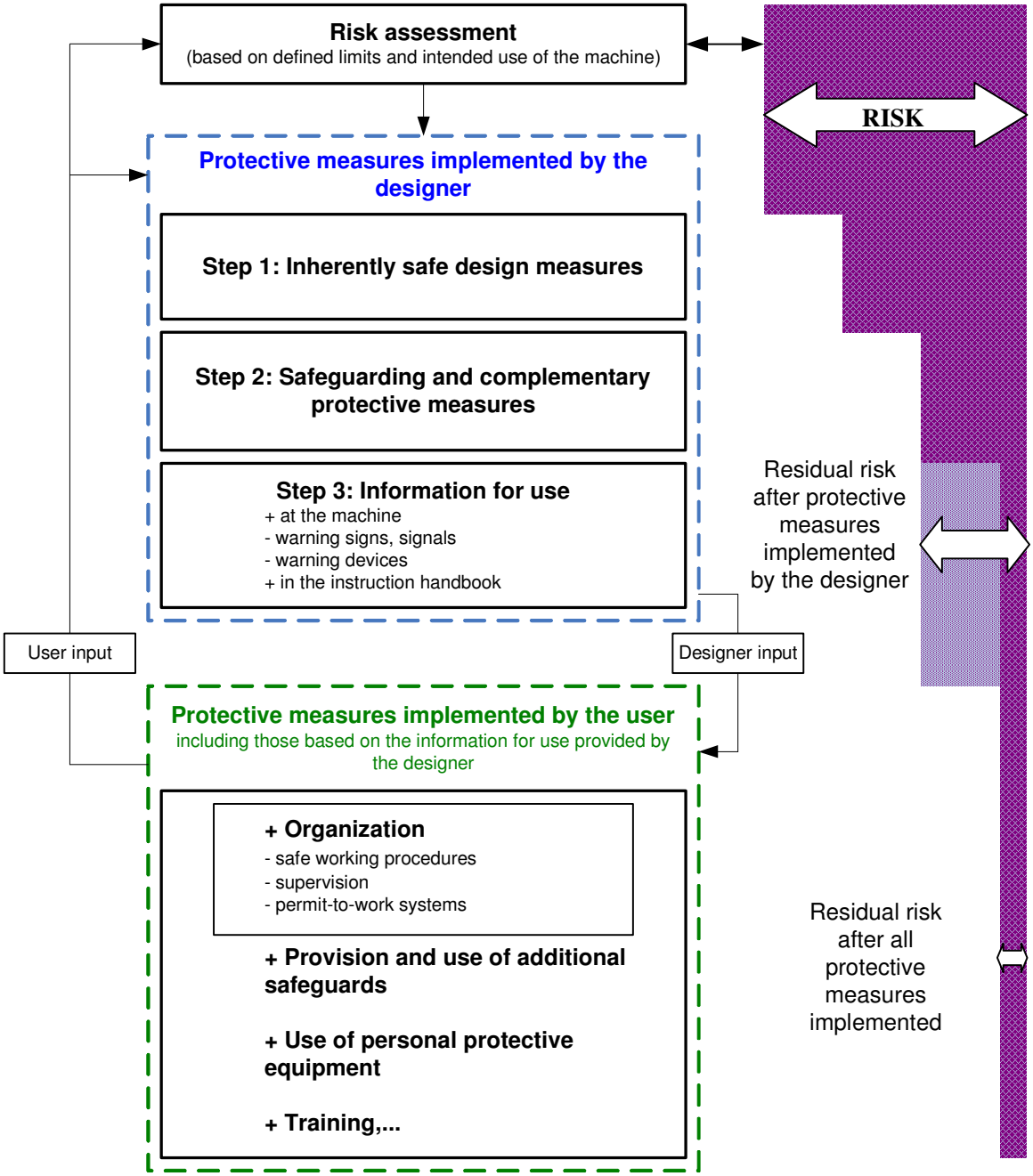

Fig. 6.3. Risk reduction process from point of view of designer

Tentative conceptual diagnostic functions to protect control system

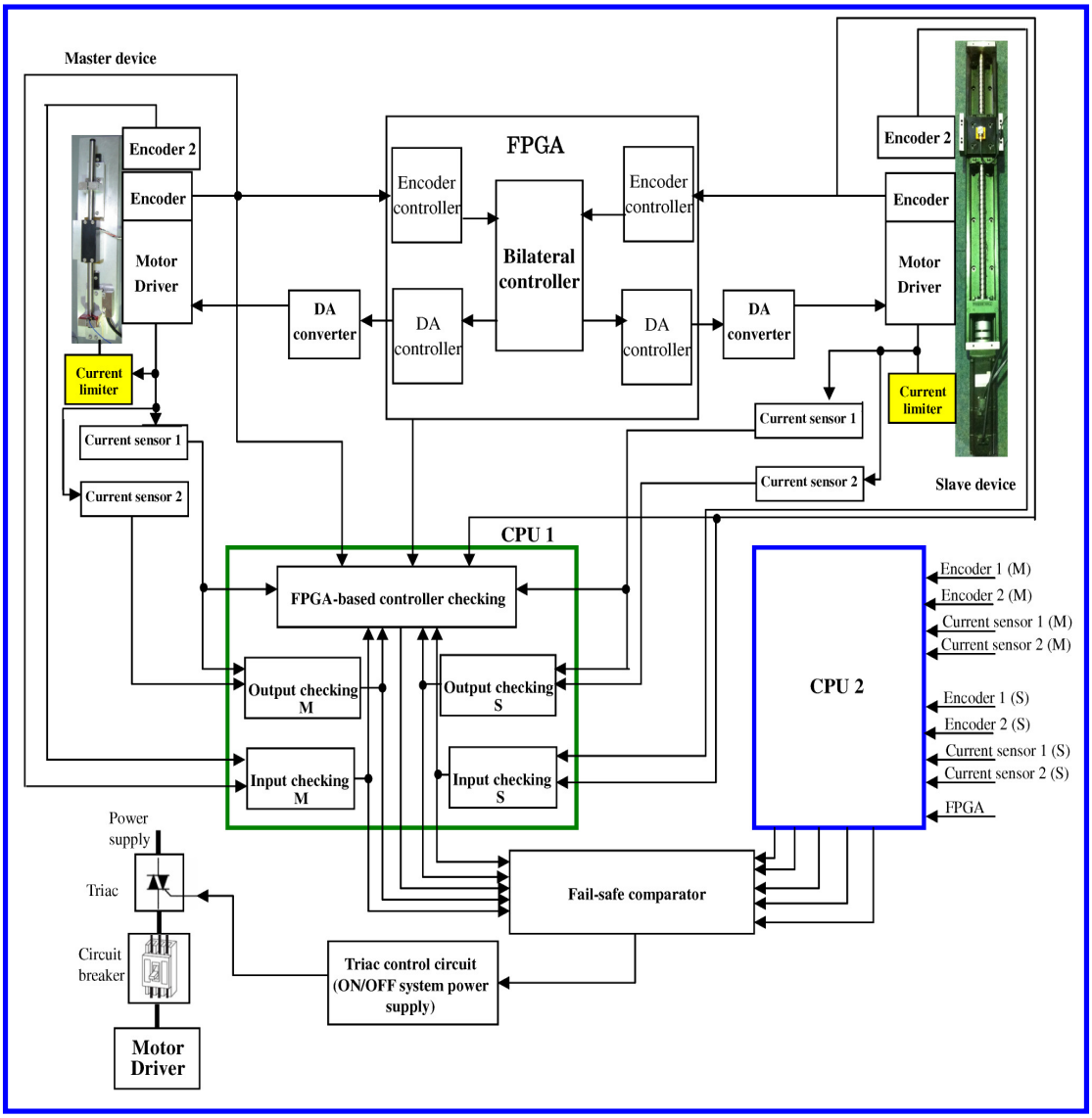

Fig. 6.4. Conceptual diagnostic functions to detect incorrect motor current and stop the control system

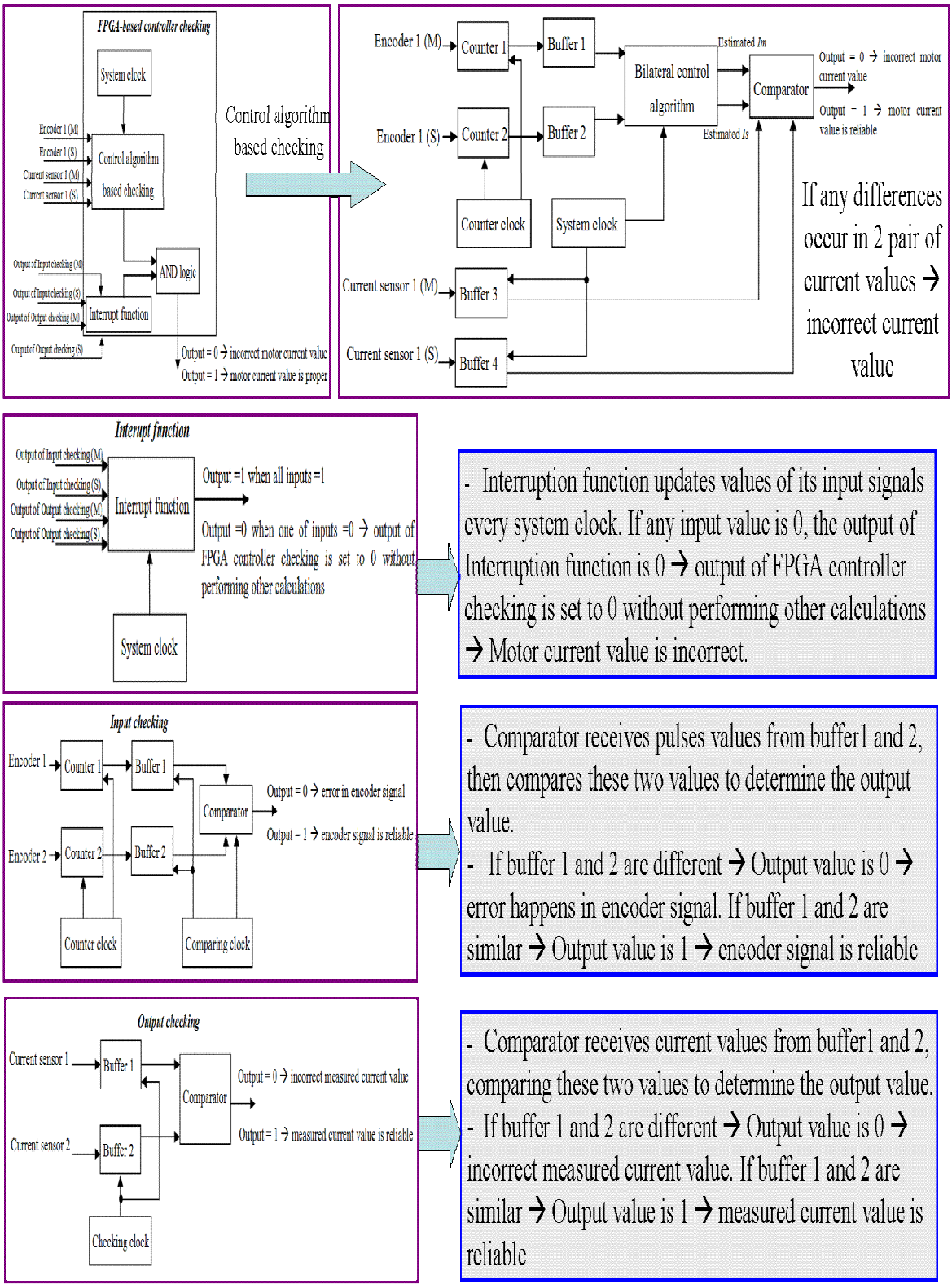

Fig. 6.5. Tentative structures of diagnostic functions in Fig. 6.4

References

[1] S. Katsura, K. Ohnishi, and K. Ohishi: “Transmission of force sensation by environment quarrier based on multilateral control”, IEEE Trans. on Industrial Electronics, Vol.54, No.2, pp.898-906 (2007)

[2] S. Katsura, W. Iida, and K. Ohnishi: “Medical mechatronics-An application to haptic forceps”, Annual Reviews in Control, Vol.29, No.2, pp.237-245 (2005)

[3] Y. Shimizu, K. Ohishi, T. Sano and S. Yasukawa: “Anti-slip/slid re-adhesion control based on disturbance observer considering bogie vibration”, Journal of Electrical Engineering in Japan, Vol.172, No.2, pp.37-46 (2010)

[4] S. Katsura, Y. Matsumoto, and K. Ohnishi: “Shadow robot for teaching motion”, Robotics and Autonomous Systems, Vol.58, No.7, pp.840-846 (2010)

[5] M. Dalvand and B. Shirinzadeh: “Motion control analysis of a parallel robot assisted minimally invasive surgery/microsurgery system (PRAMiSS)”, Robotics and Computer-Integrated Manufacturing, Vol.29, No.2, pp.318-327 (2013)

[6] Y.H. Yin, X. Yong, Z.H. Jiang, and Q.R. Wang: “Tracking and understanding unknown surface with h125igh speed by force sensing and control for robot”, IEEE Sensors Journal, Vol.12, No.9, pp.2910-2916 (2012)

[7] R.V. Patel, H.A. Talebi, J. Jayender, and F. Shadpey: “A robust position and force control strategy for 7-DOF redundant manipulators”, IEEE/ASME Transactions on Mechatronics, Vol.14, No.5, pp.575-589 (2009)

[8] H.B. Huang, S. Dong, J.K. Mills, and H.C. Shuk: “Robotic Cell Injection System With Position and Force Control: Toward Automatic Batch Biomanipulation”, IEEE Transactions on Robotics, Vol.25, No.3, pp.727-737 (2009)

[9] A. Bazaei and M. Moallem: “Improving force control bandwidth of flexible-link arms through output redefinition”, IEEE/ASME Transactions on Mechatronics, Vol.16, No.2, pp.380-386 (2011)

[10] L. Marconi and R. Naldi: “Control of aerial Robots: hybrid force and position feedback for a ducted fan”, IEEE Control Systems, Vol.32, No.4, pp.43-65 (2012)

[11] T. T. Phuong, C. Mitsantisuk, and K. Ohishi: "High performance force sensing based on Kalman-filter-based disturbance observer utilizing FPGA", IEEJ Trans. on Industry Applications, Vol.131, No.3, pp.334-342 (2011)

[12] L. Santos-Carreras, A. Sengul, M. Vollenweider and H. Bleuler: "Multimodal haptic interface for surgical robotics", IEEE Proceedings of 4th International conference on human system interaction , Yokohama, Japan, pp.60-63 (2011)

[13] N. Shimada, T. Yoshioka, K. Ohishi, and T. Miyazaki: "Smooth touch control between position control and force control for industrial robots", IEEE Proceedings of 36th annual conference IECON2010, USA, pp.1949-1954 (2010)

[14] E. Ishii, H. Nishi, and K. Ohnishi: "Improvement of performances in bilateral teleoperation by using FPGA", IEEE Trans. on Industrial Electronics, Vol.54, No.4, pp.1876-1884 (2007)

[15] E. Monmasson and M. N. Cirstea: "FPGA design methodology for industrial control systems-A review", IEEE Trans. on Industrial Electronics, Vol.54, No.4, pp.1824-1842 (2007)

[16] J. B. Huang, Z. W. Xie, H. Liu, K. Sun, Y. C. Liu, and Z. N. Jiang: "DSP/FPGA-based controller architecture for flexible joint robot with enhanced impedance performance", Journal of Intelligent and Robotic Systems, Vol.53, No.3, pp.247-261 (2008)

[17] Y. Chin Tsu, W. Wan-De, and L. Yen Tsun : "FPGA realization of a neural-network-based nonlinear channel equalizer", IEEE Trans. on Industrial Electronics, Vol.51, No.2, pp.472-479 (2004)

[18] C.U. Jung, L.N. Quy, and J.W. Jae: "An FPGA-based multiple-axis motion control chip", IEEE Trans. on Industrial Electronics, Vol.56, No.3, pp.856-870 (2009)

[19] M. Shahbazi, P. Poure, S. Saadate, and M.R. Zolghadri: "FPGA-based reconfigurable control for fault-tolerant back-to-back converter without redundancy", IEEE Trans. on Industrial Electronics, Vol.60, No.8, pp.3360-3371 (2013)

[20] L. Idkhajine, E. Monmasson, and A. Maalouf: "Fully FPGA-based sensorless control for synchronous AC drive using an extended Kalman filter", IEEE Trans. on Industrial Electronics, Vol.59, No.10, pp.3908-3918 (2012)

[21] L. Idkhajine, E. Monmasson, M.W. Naouar, A. Prata, and K. Bouallaga: "Fully integrated FPGA-based controller for synchronous motor drive", IEEE Trans. on

Industrial Electronics, Vol.56, No.10, pp.4006-4017 (2009)

[22] E. Monmasson, L. Idkhajine, and M.W. Naouar: “FPGA-based controllers”, IEEE Industrial Electronics Magazine, Vol.5, No.1, pp.14-26 (2011)

[23] L. Faa-Jeng, H. Ying-Chih, and C. Syuan-Yi: “FPGA-based computed force control system using Elman neural network for linear ultrasonic motor ”, IEEE Trans. on Industrial Electronics, Vol.56, No.4, pp.1238-1253 (2009)

[24] K. Ohnishi: “Robust motion control by disturbance observer”, Journal of Robotics and Mechatronics, Vol.8, No.3, pp.218–225, 1996.

[25] K. Ohishi, K. Ohnishi, and K. Miyachi: “Torque-speed regulation of DC motor based on load torque estimation”, in Proc. IEEJ IPEC, Tokyo, Japan, Mar 1983, Vol. 2, pp. 1209-1216.

[26] K. Ohnishi, M. Shibata, and T. Murakami: “Motion control for advanced mechatronics”, IEEE/ASME Trans. Mechatronics, Vol. 1, No. 1, pp. 56-67, Mar 1996

[27] S. Katsura, K. Irie, and K. Ohishi: “Wideband force control by position-acceleration integrated disturbance observer”, IEEE Transactions on Industrial Electronics, Vol.55, No.4, pp.1699–1706, April 2008.

[28] A. Kato, A. Muis, and K. Ohnishi: “Robust network motion control system based on disturbance observer”, Automatica, Vol.47, No.1-2, pp.5–10, 2006.

[29] T. Shibata and T. Murakami: “Power-assist control of pushing task by repulsive compliance control in electric wheelchair”, IEEE Transactions on Industrial Electronics, Vol.59, No.1, pp.511–520, Jan. 2012.

[30] H. W. Chow and N. C. Cheung: “Disturbance and response time improvement of submicrometer precision linear motion system by using modified disturbance compensator and internal model reference control”, IEEE Transactions on Industrial Electronics, Vol.60, No.1, pp.139–150, Jan. 2013.

[31] I. A. Smadi, H. Omori, and Y. Fujimoto: “Development, analysis, and experimental realization of a direct-drive helical motor”, IEEE Transactions on Industrial Electronics, Vol.59, No.5, pp.2208–2216, May 2012.

[32] C. Mitsantisuk, K. Ohishi, and S. Katsura: “Control of interaction force of twin direct-drive motor system using variable wire rope tension with multisensor integration”, IEEE Transactions on Industrial Electronics, Vol.59, No.1, pp.498–510, Jan. 2012

[33] S. Komada, N. Machii, and T. Hori: “Control of redundant manipulators considering order of disturbance observer”, IEEE Transactions on Industrial Electronics, Vol.47, No.2, pp.413–420, 2000

[34] H. Kobayashi, S. Katsura, and K. Ohnishi: “An analysis of parameter variations of disturbance observer for motion control”, IEEE Transactions on Industrial Electronics, Vol.54, No.6, pp.3413–3421, 2007

[35] L. Yu-Sheng Lu: “Sliding-mode disturbance observer with switching-gain Adaptation and its application to optical disk drives”, IEEE Transactions on Industrial Electronics, Vol.56, No.9, pp.3743–3750, 2009

[36] S. Hamasaki, M. Cao, and A. Kawamura: “Experimental verification of disturbance-observer-based active filter for resonance suppression”, IEEE Transactions on Industrial Electronics, Vol.50, No.6, pp.1140–1147, 2003

[37] Y. Zi-Jiang Yang, S. Hara, S. Kanae, and K. Wada: “Robust output feedback control of a class of nonlinear systems using a disturbance observer”, IEEE Transactions on Control Systems Technology, Vol.19, No.2, pp.256–268, 2011

[38] S. Komada, M. Ishida, K. Ohnishi, T. Hori: “Disturbance observer-based motion control of direct drive motors”, IEEE Transactions on Energy Conversion, Vol.6, No.3, pp.553–559, 1991

[39] S. Kadowaki, K. Ohishi, T. Hata, N. Iida, M. Takagi, T. Sano, and S. Yasukawa: “Antislip readhesion control based on speed-sensorless vector control and disturbance observer for electric commuter train—Series 205-5000 of the East Japan railway company”, IEEE Transactions on Industrial Electronics, Vol.54, No.4, pp.2001–2008, 2007

[40] T. Senjyu, T. Shingaki, and K. Uezato: “Sensorless vector control of synchronous reluctance motors with disturbance torque observer”, IEEE Transactions on Industrial Electronics, Vol.48, No.2, pp.402–407, 2001

[41] Y. Xiong and M. Saif: “Unknown disturbance inputs estimation based on a state functional observer design”, Automatica, Vol.39, No.8, pp.1389-1398 (2003)

[42] W. H. Chen, D. J. Balance, P. J. Gawthrop and J. O’Reilly: “A nonlinear disturbance observer for robotic manipulators”, IEEE Trans. on Industrial Electronics, Vol.47, No.4, pp.932-938 (2000)

[43] A. Kato, A. Muis, and K. Ohnishi: “Robust network motion control system based on disturbance observer”, Automatica, Vol.47, No.1-2, pp.5-10 (2006)

[44] C. Mitsantisuk, S. Katsura, and K. Ohishi: “Kalman-filter-based sensor integration of variable power assist control based on human stiffness estimation”, IEEE Trans. on Industrial Electronics, Vol.56, No.10, pp.3897-3905 (2009)

[45] Z. Jamaludin, H. Van Brussel, and J. Swevers: “Friction compensation of an XY feed table using friction-model-based feedforward and an inverse-model-based disturbance observer”, IEEE Trans. on Industrial Electronics, Vol.56, No.10, pp.3848-3853 (2009)

[46] J. Swevers, F. Al-Bender, C.G. Ganseman, and T. Projogo: “An integrated friction model structure with improved presliding behavior for accurate friction compensation”, IEEE Trans. on Automatic Control, Vol.45, No.4, pp.675-686 (2000)

[47] S.I. Han, and J.M. Lee: “Friction and uncertainty compensation of robot manipulator using optimal recurrent cerebellar model articulation controller and elasto-plastic friction observer”, IET Control Theory & Applications, Vol.5, No.18, pp.2120-2141 (2011)

[48] Y. Maeda, and M. Iwasaki: “Initial friction compensation using rheology-based rolling friction model in fast and precise positioning”, IEEE Trans. on Industrial Electronics, Vol.60, No.9, pp.3865-3876 (2013)

[49] L. Freidovich, A. Robertsson, A. Shiriaev, and R. Johansson: “LuGre-model-based friction compensation”, IEEE Trans. on Control Systems Technology, Vol.18, No.1, pp.194-200 (2010)

[50] D. Bi, Y.F. Li, S.K. Tso, and G.L. Wang: “Friction modeling and compensation for haptic display based on support vector machine”, IEEE Trans. on Industrial Electronics, Vol.51, No.2, pp.491-500 (2004)

[51] B. Friedland and Y. J. Park: “On adaptive friction compensation”, IEEE Trans. on Automatic Control, Vol.37, No.10, pp.1609–1612 (1992)

[52] C. Canudas de Wit, H. Olsson, K .J. Astrom, and P. Lischinsky: “A new model for control of systems with friction”, IEEE Trans. on Automatic Control, Vol.40, No.3, pp.419-425 (1995)

[53] L. B. Nicholas, A. L. Dale, and Y. P. Lucy: “Friction modeling and compensation for haptic interfaces”, IEEE Proceedings of Eurohaptics Conference and Symposium on

Haptic Interfaces for Virtual Environment and Teleoperator Systems, USA, pp.290-295 (2005)

[54] Q. H. Xia, S. Y. Lim, M. H. Ang Jr, and T. M. Lim: "Adaptive joint friction compensation using a model-based operational space velocity observer", IEEE Proceedings of International Conference on Robotics and Automation, USA, Vol.3, pp.3081-3086 (2004)

[55] T. Hagglund: "A friction compensator for pneumatic control valves", Journal of Process Control, Vol.12, No.8, pp.897-904, (2002)

[56] A. Pervozvanski and C. Canudas de Wit: "Asymptotic analysis of the dither effect in systems with friction", Automatica, Vol.38 , No.1, pp.105-113 (2002)

[57] J.J. Rodriguez-Andina, M.J. Moure, and M.D. Valdes: "Features, design tools, and application domains of FPGAs", IEEE Trans. on Industrial Electronics, Vol.54 , No.4, pp.1810-1823 (2007)

[58] R. Dubey, P. Agarwal, and M.K. Vasantha: "Programmable logic devices for motion control—a review", IEEE Trans. on Industrial Electronics, Vol.54 , No.1, pp.559-566 (2007)

[59] Y.Y. Tzou and H.J. Hsu: "FPGA realization of space-vector PWM control IC for three-phase PWM inverters", IEEE Trans. on Power Electronics, Vol.12 , No.6, pp.953-963 (1997)

[60] A. de Castro, P. Zumel, O. García, T. Riesgo, and J. Uceda: "Concurrent and simple digital controller of an AC/DC converter with power factor correction based on an FPGA", IEEE Trans. on Power Electronics, Vol.18, No.1, pp.334-343 (2003)

[61] R. E. Kalman: "A new approach to linear filtering and prediction problems", Journal of Basic Engineering, Trans. of the ASME, Vol.82, Series D, pp.35-45 (1960)

[62] K. Ohishi and R. Furusawa: "Actuators for motion control", IEEE Industrial Electronics Magazine, Vol. 6, No. 1, pp. 4-13, March 2012

[63] N. Miyamoto and K. Ohishi: "Online tuning method for current measurement offsets and gain deviations for SPMSM", IEEE Proceedings of 38th Annual conference on Industrial Electronics IECON 2012, Canada, pp. 1930–1935, Oct. 2012.

[64] Y. Uenaka, M. Sazawa, and K. Ohishi: "Fine self-tuning method of both current sensor offset and electrical parameter variations for SPM motor", IEEE Proceedings of 36th

Annual conference on Industrial Electronics IECON 2010, USA, pp. 835–840, Nov. 2010

[65] K. Ogata: "Modern control engineering", 3rd Edition, Prentice Hall, 1999

[66] S. Jeon and M. Tomizuka: "Benefits of acceleration measurement in velocity estimation and motion control", Control Engineering Practice, Vol. 15, pp. 325-332, 2007.

[67] T. Weigang and F. Xinxi: "An adaptive filtering algorithm of velocity estimation", Journal of Electronics, Vol.17, No.13, pp.248–253, July 2000.

[68] T. H. S. Li, Y. T. Su, S. H. Liu, J. J. Hu, and C. C. Chen: "Dynamic balance control for biped robot walking using sensor fusion, Kalman filter, and fuzzy logic", IEEE Transactions on Industrial Electronics, Vol.59, No.11, pp.4394–4408, Nov. 2012.

[69] K. Szabat and T. O. Kowalska: "Application of the Kalman filters to the high-performance drive system with elastic coupling", IEEE Transactions on Industrial Electronics, Vol.59, No.11, pp.4226–4235, Nov. 2012.

[70] C. Mitsantisuk, K. Ohishi, and S. Katsura: "Estimation of action/reaction forces for the bilateral control using Kalman filter", IEEE Transactions on Industrial Electronics, Vol.59, No.11, pp.4383–4393, Nov. 2012

[71] G.G. Rigatos: "A derivative-free Kalman filtering approach to state estimation-based control of nonlinear systems", IEEE Transactions on Industrial Electronics, Vol.59, No.10, pp.3987–3997, 2012

[72] R. Jassemi-Zargani, and D. Necsulescu: "Extended Kalman filter-based sensor fusion for operational space control of a robot arm", IEEE Transactions on Instrumentation and Measurement, Vol.51, No.6, pp.1279–1282, 2002

[73] T. Schuhmann, W. Hofmann, and R. Werner: "Improving operational performance of active magnetic bearings using Kalman filter and state feedback control", IEEE Transactions on Industrial Electronics, Vol.59, No.2, pp.821–829, 2012

[74] S.Y. Chen, "Kalman filter for robot vision: A survey", IEEE Transactions on Industrial Electronics, Vol.59, No.11, pp.4409–4420, 2012

[75] N. Kanghyun, O. Sehoon, H. Fujimoto, and Y. Hori: "Estimation of sideslip and roll angles of electric vehicles using lateral tire force sensors through RLS and Kalman filter approaches", IEEE Transactions on Industrial Electronics, Vol.60, No.3, pp.988–1000, 2013

[76] M. Elitas, S. Khan, A. O. Nergiz, and A. Sabanovic: “Task based bilateral control for microsystems application”, Automatika, Vol.52, No.2, pp.107–117, 2011.

[77] Y. Yokokura, S. Katsura, and K. Ohishi: “Stability analysis and experimental validation of a motion-copying system”, IEEE Transactions on Industrial Electronics, Vol.56, No.10, pp. 3906–3913, Oct. 2009.

[78] H. Kuwahara, T. Shimono, H. Tanaka, D. Yashiro, and K. Ohnishi: “Abstraction of action components unconstrained by alignment of haptic sensing points”, IEEE Transactions on Industrial Electronics, Vol.58, No.8, pp.3196–3204, Aug. 2011.

[79] N. Tsunashima and S. Katsura: “Spatiotemporal coupler: storage and reproduction of human finger motions”, IEEE Transactions on Industrial Electronics, Vol.59, No.2, pp.1074–1085, Feb. 2012

[80] T. Nakazaki, T. Ogata, K. Ohishi, T. Miyazaki, D. Koide, Y. Takano, and H. Tokumaru: “Focusing control system for suppressing multi-harmonic disturbances in high speed optical disk systems”, Proceedings of the 12th IEEE International Workshop on Advanced Motion Control, AMC 2012, Sarajevo, pp. 1-6, 2012

[81] G. Kostin: “Harmonic disturbance in a controlled mechanical system with friction”, Proceedings of the IEEE International Conference on Physics and Control, Russia, pp. 379-382, 2005

List of Achievements

Published Journals

1. Thao Tran Phuong, Chowarit Mitsantisuk, and Kiyoshi Ohishi: “High Performance Force Sensing Based on Kalman-Filter-Based Disturbance Observer Utilizing FPGA”, IEEJ Transactions on Industry Applications, vol. 131-D, no. 3, pp. 334-342, March, 2011.
2. Thao Tran Phuong, Ryo Furusawa, Manuel Nandayapa, Chowarit Mitsantisuk, and Kiyoshi Ohishi: “FPGA-based Wideband Force Control System with Friction-Free and Noise-Free Force Observation”, IEEJ Journal of Industry Applications, vol. 1. No. 3, pp. 178-190, November, 2012.
3. Thao Tran Phuong, Kiyoshi Ohishi, Yuki Yokokura, and Chowarit Mitsantisuk: “FPGA-based High-Performance Force Control System with Friction-Free and Noise-Free Force Observation”, has been accepted for publication in the IEEE Transactions on Industrial Electronics, and will be published in the IEEE Transactions on Industrial Electronics, vol. 60, No. 7, July, 2013

International Conference Proceedings

1. Thao Tran Phuong, Chowarit Mitsantisuk, Kiyoshi Ohishi, and Masaki Sazawa: “FPGA-based Wideband Force Sensing with Kalman-Filter-Based Disturbance Observer”, Proceedings of the 36th Annual Conference of the IEEE Industrial Electronics Society, IECON’10, Glendale, AZ., USA., pp. 1269-1274, November, 2010.
2. Thao Tran Phuong, Chowarit Mitsantisuk, and Kiyoshi Ohishi: “Multi-sensor Fusion in Kalman-filter for High Performance Force Sensing”, Proceedings of the 2011 Joint IEEE International Conference on Industrial Electronics (ICIT) & South-eastern Symposium on System Theory (SSST) , ICIT-SSST 2011, Auburn, Alabama, pp. 393-398, March, 2011.

3. Thao Tran Phuong, Ryo Furusawa, Chowarit Mitsantisuk, and Kiyoshi Ohishi: "Force Sensing Considering Periodic Disturbance Suppression Based on High Order Disturbance Observer and Kalman-filter", Proceedings of the 4th International Conference on Human System Interaction, HSI 2011, Yokohama, Japan, pp. 336-341, May, 2011.
4. Thao Tran Phuong, Chowarit Mitsantisuk, and Kiyoshi Ohishi: "Wideband Force Control System Based on Friction Free and Noise Free Observation", Proceedings of the 12th IEEE International Workshop on Advanced Motion Control (AMC), Sarajevo, Bosnia and Herzegovina, pp. 1-6, March, 2012.
5. Thao Tran Phuong, Manuel Nandayapa, Chowarit Mitsantisuk, Yuki Yokokura, and Kiyoshi Ohishi: "Force Sensation Improvement in Bilateral Control of Different Master-Slave Mechanism Based on High-order Disturbance Observer", Proceedings of the 38th Annual Conference of the IEEE Industrial Electronics Society, IECON'12, Montreal, Canada, pp. 4406-4411, October, 2012.
6. Thao Tran Phuong, Yuki Yokokura, Kiyoshi Ohishi, and Chowarit Mitsantisuk: "FPGA-based High Performance Bilateral Control of Different Master-Slave Mechanism using High-order Disturbance Observer", Proceedings of the 2013 IEEE International Conference on Mechatronics, ICM 2013, Vicenza, Italy, pp. 534-539, Feb. 27th,28th -Mar. 1st , 2013.
7. Thao Tran Phuong, Kiyoshi Ohishi and Yuki Yokokura: "Improvement of Force Sensing by Harmonics Suppression in a Motion-Copying System", The 39th Annual Conference of the IEEE Industrial Electronics Society, IECON'13, Vienna, Austria, November, 2013.
8. Thao Tran Phuong, Yuji Hirao, Takabumi Fukuda, Yasuhiro Wada, Toshimasa Miyazaki and Kiyoshi Ohishi: "Safety Technology Proposal for Force Control System", The 1st International GIGAKU Conference in Nagaoka (IGCN), Nagaoka University of Technology, Nagaoka, Japan, February 3-5, 2012.
9. Chowarit Mitsantisuk, Thao Tran Phuong, Kiyoshi Ohishi, Shiro Urushihara, and Seiichiro Katsura: "Analysis of Interaction Force of Wire-Based Robot Using Variable Wire Rope Tension Control", Proceedings of the 35th Annual Conference of the IEEE Industrial Electronics Society, IECON '09, Porto, Portugal, pp. 3059-3064, November, 2009 (Awarded IEEE IES Student scholarship).

10. Chowarit Mitsantisuk, Thao Tran Phuong, Kiyoshi Ohishi, and Seiichiro Katsura: "Combining Position and Acceleration Information for High Performance of Bilateral Control using Kalman-Filter-Based Disturbance Observer", Proceedings of the 36th Annual Conference of the IEEE Industrial Electronics Society, IECON'10, Glendale, AZ., USA., pp. 2069-2074, November, 2010.
11. Chowarit Mitsantisuk, Thao Tran Phuong, Kiyoshi Ohishi, and Seiichiro Katsura: "Sensorless Force Sensing Using Kalman Filtering Techniques for Bilateral Control System", Proceedings of the 8th edition of France-Japan and 6th Europe-Asia Congress on Mechatronics, MECATRONICS'10, Yokohama, Japan, pp. 437-442, November, 2010.

National Conference Proceedings

1. Tran Thao Phuong, Chowarit Mitsantisuk, Kiyoshi Ohishi, and Shiro Urushihara, "High performance of force control based on Kalman Filter-Disturbance Observer utilizing FPGA", Proceedings of the 2010 IEE Japan Technical Meeting on Industrial Instrumentation and Control, Tokyo, Japan, pp. 43-48, March, 2010.
2. Thao Tran Phuong, Chowarit Mitsantisuk, and Kiyoshi Ohishi: "Advantages of Acceleration Measurement in Force Sensing by Disturbance Observer", Proceedings of the 28th Annual Conference of the Robotics Society of Japan, Nagoya, Japan, September, 2010.
3. Thao Tran Phuong, Ryo Furusawa, Manuel Nandayapa, Chowarit Mitsantisuk, and Kiyoshi Ohishi: "Force Control Considering Friction Reduction Based on High-order Disturbance Observer Utilizing FPGA", Proceedings of the 54th Conference of the Automatic Control Federation, Toyohashi, Japan, November, 2011.
4. Thao Tran Phuong, Ryo Furusawa, Manuel Nandayapa, Chowarit Mitsantisuk, and Kiyoshi Ohishi: "Friction Free and Noise Free Force Observation Based on an Integration of High-order Disturbance Observer with Kalman-filter", Proceedings of the 2012 IEE Japan Technical Meeting on Industrial Instrumentation and Control, Yokohama, Japan, pp. 133-155, March, 2012.

5. Thao Tran Phuong, Manuel Nandayapa, Chowarit Mitsantisuk, Yuki Yokokura, and Kiyoshi Ohishi: "Power Assisted Bilateral Control for Different Master-Slave Mechanism", Proceedings of the 30th Annual Conference of the Robotics Society of Japan, Sapporo, Japan, September, 2012.
6. Thao Tran Phuong, Yuki Yokokura, and Kiyoshi Ohishi: "An Application of Motion-Copying System Using FPGA based Friction-Free Disturbance Observer", Proceedings of the 2013 IEE Japan Technical Meeting on Industrial Instrumentation and Control, Chiba, Japan, pp. 19-24, March, 2013.
7. Chowarit Mitsantisuk, Thao Phuong Tran, Kiyoshi Ohishi, Shiro Urushihara, and Seiichiro Katsura: "Improvement of Twin Direct-Drive Motor System for Controlling Velocity Based on Variable Wire Rope Tension Control", Proceedings of the IEE Japan Technical Meeting on Industrial Society 2009, Mie, Japan, pp. 465-470, September, 2009.
8. Chowarit Mitsantisuk, Tran Phuong Thao, Kiyoshi Ohishi, Shiro Urushihara, and Seiichiro Katsura: "Development of Disturbance Observer and its Applications to Sensorless Force Control", Proceedings of the 27th Annual Conference of the Robotics Society of Japan, Yokohama, Japan, pp. 1-4, September, 2009.